THÈSE

PRÉSENTÉE À

L'UNIVERSITÉ BORDEAUX 1

ÉCOLE DOCTORALE DES SCIENCES CHIMIQUES

par

Manuela De Leo

POUR OBTENIR LE GRADE DE

DOCTEUR

SPÉCIALITÉ : Chimie-Analytique

Développement de capteurs électrochimiques basés sur des ensembles de nanoélectrodes

---

Soutenue le 15.12.2006

Après avis de :
MM.

C.M.A.Brett	Rapporteurs
K.Kalcher	

Devant la Commission d'examen formée de :

MM.	C.M.A.Brett	Professeur, Université de Coimbra
	K.Kalcher	Professeur, Université de Graz
	P.Ugo	Professeur, Université de Venise
	A. Kuhn	Professeur, ENSCPB
	P.Pastore	Professeur, Université de Padova
	N.Sojic	Professeur, ENSCPB

Università Ca' Foscari di Venezia
Dottorato di ricerca in SCIENZE CHIMICHE 19° ciclo

L'Université Bordeaux 1
École doctorale des SCIENCES CHIMIQUES

December 2006

NANOELECTRODE ENSEMBLES FOR ELECTROCHEMICAL SENSING PURPOSES

A thesis submitted for the degree of

Doctor of Philosophy

by

MANUELA DE LEO

Supervisors: Prof. Paolo Ugo
Prof. Alexander Kuhn

Ph.D Coordinators

Prof. P. Ugo

Prof. L. Servant

Reviewers

Prof. C.M.A. Brett

Prof. K. Kalcher

Board of Examiners

Prof. C.M.A. Brett	University of Coimbra (Portugal)
Prof. K. Kalcher	University of Graz (Austria)
Prof. P. Ugo	University of Venezia (Italy)
Prof. A. Kuhn	ENSCPB (France)
Prof. P. Pastore	University of Padova (Italy)
Prof. N. Sojic	ENSCPB (France)

Contents

RESULTS AND DISCUSSION

List of Abbreviations

2D-NEEs	Two dimension- Nano electrodes ensemble
3D-NEEs	Three dimension- Nano electrodes ensemble
A_{act}	Active area
AFM	Atomic force microscopy
A_{gco}	Geometric area
CE	Counter electrode
CV	Cyclic voltammetry
D	Diffusion coefficient
E	Potential
E^0	Standard electrode potential
$E_{1/2}$	Half wave potential
F	Faraday constant
f	Fractional electrode area
FA^+	Ferrocenylmethyl-trimethylammonium
FE-SEM	Field emission scanning electron microscopy
FIA	Flow injections analysis
GDH	Glucose dehydrogenase
GOx	Glucose oxidase
I_C	Capacitive current
I_F	Faradaic current
k^0	Standard rate constant for heterogeneous electron transfer
k^0_{app}	Apparent rate constant for heterogeneous electron transfer
n	Number of electrons transferred
NAD^+	Nicotinamide adenine dinucleotide oxidized
NADH	Nicotinamide adenine dinucleotide reduced
NDEEs	Nanodisk electrode ensembles
NEEs	Nano electrode ensembles
NEE/SPS	Nano electrodes ensemble coupled with Screen printed substrate

PBE	Partially blocked surface electrodes
PMA	Phosphomolibdic acid
POMs	Polyoxometallates
q	Charge
RE	Reference electrode
SAM	Self–assembled monolayer
SEM	Scanning electron microscopy
SPS	Screen printed substrate
T	Temperature
t	Time
TEM	Transmission electron microscopy
TNFM	(4-carboxy-2,5,7-trinitro-9-fluorenylidene)malononitrile
v	Potential scan rate
WE	Working electrode
Γ	Surface coverage
ϑ	Fraction of blocked electrode surface

Summary

Recent advances in the preparation and electrochemical use of nanoelectrode ensembles (NEEs) are presented, focusing on the application of such electrode systems for the development of electrochemical biosensors.

NEE are nanotech-based electroanalytical tools which find application in a variety of fields, ranging from sensors to electronics, from energy storage to magnetic materials.

NEEs are typically prepared by *template synthesis* which consist in electroless plating of disk-shaped Au electrode elements within the pores of a microporous polycarbonate template membrane. The diameter of the pores in the template determines the diameter of the Au-nanodisks (typically 30 nm), while the density of the pores determines the number of Au-disk nanoelectrode elements per cm^2 of NEE surface and, correspondingly, the average distance between the nanoelectrode elements. These NEEs, which operate in total overlap diffusion conditions, show improved electroanalytical detection limits relative to conventional electrodes since they are characterized by very high signal/noise ratios.

Although the *template synthesis* provides a viable, simple and low cost approach to metal nanostructure synthesis (nanowires, nanotubes, etc…) for the preparation of NEEs, it showed some limitations in particular as far as reproducibility is concerned. For this reason, some improvements to the NEE fabrication procedure have been introduced and they are discussed in *Chapter 3*. This study included refinements in the gold deposition procedure and a comparison with electrochemical deposition. In order to compare performances of NEEs prepared with different ways a procedure for their standardization is developed which is based on the analytical comparison between experimental cyclic voltammograms (CV) obtained at the NEEs and CV patterns obtained by digital simulation. Assembly of NEEs on a screen printed substrate as well as their use as electrochemical detectors in flow cells are also presented in this chapter.

In *Chapter 4*, the use of NEEs for the study of the electrochemical oxidation of iodide in acidic solutions, is investigated. CV patterns display typical quasi-reversible behaviour which involves associated chemical reactions between adsorbed and solution species. The main CV characteristics at the NEE compare with those observed at millimetre sized gold disk electrodes (Au-macro), apart a slight shift in $E_{1/2}$ values and slightly higher peak to peak separation at the NEEs. The detection limit (DL) at NEEs is 0.3 μM, which is more than one order of magnitude lower than DL at the Au-macro (4 μM). The mechanism of the electrochemical oxidation of iodide at NEEs is discussed. Finally, NEEs are applied to the direct determination of iodide at micromolar concentration levels in real samples, namely in some ophthalmic drugs and iodized table salt.

In *Chapter 5*, the preparation of 3D-NEEs as well as their application as electrochemical biosensors are examined. From this viewpoint, NEEs suffer from the fact that the electrode surface useful for immobilizing mediators and/or enzymes (i.e. the active area) is very limited. For this reason, a different NEE fabrication procedure in which the nanodisk electrode elements are substituted by short nanofiber elements is proposed.

To this aim the surface of "classical" NEEs, made of gold nanodisks imbedded in the polycarbonate template, is treated with oxygen plasma or by suitable solvent mixtures (CH_2Cl_2-CH_3CH_2OH), causing the controlled etching of a part of the polycarbonate of the template membrane. The structure of the final ensemble changes from a 2-D flat structure into a 3-D one in which a "forest" of gold nanowires protrudes from the polycarbonate insulating layer. The electrochemical behaviour of fast and slow redox couples at 3D-NEEs is compared and discussed. The surface of the gold nanofibres is functionalized by electrochemically controlled adsorption of a nitrofluorenone derivate, namely (4-carboxy-2,5,7-trinitro-9-fluorenylidene)malononitrile, which is used as efficient mediator for shuttling electrons between NAD^+/NADH dependent dehydrogenase and the electrode. Finally, the adsorption of polyoxometalates is studied at 3D-NEEs with the prospect of developing hydrogen peroxide sensors.

Sommario

L'obbiettivo di questo lavoro di ricerca è lo sviluppo e l'applicazione di ensemble di nanoelettrodi (NEE) per applicazioni sensoristiche. Il lavoro è stato focalizzato sia verso la preparazione e caratterizzazione dei nanoelettrodi, sia verso l'applicazione dei NEE come rivelatori elettrochimici per biosensori e per sistemi di analisi in flusso.
Una delle tecniche più innovative per la costruzione di ensemble di nanoelettrodi e cioè di insiemi non ordinati di elettrodi nanoscopici, la cosiddetta *template synthesis* fa uso di membrane da filtrazione microporose come "stampo" per la deposizione di nanofibre di metalli all'interno dei pori.
Sebbene la *template synthesis* si sia dimostrata uno strumento valido, semplice e a basso costo, per la preparazione di nanostrutture di metalli (nanofibre, nanotubi, ecc..), tuttavia, per la preparazione dei NEE, si sono evidenziati dei limiti in particolare per quanto concerne la riproducibilità.
Sono stati quindi apportati dei miglioramenti alla procedura di fabbricazione dei NEE e in particolare alla procedura electroless di deposizione dell'oro. Al fine di testare le prestazioni elettroanalitiche dei NEEs, si è sviluppato un sistema di standardizzazione che si basa sul confronto analitico tra voltammogrammi ciclici (CV) sperimentali registrati ai NEEs e modelli di CV ottenuti da simulazione digitale.
I NEE cosi selezionati sono stati impiegati nello studio dell'ossidazione elettrochimica dello ioduro in soluzioni acide. E' stato discusso il meccanismo dell'ossidazione elettrochimica dello ioduro ai NEEs, e questi sono stati poi impiegati nella determinazione diretta dello ioduro in concentrazione micromolari in campioni reali, vale a dire in alcuni farmaci del gruppo terapeutico degli oftalmici e nel sale iodato da tavola.
Si è visto poi che l'impiego dei NEE come rivelatori in biosensori elettrochimici è limitato dal fatto che la superficie dell'elettrodo utile ad immobilizzare enzimi e/o mediatori è molto limitata (l'area attiva). Per questa ragione è stata proposta una diversa procedura di fabbricazione di NEE nella quale i nanodischi sono sostituiti da nanofibre. Per questo scopo la superficie dei NEEs tradizionali è trattata con plasma di ossigeno e con un'appropriata miscela di solventi (CH_2Cl_2-CH_3CH_2OH) causando così *l'etching* controllato di una parte della membrana di policarbonato e portando così alla formazione di strutture tridimensionali (3D-NEEs). E' stato quindi studiato il comportamento elettrochimico dei 3D-NEEs rispetto a coppie redox con proprietà cinetiche diverse ed è stata poi funzionalizzata la superficie delle nanofibre di oro con composti sia di natura organica che inorganica al fine sviluppare dei biosensori elettrocatalitici.

Résumé

L'objectif de ce travail de recherche est le développement et l'utilisation d'ensembles de nano-électrodes (NEE) pour les applications sensorielles. Les travaux se sont orientés vers la préparation et la caractérisation des nano-électrodes, ainsi que vers l'application des NEE comme dispositifs électrochimiques pour biocapteurs et pour un système d'analyse par flux.
La synthèse par template constitue une des techniques les plus innovantes pour la construction d'ensembles de NEEs (ensembles non ordonnes d'électrodes nano-scopiques). Cette technique utilise des membranes de filtration microporeuses comme «moule» pour le dépôt de nano-fibres de métal dans les pores.
Bien que la synthèse par template se soit montrée un instrument valide, simple et peu coûteux pour la préparation de nano-structures de métal (nanofibres, nanotubes, etc), la préparation des NEEs s'avère toutefois difficile, principalement en ce qui concerne la reproductibilité.
Nous avons donc apporté des améliorations à la procédure de fabrication des NEEs et plus particulièrement à la procédure de dépôt d'or par voie electroless. Afin de tester les performances électro-analytiques des NEEs, il a été développé un système de standardisation basé sur la comparaison analytique entre les voltamogrammes cycliques (CV) expérimentaux enregistrés avec les NEEs et les modèles des CV obtenus par simulation digitale.
Les NEEs ainsi sélectionnées ont été utilisé dans l'étude de l'oxydation électrochimique de l'iodure en solution acide. Le mécanisme d'oxydation électrochimique de l'iodure sur les NEEs a été discuté, et ensuite ces dernières ont été utilisées dans la détermination directe de l'iodure en concentration micromolaire des échantillons réels (médicaments du groupe thérapeutiques des ophtalmiques et sels iodés de table).
D'autre part l'utilisation des NEEs comme support de biocapteurs électrochimique s'est montrée limitée du fait que la surface de l'électrode utilisée pour l'immobilisation des enzymes et/ou des médiateurs est très restreinte. De ce fait, il a été proposé une procédure différente de fabrication des NEEs dans laquelle les nanodisques sont substitués par des nanofibres. Pour arriver à ce résultats, la surface des NEEs traditionnelles a été traitée par un plasma d'oxygène et par un mélange approprié de solvants (CH_2Cl_2-CH_3CH_2OH), ce qui conduit à la dissolution contrôlée d'une partie de la membrane du polycarbonate et aboutit ensuite à la formation de structures tridimensionnelles (3D-NEEs). Enfin, il a été étudié le comportement électrochimique des 3D-NEEs par rapport aux couples redox comportant des propriétés chimiques différentes. La surface des nanofibres d'or a été fonctionnalisée par des composés de nature soit organique soit inorganique, afin de développer des biocapteurs électrocatalytiques.

1 Introduction

The synthesis of new nanostructured materials and the study of their properties (electrochemical, catalytical and optical) compared to those of macroscopic samples of the same materials, are attracting increasing interest in modern chemical science. The transition between bulk and molecular scales often leads to dramatic changes in the properties of a material, which can be interesting for the practical applications in a variety of areas, including chemistry, physics, electronics, optics, materials and biomedical science [1-4]. This trend includes the preparation, characterization and electrochemical applications of electrodes with critical dimensions in the nanometer range. Among other more complex and expensive procedures, the preparation of nanoelectrodes using microporous membranes as templates distinguishes itself by its simplicity and wide applicability.

First attempts in such direction started at the end of 1980s in Charles Martin's laboratory [5,6], shortly followed by Uosaki and coworkers [7], who proposed the new idea of using pre-formed microporous membranes to build specially featured electrodes inside the pores of the membrane, so obtaining an integrated membrane-nanoelectrodes device. These nanostructured electrodes showed quickly to be very useful for a variety of specialized functions spanning from chemical analyses and sensing [8] to photoelectrochemistry [9] and electrochemical energy storage [10, 11].

The first prototype nanoelectrode ensemble (NEE) was built using alumina microporous membrane as template [5-7], which was then matched by track-etched polymeric membranes [2, 12] commercially available as ultrafiltration membranes (for sophisticated biological separations). All these membranes contain monodispersed pores of very small diameter; the pore diameter determines the nanoelectrode diameter and the pore density controls the distance between the nanoelectrode elements. Since the thickness of the templating membrane is usually much larger than the pore diameter, the obtained nanostructures are characterized by high aspect ratio (that is the length/diameter ratio), which can be as high as 600 or more.

Other approaches are based on exploiting as nanoelectrodes the defects generated in a self-assembled monolayer [13-16]. Recently, metal nanostructures have been obtained also using as templates the pores created by self-assembly of block copolymers under the influence of applied electric fields and high temperatures [17,18].

For a recent review on self-assembly and nanofabrication in polymer matrices see reference [19]. Those interested also in other methods for the fabrication of nanoelectrodes and arrays are addressed to a recent review by Arrigan [20].

The use of pre-formed microporous membranes as template for the synthesis of nanomaterials was somehow revolutionary since it made accessible to almost any laboratory a simple but efficient procedure for the easy preparation of nanomaterials of interest not only to the electrochemist, but to all material scientists [21]. What is needed for the membrane based synthesis of nanomaterials is, in fact, very simple equipment, such as an apparatus for metal deposition and basic electrochemical instrumentation.

Historically, fundamentals of template synthesis in microporous membranes were introduced by Possin [22] and refined by Williams and Giordano [23] who prepared different metallic nanowires with diameters as small as 10 nm within the pores of etched nuclear damage tracks in mica. The technique refined progressively with time, up to achieving the preparation of very sophisticated nanostructures such as, for instance, conically shaped nanoelectrodes with controlled vertex angle, obtained very recently by fine tuning the etching of the pores in the membrane [24, 25].

Templating membranes can be used to produce nanostructured electrode system not only via template metal deposition, but also using other methods such as sol-gel [26-28] or chemical vapour deposition [26,29]. This chapter will examine specifically the preparation, characterization and electrochemical application of ensembles of nanodisk and nanofibre electrodes obtained by using microporous membranes as templates, together with their electroanalytical applications.

1.1 Templating membranes

1.1.1 Comparison between templating membranes

There are two main types of microporous membranes available for the template deposition of metal nanowires and related nanostructures: track-etched polymer and microporous alumina membranes. Both types of membranes are commercially available, special geometries can be obtained on request from the producers; note that alumina membranes can be home-made in certain laboratories.

The main morphological difference between alumina and track-etched polymer membranes is that the alumina membranes, which are prepared by controlled anodization of aluminium [30, 31] are characterized by very high pore densities so that the ratio between the total pore area and the overall geometric area is a number not much smaller than unity (see Fig. 1.1-A). On the contrary, as shown in Fig. 1.1-B, track-etched polymeric membranes are indeed characterized by much smaller pore densities. They are prepared by irradiation of the polymer foil with nuclear fission fragments of heavy elements such as californium or uranium or by ion beams from accelerators. The tracked zone is then removed by a chemical etching agent, typically a solution of a strong alkali.

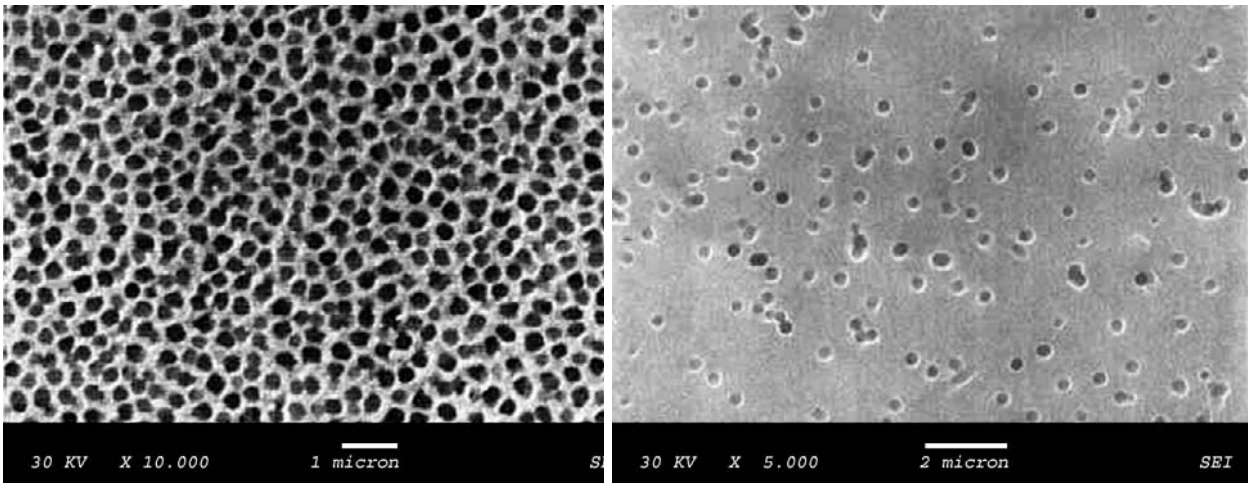

Figure 1.1
SEM images of commercial microporous membrane with pores of 200 nm diameter: a) alumina; b) track-etched polycarbonate.

The chemical etching determines the pore size and shape [32-34], while the time of tracking determines the pore density [32, 35]. Polymeric materials most widely used for preparing track-etched porous membranes are polycarbonate, polyethylene terephthalate and polyimide [32].

Advantageous characteristics of the track etched membranes over porous alumina films are their flexibility (alumina films are brittle) and their smooth surfaces, a problem with track-etched membranes is that the pores created by fission fragment tracks are not always parallel to each other (or even perpendicular to the membrane surface), and the pore positions are randomly distributed, unless special control procedure are applied [36]. On the other hand, the pores in the alumina membranes can be connected on one side of the membrane [37]. Although both kind of membranes can be used for preparing NEEs, track-etched polymers are preferred since they allow higher distances between the nanoelectrode elements, as required in the case of analytical/sensing applications.

For this reason, this thesis focuses on NEEs prepared using commercially available track-etch membranes as template.

1.1.2 Preparation of track-etched polymer membranes

There are two basic methods for producing latent tracks in the polymer foils to be transformed into porous membranes. The first method is based on the irradiation with fragments from the fission of heavy nuclei such as californium or uranium [38] in a nuclear reactor. Typical energy losses of the fission fragments are about 10 keV/nm. The fission fragments coming from a thin layer target have an almost isotropic angle distribution. To create an array of latent tracks penetrating the foil, a collimator is normally used.

The advantages of the tracking with fission fragments are: a) good time stability of the particle flux; b) a non parallel particle flux (enables the production of a high porosity and low percentage of pore channels); c) relatively low cost.

The limitations of the method are: a) contamination of the tracked foil with radioactive products ("cooling" of the irradiated material is needed, which usually takes a few months); b) limited thickness of the membrane to be tracked; c) limited

possibilities of controlling the angle distribution of the tracks; d) fragments of different masses and energies produce tracks with different etching properties.

The second method is based on the use of ion beams in accelerators. The intensity of the ion beam should be at least 10^{11} ions per second. To irradiate large areas a scanning beam is normally used.

The advantages of the ion beam accelerator tracking method are: a) no radioactive contamination of the material when the ion energy is below the Coulomb barrier; b) identical bombarding particles leads to tracks with the same etching properties; c) large range of high energy particles makes possible the tracking of thicker membranes; d) better conditions for producing high–density (>10^9 cm^{-2}) track arrays; e) particles heavier than fission fragments can be used (^{238}U for example); f) it is easier to control the impact angle and produce arrays of parallel tracks or create some particular angular distributions for getting rid of merging pores.

Very recent advances showed that with ion beams it is possible to control the number and the geometrical distribution of the tracks. For this aim, the sample is covered by a metallic mask of small diameter (0.1 mm) so that the ions can penetrate the film only within the small area. By registering the ions passing through the film and shutting down and/or moving the membrane after one single ion had passed through [39, 40] it is possible to obtain single pore membranes or membrane with geometrically patterned arrays of tracks (and pores). The limitations of the ion beam accelerator method are: a) relative instability of the particle flux; b) higher costs compared to irradiation.

Chemical etching is the process of pore formation during which the damaged zone of a latent track is removed and transformed into a hollow channel (pore). The most widely used etching agents are alkaline solutions (KOH or NaOH). The simplest description of the etching process is based on two parameters: the bulk etch rate (V_B) and the track etch rate (V_T). While V_B depends on the material, etchant composition and the temperature, V_T depends on additional parameters, such as sensitivity of the material, irradiation and post-irradiation conditions, etching conditions [32].

It was shown that a strict control of the etching conditions (material, etchant composition and temperature) allows one to control the shape of the pores, obtaining, for instance, funnel-like or conically shaped pores [35, 40]. In these cases etching is performed asymmetrically, so that $V_T > V_T$, this ratio changing through the thickness of the membrane. Typically, in a U-tube cell the membrane separates an alkaline etching solution (usually KOH) from a stopping solution, typically a weak acid solution (HCOOH). A potential of some tens of V is applied across the membrane by two Pt electrodes. The electrode in the etching solution serves as the anode, and the electrode in the stop solution is the cathode. The application of a potential across the membrane is stopped as soon as a monitoring amperemeter registers an increase of current up to a pre-set value, typically 1 mA. The membrane is then immediately immersed (both sides) in the stopping medium, so blocking the asymmetrical etching; at the end of the process, conical nanopores of controlled shape are obtained [35].

1.2 Membrane templated deposition of metals

1.2.1 Electrochemical deposition of metals

Electrochemical deposition of metals in the pores of templating membranes requires that one side of the membrane is in direct contact with a metallic layer. This can be produced by plasma or vacuum deposition of a metal layer on one side of the membrane [41], or by tightly attaching the membrane on the surface of a solid electrode [5]. These procedures require that the membrane film is robust enough to tolerate this kind of manipulation; for plasma or vacuum deposition the thickness required is usually > 10 μm for track etched membrane and > 30 μm for alumina membranes [41]. The metal which produces the conductive layer can be the same or different from the one which will provide the final template structure; in some cases, to improve adhesion of the sputtered or evaporated metal layer, a thin film of reactive metals such as chromium or titanium is deposited first [42].

The scheme for electrochemical template synthesis is shown in Fig. 1.2 [12]. For performing the template deposition, the coated film is placed in an electrochemical cell where the template membrane acts as the cathode and a counter electrode is the anode. The deposition can be carried out both under galvanostatic or potentiostatic conditions.

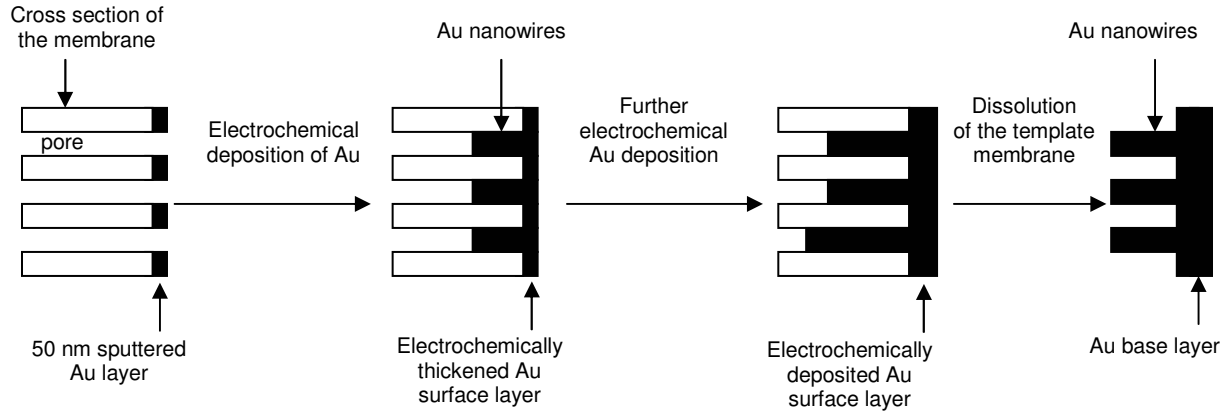

Figure 1.2
Scheme for electrochemical template synthesis.

The typical final products of the electrochemical deposition are solid nanoparticles and not hollow structures (such as for instance, nanotubes or nanocapsules). The electrochemical process consists in fact in the growth and filling of the pores, starting from the bottom metallic layer and progressing towards the open end of the templating pore (see Fig. 1.2).

In a potentiostatic electrochemical deposition three distinct regions characterise the time evolution of the current during the process [43]. With reference to the typical behaviour shown in Fig. 1.3, in region I metal wires grow in the pores, in region II the pores are completely filled and in region III the growth proceeds on the outer face of the templating membrane. Stopping the electrodeposition at step I leads to the formation of nanofibres and at step II to "mushroom" shaped nanostructures (see Fig. 1.3-B and C).

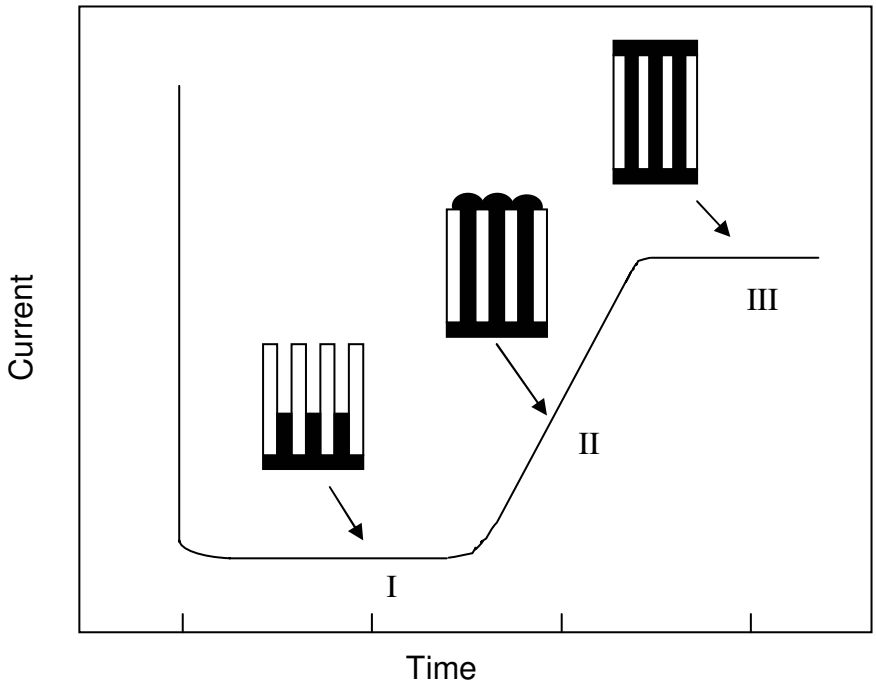

Figure 1.3
Dependence of the electrochemical reduction current on time for the potentiostatic deposition of a metal in a microporous membrane. In region I metal wires grow in the pores, in region II the pores are just completely filled (transition region to bulk growth) and in region III, growth commences over the whole membrane.

Electrodeposition of metals has been studied for obtaining gold nanowires in alumina [44-46], mica [23] and polycarbonate [42] microporous templates. Also other metals were studied with this respect, such as Co [42, 47- 49], Ni [42, 48, 50], Cu [42, 51], Pt and Pd [52]. With the goal of obtaining nanowires with special properties, even alloys such as NiFe [48], FeSiB [50] or salts such as Bi_2Te_3 [53, 54] and CdS [55] have been deposited electrochemically in microporous templates.

One problem encountered for electrochemical deposition of metals in polycarbonate templates is related to the low wettability of this polymer, even after impregnation with polyvinyl pyrrolidone. To overcome this problem, Mallouk and co-workers proposed the addition of 1-2% gelatine to the electrodeposition baths [56-59].

1.2.2 Electroless deposition of metals

By taking into account that templating membranes are made of insulating material, the possibility to exploit chemical deposition methods such as electroless deposition should be considered.

Electroless metal deposition involves the use of chemical reducing agents to plate a metal from a solution onto a surface. The key requirement for this process is to arrange the chemistry so that the kinetics of homogeneous electron transfer from the reducing agent to the metal ion is very slow. A catalyst that accelerates the rate of metal ion reduction is then applied to the surface to be coated. As a consequence the metal ion is reduced preferentially at the surface incorporating the catalyst so that only this surface is coated with the desired metal. The thickness of the metal film deposited can be controlled by varying the plating time [9].

The principles of electroless deposition in templates are exemplified for the typical case of Au deposition, as developed in Martin's laboratory for the template fabrication of nanoelectrode ensembles, nanotubes and other differently shaped gold nanomaterials. The electroless plating of gold [12] consists of three steps; at first a "sensitizer" (Sn^{2+}) is applied to the surface (pore walls plus faces) of the template membrane. This is accomplished by simply immersing the membrane into a solution containing $SnCl_2$. The sensitised membrane is then activated by immersion into an aqueous silver-ammonia solution, that causes a redox reaction in which the surface-bound (Sn(II) is oxidised to Sn(IV) and Ag^+ is reduced to elemental Ag. As a result, the pore walls and membrane faces become coated with discrete Ag nanoparticles. The Ag-coated membrane is then immersed into an Au plating bath. The Ag particles are galvanically displaced by Au and the pore walls and membrane faces become coated with Au particles. These particles catalyse the reduction of Au(I) on the membrane surfaces using formaldehyde as the reducing agent. If the plating procedure is stopped after a relatively short time before the Au nanowires are obtained, Au nanotubes with a length corresponding to the complete thickness of the template membrane are formed within the pores.

For filling completely the pores to obtain nanowires, the electroless plating must be extended up to 24 hours. In order to slow down the kinetics of the deposition the process is performed operating in the vicinity of 0°C. The Au electroless plating bath can be composed by a commercial solution containing $NaAu(SO_3)_2$ (Oromerse Part B, from Technics Inc.) [12], but also home-made electroless plating solutions have been used [60].

In contrast to the electrochemical template deposition, in the electroless method the growth of the metal layer starts from the sensitised/activated sites located on the pore walls, so that the deposition proceeds from the pore walls to the centre. This is the reason why by stopping the deposition at short time, hollow metal nanomaterials (e.g. nanotubes) can be prepared [61]. For the nanotube formation, the control of the electroless bath at pH ≈ 8-10 was proposed [62]. These nanotubes can be separated from the template membrane or can be kept in the template membrane. This procedure allows one to obtain separation membranes with metalized pores [63, 64], whose inner surface can be functionalised chemically, using, for instance, well known thiol chemistry [62].

For the preparation of the so-called nanoelectrode ensembles, metal nanowires must be obtained and kept inside the guest membrane through a solid sealing with the polymer membrane. This is obtained when shrinking the polymer by heating the ensemble just above the glass transition temperature of the polymer (150°C for polycarbonate).

For some specific applications, mixed electroless/electrochemical deposition of metals inside the pores of template membranes has been used. As an example, the fabrication of Au-Te nanocable, with a radial metal-semiconductor structure was carried out by electrochemical deposition of Te inside Au nanotubes previously obtained by electroless deposition [65].

Also other metals such as Cu [66], Pd [67], Ni-P [68] can be deposited in polycarbonate templates by suitable electroless deposition procedures.

1.3 Template nanoelectrode ensembles

Nanoelectrode ensembles (NEEs) and arrays (NEA) are advanced nanostructured electrode systems which are finding application in a variety of fields ranging from sensors to electronics, from energy storage to magnetic materials [9]. The difference between NEEs and NEAs is that in the former the spatial distribution of the nanoelectrodes is random while in the array it is ordered. In the following we will refer mainly to NEEs prepared by using microporous membranes as templating systems and containing randomly distributed pores.

They are prepared by filling the pores of a template with metal nanowires so that in the final ensemble, only the surface of the nanodisk is exposed to the sample solution. The density of the pores in the template determines the number of Au-disk nanoelectrode elements per cm^2 of NEE surface and, correspondingly, the average distance between the nanoelectrode elements.

The scheme of a NEE together with the typical assembly used to transform a piece of golden membrane into a handy NEE are shown in Fig. 1.4. Specific details can be found in the first original papers [12, 69], as well as in recent reviews [8, 9, 70]. At the present status of research, in this kind of NEEs all the nanoelectrodes are connected to each other by a back metal current collector, so that all the nanoelectrodes experience the same applied potential.

As illustrated in Fig. 1.5, depending on whether the template is completely kept on site, partially etched or fully removed, it is possible to obtain nanoelectrodes ensembles with very different geometries. Theoretical treatment of the electrochemical behavior of these different geometries is still at a preliminary stage. Such analysis was developed systematically only for the nanodisk case, as will be presented in the following section.

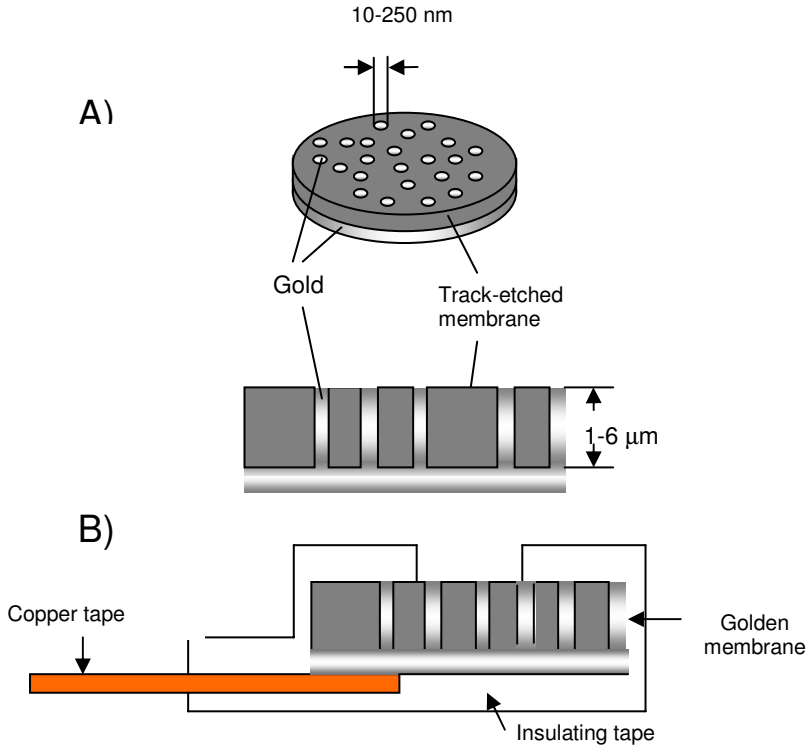

Figure 1.4
A) Scheme of a Au NEE deposited at a polycarbonate membrane. B) Schematic diagram of the typical assembly of the nanoelectrode ensembles

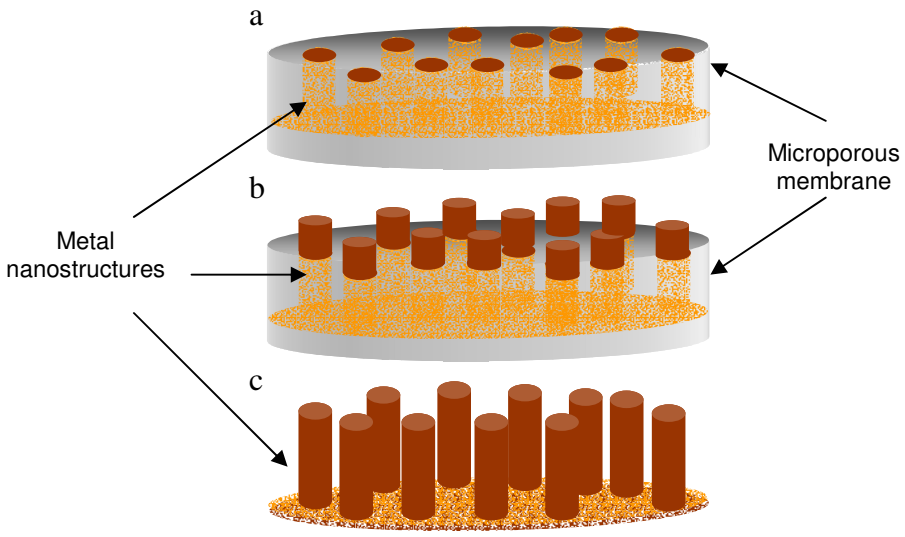

Figure 1.5
Different geometries for templated nanoelectrode ensembles: a) ensemble of nanodisks; b) ensemble of partially naked nanowires; c) ensemble of completely naked nanowires.

1.3.1 Diffusion at nanodisk electrode ensembles

The electrochemical characteristics that distinguish nanodisk electrode ensembles (NDEE) from conventional macro (mm-sized) or even ultramicro (μm-sized) electrodes are:

- dramatic lowering of double layer charging (capacitive) currents [2,12];
- extreme sensitivity to the kinetics of the charge transfer process [71] which means capability to measure very high charge transfer rate constants [13].

Since these characteristics are specific for ensembles of nanodisks electrodes, in case of experimental inability to get direct morphological information about the NDEE structure by e.g. electron or scanning probe microscopy [72], the lack of some of these characteristics, such as the persistence of high capacitive currents, should be taken as a diagnostic indication for a failure in the preparation procedure. From a voltammetric viewpoint, NDEE can be considered as ensembles of disc ultramicroelectrodes separated by an electrical insulator interposed between them. An ultramicroelectrode is considered as an electrode with at least one dimension comparable or lower than the thickness of the diffusion layer (typically < 25 μm). At such small electrodes, edge effects from the electrode become relevant and diffusion from the bulk solution to the electrode surface is described in terms of radial geometry instead of the simpler linear geometry used for larger (>100 μm) electrodes. A NDEE can be considered as a large assembly of very small ultramicrolectrodes confined in a rather small space. Since the number of nanodisk elements per surface is large (10^6-10^8 elements/cm^2), all the nanoelectrodes are statistically equivalent and the different contribution of the elements at the outer range of the ensemble can be considered as negligible [73, 74], even in NDEEs of an overall area as small as 10^{-2}-10^{-3} cm^2 [73].

NDEEs can exhibit three distinct voltammetric response regimes depending on the scan rate or reciprocal distance between the nanoelectrode elements [75, 76]. When the radial diffusion boundary layers overlap totally (radius of the diffusion hemisphere larger then the average hemidistance between electrodes, slow scan rates) NDEEs behave as planar macroelectrodes with respect to Faradaic currents (total overlap conditions).

When diffusion hemispheres become smaller (higher scan rates), the current response is dominated by radial diffusion at each single element (pure radial conditions). At very high scan rates, the linear active state is reached in which the current response is governed by linear diffusion to the individual nanodisk (linear active conditions). Fig. 1.6 sketches the situation encountered for the total overlap and pure radial regimes, being characterized by the higher signal/background current ratios (see below). These two regimes are those typically used for analytical and sensing applications.

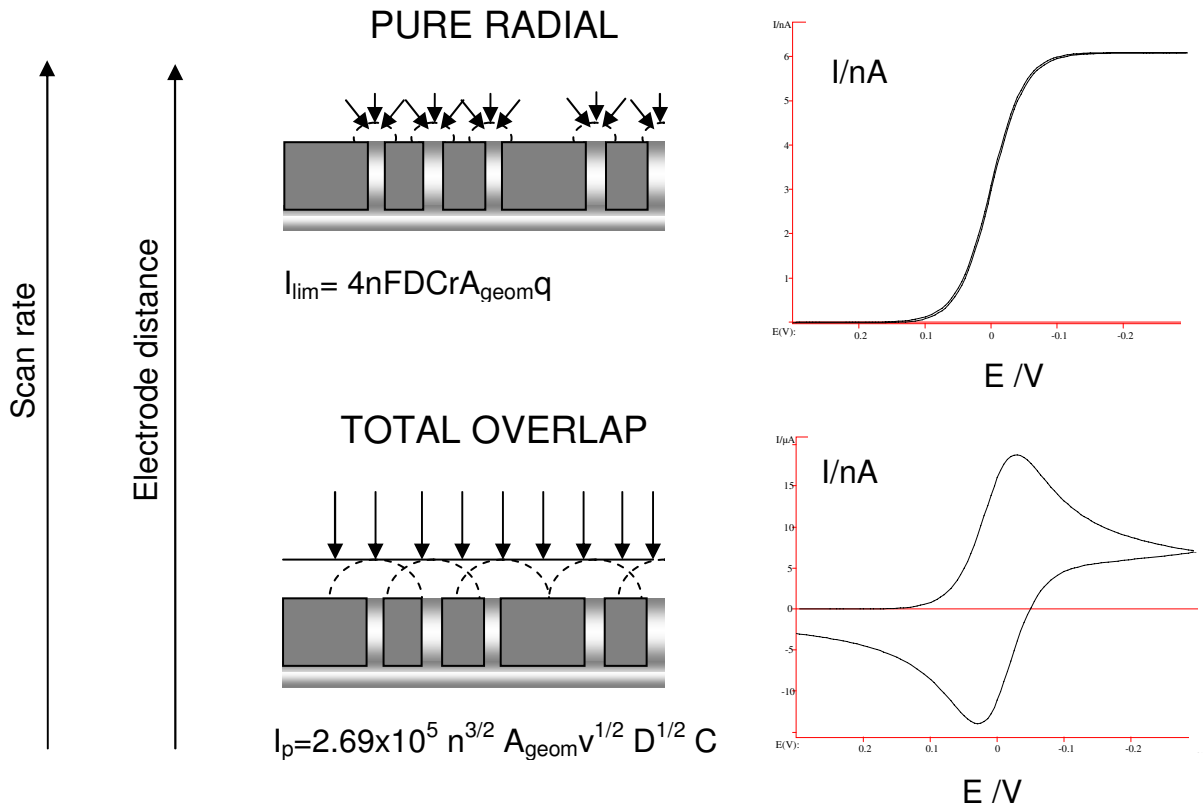

Figure 1.6
Typical diffusive regimes observed at nanoelectrode ensembles as a function of the scan rate and/or nanoelectrodes distance.

The diffusion regime usually observed at NDEEs prepared from commercial track-etched membranes is the total overlap regime [12]. Transition from one regime to the other as a function of the nanoelement distance was demonstrated experimentally using specially made membranes [75].

1.3.2 Signal to background current ratios

In the total overlap diffusion regime, NDEEs show enhanced electroanalytical detection limits, relative to a conventional millimeter-sized electrode. This is because the Faradaic current (I_F) at the NDEE is proportional to the total geometric area (A_{geom}, nanodisks plus insulator area) of the ensemble, while the double-layer charging current (I_C) is proportional only to the area of the electrode elements (active area, A_{act}) [12]. In voltammetry, I_C is the main component of the noise.

Faradaic-to-capacitive currents at NDEEs and conventional electrodes with the same geometric area are related by eq. 1.1 [12, 70]:

$$(I_F/I_C)_{NDEE} = (I_F/I_C)_{conv} A_{geom}/A_{act} \quad (1.1)$$

This ratio at the NDEE is higher, compared to a conventional electrode of the same geometric area, by a proportionality factor that is the reciprocal of the fractional electrode area f, defined as

$$f = A_{act}/A_{geom} \quad (1.2)$$

Typical f values for NDEEs are between 10^{-3} and 10^{-2}. Faradaic currents at NDEEs are equal to those recorded at macro electrodes of the same geometric area, however at NDEEs background currents are dramatically lowered. As a consequence, signals for analytes at concentrations lower than micromolar, are significantly better resolved from the background current. Such an improvement in the Faradaic to capacitive current ratios explains why detection limits (DLs) at NDEEs can be 2-3 orders of magnitude lower than with conventional electrodes [2, 12, 77].

It was shown that improvements in signal/background current ratios at NDEEs are independent from the total geometric area of the ensemble [73]. This is true if the fractional area is kept constant and if the dimensions of the ensemble are lowered to a size still large enough to contain a large number of nanoelements (for instance, NDEE with A_{geom} of 0.005 cm^2 contains $4.8x10^6$ nanoelectrodes).

Note that NDEEs warrant an independence on the ensemble size for overall geometric areas lower than those required for achieving comparable results with arrays of micrometer sized electrodes [74]. This is because the real nanometer size of the electrodes and very high number of elements per cm^2.

This is particularly attractive when thinking to apply the advantages of the use of arrays/ensembles of micro- nanoelectrodes to analyses in samples of very small volume or for "in vivo" biomedical applications. For a given overall geometric area, it is evident that the I_F/I_C is maximum when the total overlap regime is operative. In the case of a pure radial regime, only a certain percentage of the geometric area of the ensemble contributes to the production of a Faradaic current while, in the total overlap regime, this percentage is 100%. On the other hand, it is worth stressing that for NDEEs or NEAs with the same active area, higher Faradaic currents are achieved when operating under pure radial conditions [74]; this is the regime of choice for obtaining the maximum improvement of detection limits when there is no constrain in increasing the distance between the nanoelectrode elements and/or the overall geometric area of the ensemble.

When using Au-NDEEs for trace analysis the accessible potential window is influenced by the high amplification levels on the background signals. The accessible limit depends indeed on the current scale (e.g. nA or pA) at which the signal is recorded and is really an arbitrary definition. Working at nA scales, on the positive side the accessible limit is about 0.7 V vs Ag/AgCl and is related to the formation of a surface oxide layer [12]. On the negative side it depends on the hydrogen evolution reaction and shifts negatively by increasing the solution pH (e.g., approximately – 0.75 V vs Ag/AgCl at pH 7). It was shown that NDEEs can be advantageously used not only as naked nanoelectrode ensembles, but also as polymer coated devices [2]. For instance, the overall surface of a NDEE (insulator and nanodisks) can be easily coated by a thin layer of an ionomer coating. In the cited literature example [2], the ionomer of choice was the polyestersulphonate Eastman AQ55®, which was applied as a water dispersion, i.e. using a solvent which does not damage the NDEE surface (the polycarbonate template can be damaged by organic solvents).

Such an approach showed that it was possible by this way to combine successfully the preconcentration capabilities of ionomer coated electrodes [8, 69, 77] with the increased Faradaic / capacitive current ratio typical of NDEEs.
The ability of NDEEs to allow well resolved cyclic voltammograms for trace redox species has interesting consequences also for adsorption related problems, as in the case of small organic redox molecules and some biomacromolecules as well. If adsorption is concentration dependent, then lowering the solution concentration below the adsorption limit can sometimes overcome the problem. This was demonstrated to be the case for some phenothiazines [77], commonly used as redox mediators in biosensors, and for the heme-containing enzyme cytochrome *c* [79].

1.3.3 Electron transfer kinetics

An important characteristics of NDEEs is that electron transfer kinetics appear slower than at single electrodes [12]. Being composed of a large number of nanodiscs metal elements surrounded by a large surface of insulating material (the guest membrane), NDEEs can be considered as electrodes with a partially blocked surface (PBE); the nanodiscs electrodes are the unblocked surface and the template membrane is the blocking material. According to the pioneering model elaborated by Amatore et al. [71], the current response at this kind of electrodes is identical to that at a naked electrode with the same overall geometric area, but with a smaller apparent standard rate constant for the electron transfer which decreases as the coverage with the blocking agent increases. Such an apparent rate constant ($k°_{app}$) is related, in fact, to the true standard charge transfer rate constant (k°), by the relationship [71]:

$$k°_{app} = k°(1 - \vartheta) = k° f \qquad (1.3)$$

where ϑ is the fraction of blocked electrode surface and f is the fraction of the electrode surface that is Au nanodisks (see eq. 1.2).
From a mechanistic viewpoint, NDEE are an advantage since they allow one to obtain experimentally very large k° values [80]. What is measured at NDEE is the smaller $k°_{app}$, which can be converted into the larger k° by eq. (1.3) [13, 77].

Further understanding of the electrochemical behavior of NDEEs will probably take advantage from recent studies devoted to modeling by digital simulation the voltammetric behavior of regular [81] and random arrays [82] of ultramicroelectrodes.

1.4 Electrodes with highly controlled surfaces

Modification of electrode surface with catalytically active molecules is an extremely attractive method for controlling the chemical and electronic properties of electrodes. Most of the fundamental studies have been performed on classical flat electrode surface. However, for some applications, such as in vivo measurements, it is important to use very small electrodes with the result that the measured currents are quite small due to the limited active surface area [83, 84]. In all these cases template synthesis of nanostructures and nanoelectrodes can be used as a valuable tool to prepare high surface area arrays. Moreover high surface area nanoelectrode systems appear very attractive also as building blocks for self assembly of supramolecular architectures for sensors development.

1.4.1 Macroporous electrodes

In the context of template synthesis, recently various methods to increase the electrode surface area were proposed, for example by using colloidal crystal built from polymer particles as endo templates for subsequent metals electrodeposition [85,86] or by using Langmuir Blodgett technique to assembly colloidal crystals as template for the synthesis of metallic macroporous materials [87].
These methods have shown the advantage to give a good control of pore size, so allowing a rational design of electrodes with a controllable electrocatalytic activity.

1.4.2 High surface nanoelectrodes: etching processes

Notwithstanding their interesting behavior and related analytical advantages [70], ensembles of nanodisk electrodes can present some limitations with respect to their use as sensors when the electrode surface has to be functionalized.

In fact, when immobilizing chemical reactants or electrocatalysts on the electrode surface one has to take into account the very low value of the active area of the ensemble, which can be 10^2–10^3 times smaller than the overall geometric area.
It was recently shown [88] that the small surface area of the nanodisk electrodes of an ensemble can be increased in a controlled way by suitable etching, in order to partially remove the upper layers of the PC template membrane. This causes the structure of the final ensemble to change from a flat 2-D surface, made of metal nanodisks imbedded into the PC, to a 3-D structure made of gold nanowires partially protruding from the PC insulating layer. Such an approach is summarized in Scheme of Fig. 1.7.

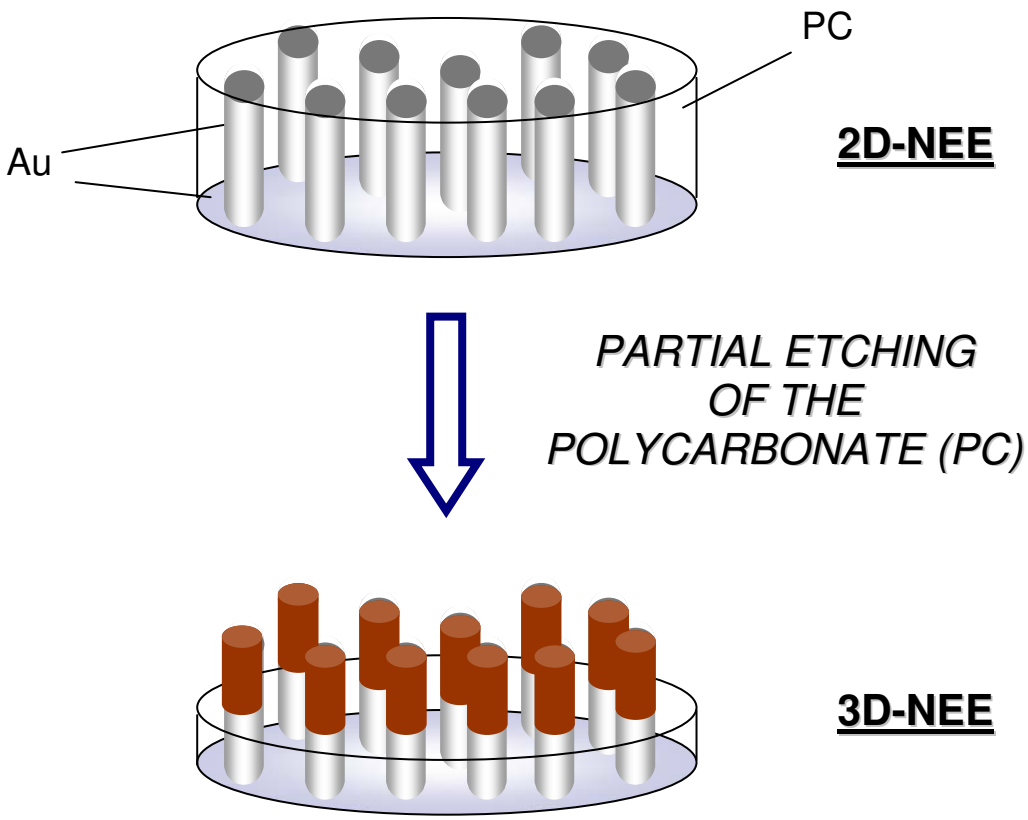

Figure 1.7
Schematic drawing of the effect of the etching on the NEE structure

Martin et al. [88] first proposed O_2 plasma as a way for achieving the controlled removal of PC. This method was recently applied to the preparation of 3D-NEEs functionalized with ss-DNA for DNA sequencing [89, 90]. These publications described enhanced electrocatalysis of redox reporters at DNA-modified 3D-NEEs. The authors suggested that the 3D-NEE architecture of the nanowires could facilitate the electrocatalytic reaction because of enhanced diffusion around the nanofibres.

Recently, Zosky and Krishnamoorthy [91] proposed to substitute the plasma etching with a simpler chemical etching method based on the partial dissolution of the PC membrane in suitable solvent mixtures. It was reported that after the chemical etching, in spite of the expected increase of active area, double layer charging current did not increase significantly with respect to 2D-NEEs. On the other hand, it was reported that the faradaic current for a reversible redox probe (e.g 10mM α-methylferrocenemethanol) increases with the etching of the NEE surface.

Notwithstanding the interesting results presented in these papers [89-91], the preliminary explanation of the observed phenomena appears somehow arguable. Indeed, the effects that a high density of metal nanowires (approximately $6 \cdot 10^8$ nanofibres/cm^2 [12]), and consequently also the overlap of the diffusion layers [12,71] should have on the electrochemical response of these 3D-NEEs, were neither taken into account, nor yet discussed.

When thinking to exploit high surface NEEs as efficient electrodes for advanced sensors or in electroanalysis, it is clearly valuable to obtain more precise information on their peculiarities and, eventually, limits.

Goal of the thesis

As above evidenced, NEEs have been introduced and studied since more than one decade and have shown to be valuable electroanalytical tools, in particular, as far as improved signal/noise ratios and miniaturization are concerned. This notwithstanding, some points on the preparation and characterization as well as on their application in electroanalysis and sensors still need additional research efforts. From this arise the main objectives of this thesis which can be summarized in the following main goals:

1. improvement of the NEEs preparation methods and standardization of the whole manufacturing process in order to get a valid and fast tool for evaluating the performances of these devices;
2. analytical study of the possibility to use NEEs for trace determinations in real samples of practical interest, focusing on an analyte that would require preconcentration steps to be determined with traditional electrodes. For this purpose the iodide anion has been chosen, in view of performing its analysis, also at traces concentration levels, thanks to the high signal/noise ratios, typical for NEEs.
3. study the effect of the increase in active electrode area, via the etching procedure, on the electrochemical behaviour. In particular, the preliminary study of 3D-NEE applications for instance as electrochemical detectors in mediated biosensors.

References

[1] H.Bracht, S.P.Nichols, W.Walukiecwicz, J.P.Silveira, F.Briones, E.E.Haller, *Nature* **2000,** 408, 67.

[2] P.Ugo, L.M.Moretto, S.Bellomi, V.P.Menon, C.R.Martin, *Anal. Chem.* **1996,** 68, 4169.

[3] A.Malinauskas, *Synth. Met.* **1999,** 107, 75.

[4] R.Gref, Y.Minamitake, M.T. Peracchia, V.Trubetskoy, V.Torchilin, R.Langer, *Science* **1994,** 263, 1600.

[5] R.M.Penner, C.R.Martin, *Anal. Chem.* **1987,** 59, 2625.

[6] I.F.Cheng, C.R.Martin, *Anal.Chem.* **1988,** 60, 2163.

[7] K.Uosaki, K.Okazaki, H.Kita, H.Takahashi, *Anal.Chem.* **1990,** 62, 652.

[8] P.Ugo, in *Encyclopedia of sensors*, American Scientific Publishers, Stevenson Ranch, USA, **2005** - in press.

[9] C.R.Martin and D.T.Mitchell, in *Electroanalytical Chemistry, a Series of Advances,* edited A. J. Bard, I. Rubinstein, Marcel Dekker, New York **1999**, vol. 21, p. 1.

[10] F.Nazar, G.Goward, F.Leroux, M.Duncan, H.Huang, T.Kerr, J.Gaubicher, *Int. J.Inorg. Mat.* **2001**, 3, 191.

[11] M.Hirshes, *Mat. Sci. Eng. B,* **2004**, B-108, 1.

[12] V.P.Menon, C.R.Martin, *Anal. Chem.* **1995**, 67, 1920.

[13] E.Sabatani, J.Rubinstein, *J. Phys. Chem.* **1987**, *91*, 6663.

[14] O.Chailapakul, L.Sun, C.J.Xu, R.M.Crooks, *J. Am. Chem. Soc.* **1993**, 115, 12459.

[15] G.L.Che, C.R.Cabrera, *J. Electroanal. Chem.* **1996**, 417, 155.

[16] W.S.Baker and R.M.Crooks, *J. Phys. Chem. B,* **1998**, 102, 10041.

[17] E.Jeonng, T.H.Galow, J.Schotter, M.Bal, A.Ursache, M.T.Tuominen, C.M.Stafford, T.P.Russel, V.M.Rotello, *Langmuir* **2001**, 17, 6396.

[18] W.Cheng, S.Dong, E.Wang, *Anal. Chem.* **2002**, 74, 3599.

[19] T.Liu, C.Burger, B.Chu, *Nanofabrication in polymer matrices, Pro. Polym. Sci.* **2003**, 28, 5.

[20] D.W.M.Arrigan, *Analyst* **2004**, 129, 1157.

[21] J.C.Hulteen and C.R.Martin, *J. Mater. Chem*. **1997**, 7, 1075.

[22] G.E.Possin, *Rev. Sci. Instrum*. **1970**, 41, 772.

[23] W.D.Williams, N.Giordano, *Rev. Sci. Instrum*. **1984**, 55, 410.

[24] P.Scopece, *PhD Thesis,* University of Venice, Italy **2004**.

[25] P.Scopece, L.A.Baker, P.Ugo, C.R.Martin, submitted.

[26] B.B.Lakshmi, C.J.Patrissi, and C.R.Martin, *Chem. Mater*. **1997**, 9, 2544.

[27] C.J.Patrissi and C.R.Martin, *J.Electrochem.Soc.* **1999**, 146, 3176.

[28] N.Li, C.R.Martin, and B.Scrosati, *J. Power Sources* **2001**, 97-98, 240.

[29] G.Che, K.B.Jirage, E.R.Fisher, C.R.Martin, and H.Yoneyama, *J. Electrochem. Soc.* **1997**, 144, 4296.

[30] J.W.Diggle, T.C.Downie, C.W.Goulding*, Chem. Rev*. **1969**, 69, 365.

[31] A.Despic, V.P.Parkhutik, in *Modern Aspects of Electrochemistry,* edited, J. O'M. Bockris, R.E. White, B.E. Conway, Plenum Press, New York, **1989**, vol. 20, p. 401.

[32] P.Apel, *Radiat. Meas.* **2001**, 34, 559.

[33] Z.Siwy, A.Fulinski, *Phys. Rev. Lett.* **2002**, 89, 103.

[34] Z.Siwy, D.Dobrev, R.Neumann, C.Trautmann, K.Voss, *Appl. Phys. A* **2003**,76, 781.

[35] N.Li, S.Yun, C.C.Harrell, C.R.Martin, *Anal.Chem*. **2004**, 76, 2025.

[36] L.D.D.Pra, E.Ferain, R.Legras, and S.Demoustier-Champagne, *Nucl. Instrum. Meth. Phys. Res. B* **2002**, 196, 81.

[37] P.Ugo, L.M.Moretto, G.A.Mazzocchin, P.Guerriero, C.R.Martin, *Electroanalysis* **1998**, 10, 1168.

[38] R.L.Fleisher, P.B.Price, and R.M.Walker, *Nuclear Tracks In Solids, Principle and Applications,* Berkley, CA, **1975**.

[39] R.Spohr, *Methods and device to generate a predetermined number of ion tracks,* Germany, Patent number DE 2951376C2, **1983**.

[40] P.Y.Apel, Y.E.Korchev, Z.Siwy, R.Spohr, and M.Yoshida, *Nucl. Inst. Meth. Phys. Res. B* **2001**, 184, 337.

[41] C.A.Foss-Jr, in *Metal Nanoparticles, Synthesis, Characterization and Applications* edited D. L. Feldheim and J. C.A. Foss, Marcel Dekker, NY **2002** chap. 5.

[42] C.Schönenberger, B.M.I.v.d.Zande, L.G.J.Fokkink, M.Henny, C.Schmid, M.Krüger, A. Bachtold, R. Huber, H. Birk, and U. Staufer, *J.Phys.Chem. B* **1997**, 101, 5497.

[43] T.M.Whitney, J.S.Jiang, P.C.Searson, C.L.Chien, *Science* **1993**, 261, 1316.

[44] C.J.Brumlik and C.R.Martin, *Anal.Chem.* **1992**, 64, 1201.

[45] B.M.I.v.d.Zande, M.R.Böhmer, L.G.J.Fokkink, and C.Schönenbergher, *Langmuir* **2000**, 16, 451.

[46] X.Y.Zhang, L.D.Zhang, Y.Lei, L.X.Zhao, and Y.Q.Mao, *J.Mater.Chem.* **2001**, 11, 1732.

[47] L.Piraux, S.Dubois, and S.D.Champagne, *Nucl. Inst. Meth. Phys. Res. B* **1997**, 131, 357.

[48] H.Chiriac, A.E.Moga, M.Urse, and T.A.Óvári, *Sensors and Actuators A* **2003**, 106, 348.

[49] J.Verbeeck, O.I.Lebedev, G.V.Tendeloo, L.Cagnon, C.Bougerol, and G.Tourillon, *J. Electrochem. Soc.* **2003**, *150, 468.*

[50] K.R.Pirota, D.Navas, M.Hernández-Vélez, K.Nielsch, and M.Vásquez, *J.Alloys and Compounds* **2004**, 369, 18.

[51] Y.Konishi, M.Motoyama, H.Matsushima, Y.Fukunata, R.Ishii, and Y.Ito, *J. Electroanal. Chem*. **2003**, 559, 149.

[52] M.Platt, R.A.W.Dryfe, and E.P.L.Roberts, *Electrochim. Acta* **2004**, 49, 3937.

[53] S.A.Sapp, B.Lakshmi, and C.R.Martin, *Adv. Mat.* **1999**, 11, 402.

[54] A.L.Prieto, M.S.Sander, M.S.M.González, R.Gronsky, T.Sands, and A.M.Stacy, *J. Am. Chem. Soc.* **2001**, 123, 7160.

[55] D.Routkevitch, T.Bigioni, M.Moskovits, J.M.Xu, *J. Phys. Chem.* **1996**, 100, 14037.

[56] M.Tian, J.Wang, J.Kurtz, T.E.Mallouk, M.H.W.Chan, *Nano Lett.* **2003**, 3, 919.

[57] M.L.Tian, J.Wang, J.Snyder, J.Kurtz, Y.Liu, P.Schiffer, T.E.Mallouk, M.H.W.Chan, *Appl. Phys. Lett.* **2003**, 83, 1620.

[58] J.Wang, M.Tian, T.E.Mallouk, M.H.W.Chan, *J.Phys.Chem. B,* **2004**, 108, 841.

[59] J.G.Wang, M.L.Tian, T.E.Mallouk, M.H.W.Chan, *Nano Lett.* **2004**, 4, 1313.

[60] J.Gu, J.Shi, L.Xiong, H.Chen, L.Li, and M.Ruan, *Solid State Sciences* **2004**, 6, 747.

[61] M.Wirtz and C.R.Martin, *Advanced Materials* **2003**, 15, 455.

[62] K.B.Jirage, J.C.Hulteen, and C.R.Martin, *Anal. Chem.* **1999**, 71, 4913.

[63] K.B.Jirage, J.C.Hulteen, and C.R.Martin, *Science* **1997**, 278, 655.

[64] J.C.Hulteen, K.B.Jirage, and C.R.Martin, *J. Am. Chem. Soc.* **1998**, 120, 6603.

[65] J-R.Ku, R.Vidu, R.Talroze, P.Stroeve, *J. Am. Chem. Soc.* **2004**, 126, 15022.

[66] B.Bercu, I.Enculescu, and R.Spohr, *Nucl. Instr. and Meth. B* **2004**, 225, 497.

[67] R.A.W.Dryfe, A.O.Simm, and B.Kralj, *J. Am. Chem.Soc.* **2003**, 125, 13014.

[68] Y.-L.Tai and H.Teng, *Chem. Mater.* **2004**, 16, 338.

[69] R.V.Parthasarathy and C.R.Martin, *Nature* **1994**, 369, 298.

[70] (a) P.Ugo, L.M.Moretto, F.Vezzà, *ChemPhysChem.* **2002** 3, 917; (b) P.Ugo, L.M.Moretto, F.Vezzà in *Sensors Update,* edited H. Baltes, G.K. Fedder, J.G. Korvink, Wiley-VCH, Weinheim, **2003** vol. 12, p. 121.

[71] C.Amatore, J.M. Saveant, D. Tessier*, J. Electroanal. Chem.* **1983**, 147, 39.

[72] W.S.Baker, R.M.Crooks, *J. Phys. Chem. B* **1998**, 102, 10041.

[73] L.M.Moretto, N.Pepe, P.Ugo, *Talanta* **2004**, 62, 1055.

[74] H.J.Lee, C.Beriet, R.Ferrigno, H.H.Girault, *J. Electroanal. Chem.* **2001**, 502, 138.

[75] J.C.Hulteen, V.P.Menon, C.R.Martin, *J. Chem. Soc. Faraday Trans.* **1996**, 92, 4029.

[76] J.F.Cheng, L.D.Whiteley, C.R.Martin, *Anal. Chem.* **1989**, 61, 762.

[77] B.Brunetti, P.Ugo, L.M.Moretto, C.R.Martin, *J. Electroanal. Chem*. **2000**, 491, 166.

[78] P.Ugo and L.M.Moretto, *Electroanalysis* **1995**, 7, 1105.

[79] P.Ugo, N.Pepe, L.M.Moretto, M.Battagliarin, *J. Electroanal. Chem*. **2003**, 560, 51.

[80] A.J.Bard, L.Faulkner, *Electrochemical Methods*, 2nd ed., Wiley, New York, **2000**.

[81] B.A.Brookes, T.J.Davies, A.C.Fisher, R.G.Evans, S.J.Wilkins, K.Yunus, J.D.Wadhawan, R.G.Compton, *J. Phys. Chem. B* **2003**, 107, 1616.

[82] T.J.Davies B.A.Brookes, A.C.Fisher, K.Yunus, S.J.Wilkins, P.R.Green, J.D.Wadhawan, R.G.Compton, *J. Phys. Chem. B* **2003**, 107, 6431.

[83] R.W.Murray, A.G.Ewing, R.A.Durst, *Anal. Chem*. **1987**, 59, 379A.

[84] R.W.Murray, *Molecular design of Electrode Surface,* Wiley-Interscience, New York, **1992**.

[85] O.D.Velev, P.M.Tessier, A.M.Lenhoff, E.W.Kaler, *Nature* **1999**, 401, 548.

[86] P.N.Bartlett, P.R.Birkin, M.A.Ghanem, *Chem. Commun*. **2000**, 1671.

[87] R.Szamocki, S.Reculusa, S.Ravaine, P.N.Bartlett, A.Kuhn, R.Hempelmann, *Angew. Chem. Int. Ed*. **2006**, 45, 1317.

[88] S.Yu, N.Li, J.Wharton, C.R.Martin, *Nano Lett*. **2003**, 3, 815.

[89] R.Gasparac, B.J.Taft, M.A.Lapierre-Devlin, A.D.Lazareck, J.M.Xu, and S.O.Kelly, *J. Am. Chem. Soc.* **2004**, 126, 12270.

[90] M.A.Lapierre-Devlin, C.L.Asher, B.J.Taft, R.Gasparac, M.A.Roberts, S.O.Kelley, *Nano Lett*. **2005**, 5, 1051.

[91] K.Krishnamoorthy, C.G.Zoski, *Anal. Chem*. **2005**, 77, 5068.

2 Experimental

2.1 Apparatus

Electrochemical apparatus

All electroanalytical measurements were carried out at room temperature (22±1°C) using a three-electrode single-compartment cell equipped with a platinum coil counter electrode and a Ag/AgCl (KCl saturated) reference electrode. All potential values are referred to this reference electrode. A CH660A or an Autolab PG-STAT 10 potentiostat controlled via PC by their own software were used for voltammetric measurements.

Conventional "macro" gold electrodes, named "Au-macro" for brevity, were prepared from a golden glass plate (thickness 1 mm) coated with nickel 80 ° A, chromium 20 and gold 3900 °A on the outer surface. They were purchased from ACM France. The golden plate was cut into slides (ca. 2.5 cm×1.0 cm) and the geometric area of the electrodes (0.07 cm^2) was defined, as it was made for the NEE, by the diameter of a hole punched in a strip of insulating tape which covers all the golden surface apart the hole. The electrical contact was made with a copper tape before placing the insulating tape.

Before each set of measurements, the surface of the Au-macro electrodes was cleaned electrochemically by cycling in 0.5M H_2SO_4 between -0.1V and 1.5 V at 100 mVs^{-1}.

Flow cell system

The home made flow cell used for the characterization of NEE/SPS (see below) is shown in Fig. 2.1. The microcell was tailored with appropriate dimensions and inner electrical connections, in order to tightly lodge the screen printed substrate on the bottom surface of the Perspex block. The NEE/SPS was screwed between these two polymer blocks, leaving two holes in the upper side equipped for connection to the sample loop (125 μL) via Teflon tubing. A peristaltic pump (Minipuls-3 from Gilson™) was used to propel solution along a FIA system.

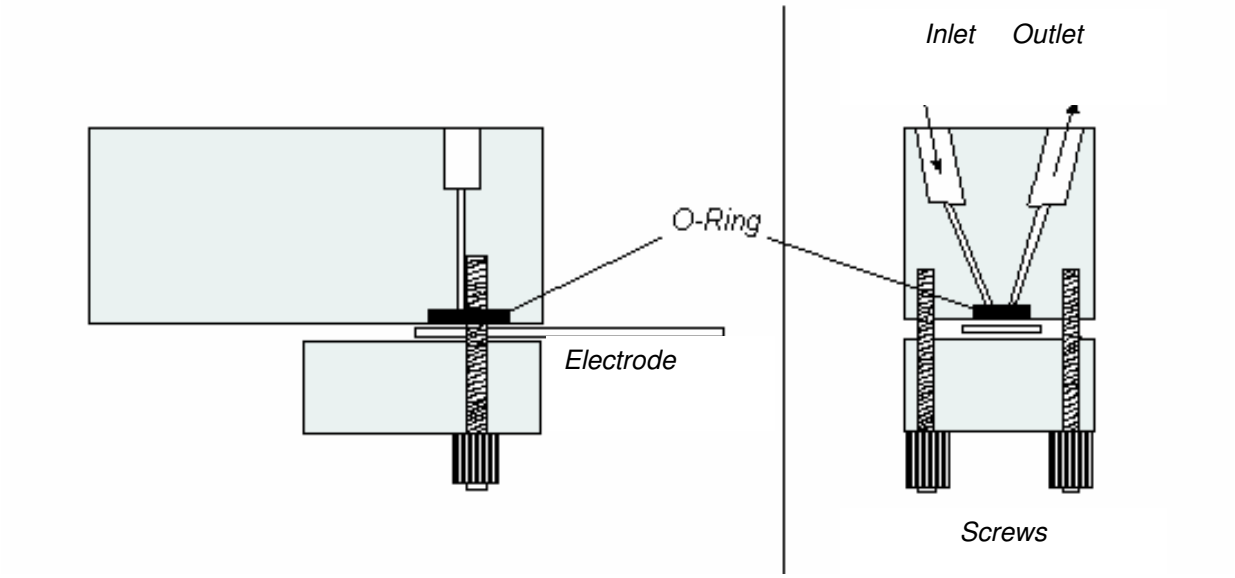

Figure 2.1
Flow cell system

Microscopy apparatus

Scanning electron microscopy (SEM) analyses were performed using a JEOL JSM 5600 instrument, while transmission electron microscopy (TEM) measurements were carried out using a JEOL JEM 3010.

Field-Emission Scanning electron micrographs (FE-SEM) were performed at the Lilit Lab, Synchrotron Facility, INFM- Trieste-Italy; samples were made conductive by sputtering a thin layer of Au-Pd alloy using a vacuum sputter coater.

For electrochemical depositions, one face of the PC membranes was made conductive by evaporation of a thin layer of gold using an Edwards Auto 306 Vacuum Evaporator (pressure = $2x10^{-6}$ mbar; deposition speed = 0.05 Å/s)

AFM analysis were performed using a NTEGRA (NT MDT) Microscopy with a Scanning Image Processor, SPIP v 4.2, Image Metrology A/S 1998-2005. Measurements were done in contact mode.

2.2 Materials

2.2.1 Membranes and gold plating

Polycarbonate filtration membranes (SPI-Pore, 47 mm filter diameter, 6 μm filter thickness) with a nominal pore diameter of 30 nm and coated by the producer with the wetting agent polyvinylpyrrolidone (PVP) were used as the templates to prepare the NEEs.

Commercial gold electroless plating solution (Oromerse Part B, Technic Inc.) was diluted (40 times with water) prior to use. For the gold deposition we used the commercial gold-plating-bath ECF-60 (Technic Inc.).

2.2.2 Chemicals

(Ferrocenylmethyl)dimethylamine (Aldrich) was reacted with methyl iodide to form the quaternary ammonium iodide [1]. This was then converted to (ferrocenylmethyl) trimethylammonium hexafluorophosphate ($FA^+PF_6^-$) using $AgPF_6$.

Phosphomolybdic acid, $H_3PMo_{12}O_{40}$, (PMA) was purchased from Sigma; tris-buffer and calcium chloride dihydrate and glucose were purchased from Merck and Sigma, respectively, and used as received. Glucose solutions were left 12 h for equilibration before use. tris buffer was prepared by dissolving the adequate amount of compound and adjusting to pH 8 by addition of concentrated HNO_3. (4-carboxy-2,5,7-trinitro-9-fluorenylidene) malononitrile (TNFM) was prepared according to the literature and was used as 5 mM solution in tris-buffer [2].

The reduced form of β-nicotinamide adenine dinucleotide (NADH) was purchased as the sodium salt with 98% purity (Sigma). NAD^+ was also obtained from Sigma with 99% purity. Glucose dehydrogenase from bacillus megaterium (Sigma) had an activity of 50-150 units per milligram.

All other reagents were of analytical grade and were used as received. Purified water was obtained using a Milli-Ro plus Milli-Q (Millipore) water purification system.

2.2.3 Real samples

The examined ophthalmic drugs were Facovit (Teofarma S.r.l, Italy) and Rubjovit (S.I.F.I. S.p.A, Italy). The declared composition of 100mL of Facovit solution is, for active components: 100 mg potassium iodide, 100 mg rubidium iodide, 10 mg propionate testosterone and 5 mg riboflavin; excipients: monosodium phosphate dihydrate, disodium phosphate dihydrate, polysorbate 80, (hydroxypropyl)methyl cellulose and benzalconium chloride. The composition of 100 mL of Rubjovit solution is: 800 mg rubidium iodide, 1.2 g sodium iodide, 500 mg calcium formate, 225 mg sodium ascorbate, 200 mg ascorbic acid and 250 mg thiamine hydrochloride; excipients are boric acid, thiourea, phenol and lactose monohydrate. For the analysis, the drug was at first diluted (1:10 for Facovit and 1:100 for Rubjovit) with 0.1M H_2SO_4, then an aliquot of this solution was added to 20mL of 0.1M H_2SO_4 in the electrochemical cell.

The sample of commercially available iodized table salt (Salinen, Ebensee, Austria) was bought at a local grocery. It contained a declared value of 3 mg of potassium iodide in 100 g of salt. The samples were prepared by dissolving 58.5 g (approximately equivalent to 1 mol of NaCl) of the salt in 250mL of sulphuric acid, pH 1.0, and an aliquot of this solution (typically 400 μL) was added to 20mL of sulphuric acid, pH 1.0, in the electrochemical cell.

2.3 Fabrication of nanodisk electrode ensembles (2D-NEEs)

2.3.1 Electroless gold deposition

In this work, gold 2D-NEEs were prepared via electroless or electrochemical procedures. The main step of "classical" template of electroless deposition [3] are described and sketched in Fig. 2.2: after wetting for 2 h in methanol, the polycarbonate template membrane was sensitized with Sn^{2+} by immersion into a solution that was 0.026 M in $SnCl_2$ and 0.07 M in trifluoroacetic acid in 50:50 methanol-water for 45 minutes (Step a)). After rinsing with methanol for 5 min, the sensitized membrane was immersed for 10 min in 0.029 M $Ag[(NH_3)_2]NO_3$ (Step b)) The membrane was then immersed into the Au plating bath which was $7.9x10^{-3}$ M in $Na_3Au(SO_3)_2$, 0.127 M in Na_2SO_3. After waiting 30 minutes, 0.625 M formaldehyde was added to the plating bath (Step c)).

The temperature of the bath was 0-2 °C. Electroless deposition was allowed to proceed for 15 hours, after which an additional 0.3 M formaldehyde was added. Deposition was continued for another 9 hours, after which the membrane was rinsed with water and immersed in 10% HNO_3 for 12 hours. The membrane was then rinsed again with water and dried.

After the sensitization (step a), in which Sn^{2+} is adsorbed on the pore walls and membrane faces via coordination to the PVP which impregnate the PC membrane [3], discrete nanoscopic *Ag* particles are deposited according to the following reaction (step b):

$$Sn^{2+} + 2Ag^{+} \rightarrow Sn^{4+} + 2Ag^{0} \qquad (2.1)$$

In the next step, the *Ag* particles are galvanically displaced by *Au* since gold is a more noble metal, as follows:

$$Au^{+} + Ag^{0} \rightarrow Au^{0} + Ag^{+} \qquad (2.2)$$

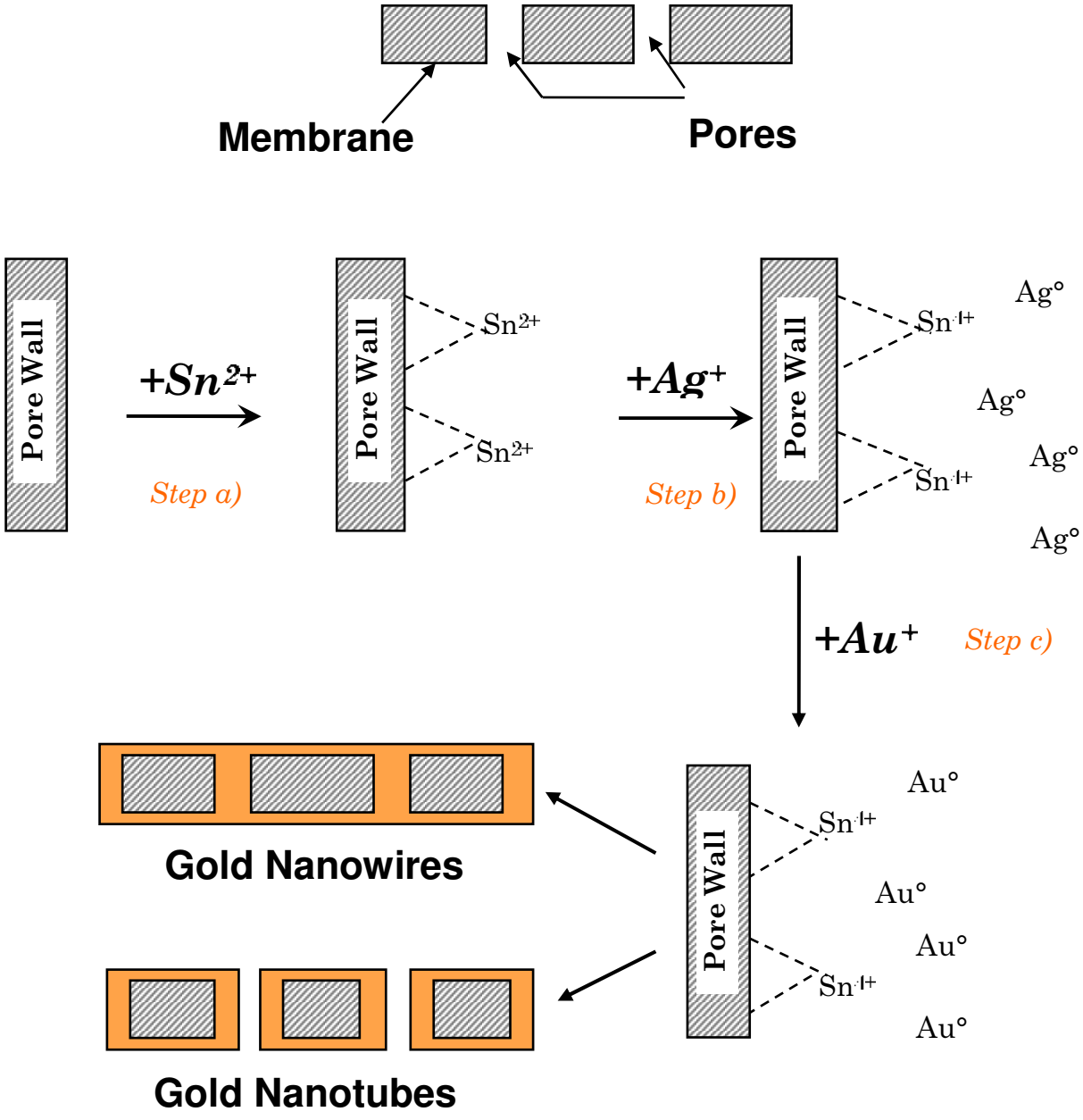

Figure 2.2
Electroless deposition procedure: Steps a) sensitization with Sn^{2+} ; b) activation in a solution of $AgNO_3$ that causes a redox reaction in which the surface-bond Sn^{2+} is oxidized to Sn^{4+} and the Ag+ is reduced to elemental Ag; c) reduction of gold: the Ag particles are galvanically displaced by Au since gold is a more noble metal.
The bulk reaction is performed adding formaldehyde as the reducing agent and the deposition time could be modified in order to get nanowires or nanotubes.

As a result, the pore walls and faces become coated with Au nanoparticles. These particles are excellent catalytic sites for the oxidation of formaldehyde and facilitate the concurrent reduction of *Au(I)* to *Au(0)* (step c). As a result, gold plating continues on the gold particles, with formaldehyde as the reducing agent. This reaction can be represented as follows:

$$2Au^{+} + HCHO + 3OH^{-} \rightarrow HCOO^{-} + 2H_2O + 2\,Au^{0} \qquad (2.3)$$

Overall, *Au* plating was continued for 24 h, resulting in the deposition of continuous Au nanowires (see below) within the pores and on both membrane faces (Fig.2.3). Usually the pH of the Au plating bath was kept around 12 to deposit nanowires, but it was adjusted to pH 10 and even lower by addition 0.5M H_2SO_4 in experiments where the influence of pH on the deposition was studied. After plating, the gold coated membrane was thoroughly rinsed with water and then immersed in 10% nitric acid for 12 h to dissolve any residual *Sn* or *Ag* that might be left in the membrane. Once the membrane is rinsed thoroughly in water and air-dried, it can be used for NEEs fabrication.

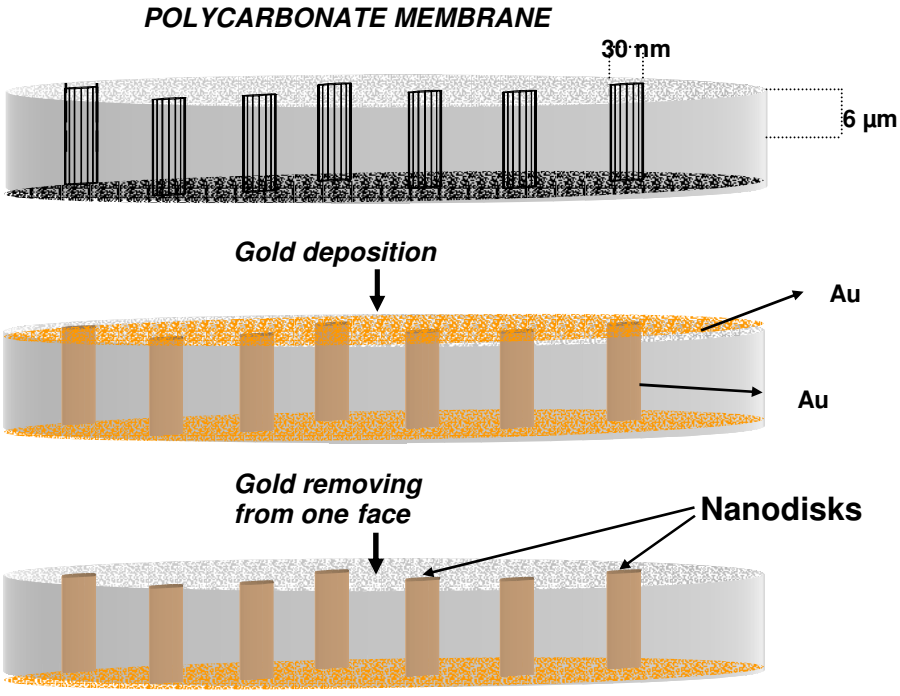

Figure 2.3
Gold deposition in template membrane and disk shaped nanoelectrode ensembles formation.

2.3.2 Electrochemical deposition

This kind of assembly was also used to electroplate gold nanofibres in PC membranes with pores of 30nm. For this purpose, at first, one of the PC membrane faces was made conductive by depositing a thin gold layer by metal evaporation under vacuum, then a piece of copper tape (to act as current collector) and aluminium tape (to give mechanical strength) were attached to this gold layer; as shown in Fig.2.4. Note that the membrane face without gold was used as the upper face of the assembly. Details of the assembly as well as the three-electrodes cell, are sketched in Fig.2.5.

A Pt coil was used as counter electrode, a Ag/AgCl (KCl saturated) was the reference electrode and the Au- coated back of the membrane was the working electrode.

Electrodepositions were performed at room temperature using a commercial gold electrodeposition bath under potentiostatic control (applied potential of -1.1 V), without any stirring of the solution.

A similar procedure was used to deposit copper nanofibres inside PC membranes with a pore diameter of 100nm. Since the pores were bigger, instead of evaporating gold on one side of the membrane, one face of the membrane was made conductive by gold electroless deposition (see above), however the deposition was performed at room temperature, in order to accelerate the deposition kinetics. During the electroless deposition, one face of the membrane was protected from gold deposition by shielding with a layer of Parafilm®.

After removal of this protection layer, electrodeposition was performed as illustrated in Fig. 2.4 using as plating bath an aqueous solution containing 0.5 M $CuSO_4 \cdot 5H_2O$, 1% w/w gelatine, pH 1 (by H_2SO_4); the potential to the working electrode was -0.1V vs Ag/AgCl.

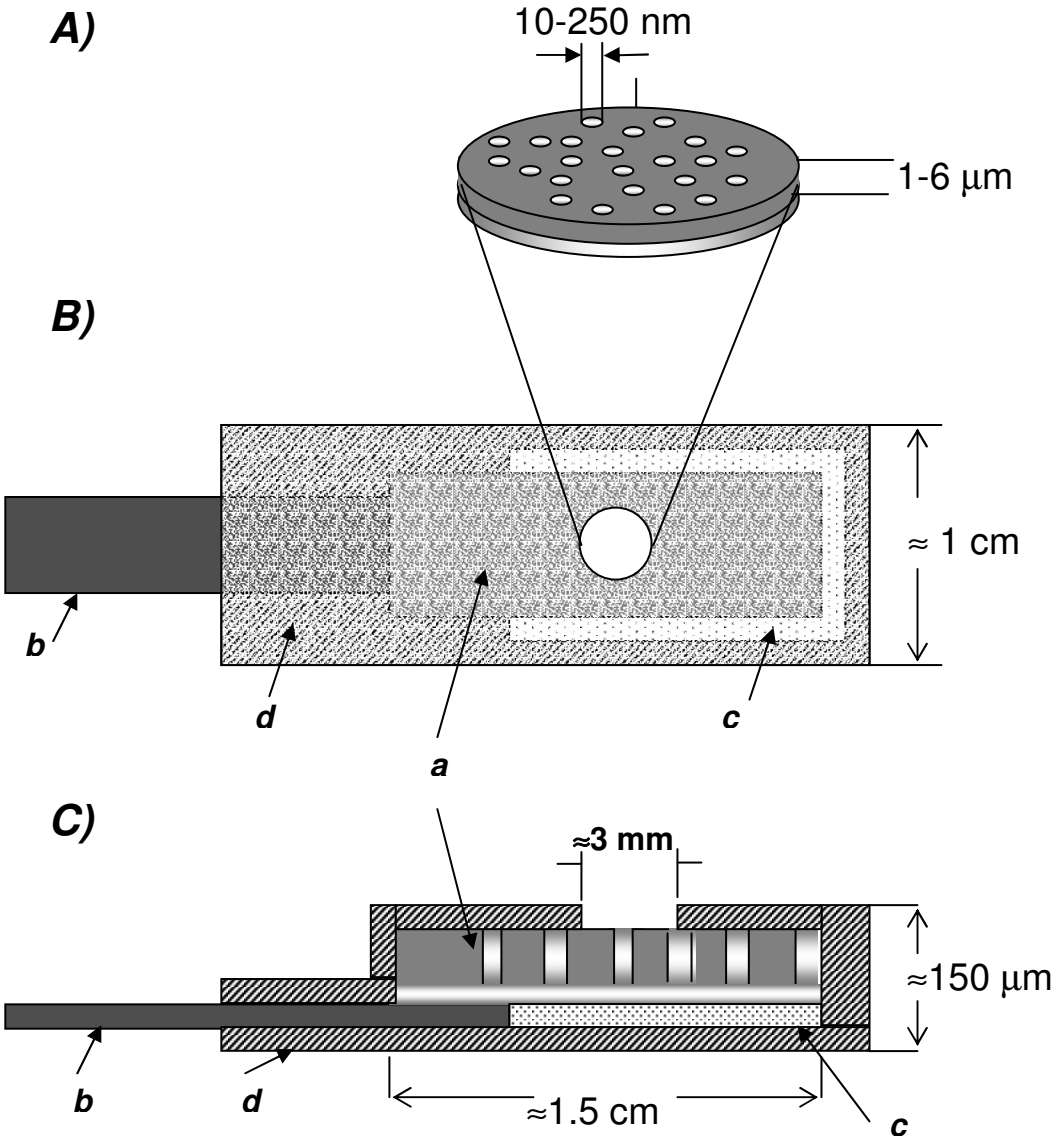

Figure 2.4
Scheme of a Au-NEE prepared using a track-etched polycarbonate membrane as template A). Particular of the section of the active area; B) top view, C) section of the all NEE ready for use as working electrode. (a): track-etched golden membrane; (b): copper adhesive tape with conductive glue to connect to instrumentation; (c): aluminum adhesive foil with non-conductive glue; (d): insulating tape. Note: the dimensions of the pores (nanofibers) are only indicative and not in scale.

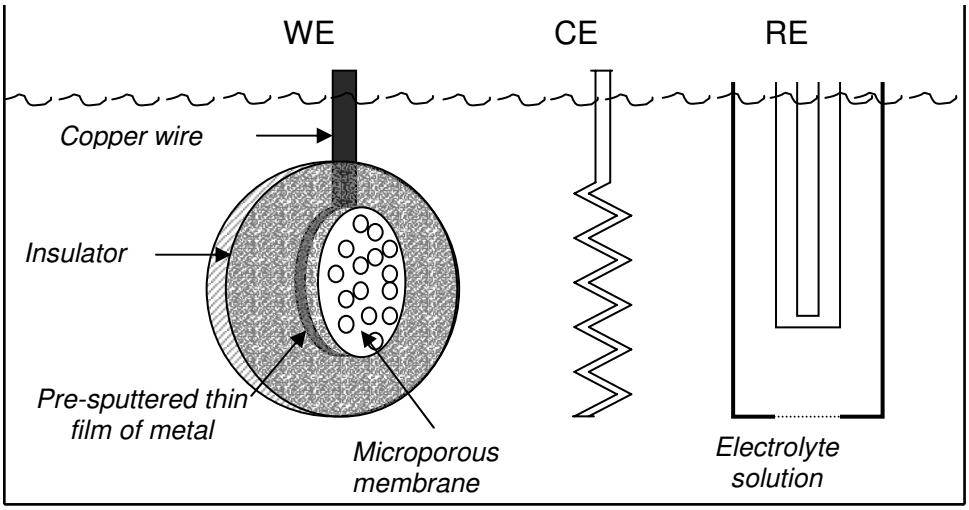

Figure 2.5
Electrochemical template deposition of metals: scheme of the electrochemical cell

2.3.3 NEE assembly

The scheme of a NEE together with the typical assembly used to transform a piece of golden membrane into a handy NEE are shown in Fig. 2.4.

A piece of conducting adhesive copper tape (~5x60 mm) is first affixed to a small square (with a dimension of ~10 mm) of adhesive non-conducting aluminum tape and then to a ~5x5 mm piece of the gold coated membrane, so that only a small part of the membrane is in contact with the copper, which acts as electron collector. The biggest part of the membrane is fixed to the aluminium, since the adhesive of the copper tape contains Ni particles that could damage the membrane.

The upper Au surface layer from the piece of gold coated membrane is removed carefully by cotton stick, previously wetted with ethanol, to exposes the disk- shaped ends of the Au nanowires within the pores of the membrane. These nanodisks will become the active electrode elements. At this point, the NEE assembly is heat-treated at 150 °C for 15 min; this produces a shrinkage of the PC that improves the sealing between the Au nanowires and the pore walls.

Finally, strips of non conductive tape (Monokote, coloured Mylar film ready with polyethylene heat curable glue) are applied to the lower and upper surfaces of the assembly to insulate the Al and Cu tapes. A hole, with a diameter of 3mm, is punched into the upper piece of insulator tape prior to its placement on the assembly. This hole defines the area of the NEE that is exposed to the solution. We refer to this area as the geometric area of the NEE (0.07 cm^2).

2.3.4 NEEs coupled with disposable screen printed substrate (SPS)

The association of Au-NEEs with graphite screen printed substrate (SPS) was used in order to couple the high electroanalytical sensitivity, deriving from the nanosized properties of NEEs, with the feasibility and versatility of the screen printing technology.

Conducting and insulating inks were printed on 0.3–0.5 mm thick polyvinyl-chloride (PVC) substrates using a HT10 Fleischle™ screen printer (Brackenheim, Germany). Silver and carbon-graphite pastes for the conducting paths and WE, Ag/AgCl for RE and insulator pastes were all from GWENT Electronics Materials Inc™. Templates for planar concentric lay-out and specific three-electrode probes were previously designed (Fig. 2.6) [4,5].

In order to assemble NEE/SPS, Au-NEE membrane was one side peeled and soaked on the golden side of a wet graphite ink pad. Either a vacuum pen or a vacuum-controlled silicone rubber tube was conveniently used for placing the inked membrane on the graphite WE of a pre-printed SPS. Afterwards, the device was completed by printing insulator and RE layers as in common screen printing procedure. In each case, the geometric area of the WE is defined by the insulator geometry (2.53 mm^2).

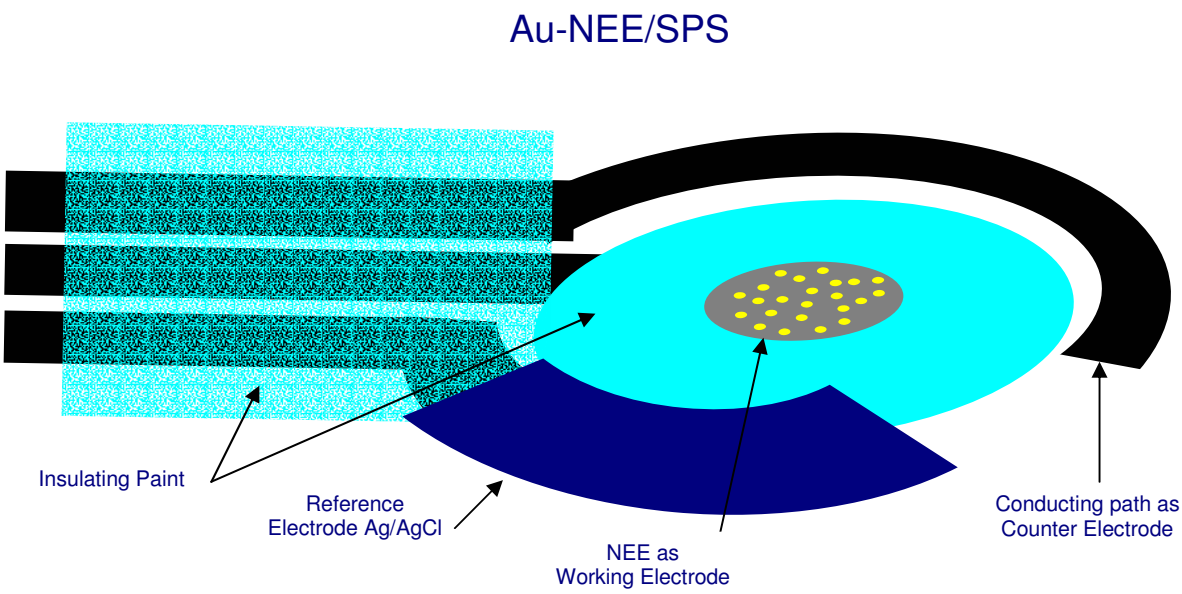

Figure 2.6
NEE/SPS assembly. Sequence of the printing steps: first graphite-based pastes with an optimized concentric lay-out were prepared; Au-NEE membrane is first one side peeled and soaked on the golden side of a wet graphite ink and then placed on the graphite working electrode; afterwards, device is completed by printing insulator and reference layers

2.4 Etching of polycarbonate: from 2D-NEEs to 3D-NEEs

Etching procedures

3D-NEEs were obtained from 2D-NEEs by two different etching procedures: one using O_2/Ar plasma [6] and the other using as chemical etching agent a solvent mixture of dichloromethane and ethanol [7]. However, the CH_2Cl_2/C_2H_5OH ratio used by us was dramatically lower than the one used by other authors [7].

Plasma etching

The surface of a 2D-NEE was exposed to a O_2/Ar plasma using a Plasma Asher system (EMITECH K1050X) with the following experimental parameters: power 100W, flow rate O_2 = 30 cm^3 min^{-1}, flow rate Ar = 10 cm^3 min^{-1}; typical etching time = 30 seconds.

Chemical etching

2D-NEEs were dipped in a solvent mixture of 1:9 dichloromethane-ethanol for a few seconds (namely 2, 5 and 10 seconds) and then dipped in pure ethanol to stop the etching process; finally, they were abundantly rinsed with water.

Note that dichloromethane acts as the etching agent for PC, while ethanol is used to dilute CH_2Cl_2 in order to decrease its etching power, thus allowing a better control of the length of the exposed nanowires.

References

[1] A.Lombardo, T.I.Bieber, *J. Chem. Educ.* **1983**, 60,1080.

[2] N.Mano, A.Kuhn, *J.Electroanal. Chem*. **1999**, 477, 79.

[3] V.P.Menon, C.R.Martin, *Anal. Chem*. **1995**, 67, 1920.

[4] W.Vastarella, B.Lanza, A.Masci, R.Pilloton, *Proceedings of the 9th Italian Conference on Sensors and Microsystems*, Word Scientific, Ferrara, **2004**.

[5] W.Vastarella, M.DeLeo, J.Maly, A.Masci, L.M.Moretto, R.Pilloton, *Procedings of the AISEM*, Lecce, **2005**.

[6] S.Yu, N.Li, J.Wharton, C.R.Martin, *Nano Lett*. **2003**, 3, 815.

[7] K. Krishnamoorthy, C.G.Zosky, *Anal. Chem*. **2005**, 77, 5068

3 Preparation and characterization of NEEs

3.1 Introduction

Many years of practice in the preparation and electrochemical use of NEEs indicated that the "classical" procedure for their preparation [1] presents some limits in particular as far as reproducibility, between different NEEs in the same preparation batch, is concerned. For instance, in our laboratory, when using the traditional procedure, the percentage of NEEs, which display electrochemical characteristics peculiar of NEEs, was typically around 30-40%. This can be attributed mainly to problems in the full chemical control of the gold deposition. An uncontrolled deposition can causes i) uncontrolled changes in the active area of the NEEs (in particular the number of nanodisks that compose the ensemble); ii) failures in the electrical contact between the nanoelectrodes and the signal collector. These two factors influence the electrochemical response of NEEs because they determine the double layer charging current (which depends on the A_{act}), the diffusional regime (radial instead of total overlap when not all the pores are filled with gold) and the background currents due to drops (as consequence of not optimal electrical contact).

In the literature there are more and more examples for using template synthesis to get nanostructures (made of different materials and with different shapes) [2-5], but the application of this method to produce NEEs is not so widespread, probably as a consequence of such reproducibility problems.

For this reason, in this thesis, the parameters that regulate the template deposition of gold have been further investigated. Particular attention was put on the optimization of the electroless deposition as well as on the possible alternative use of an electrochemical deposition.

Finally in order to check whether these changes lead to real improvements, a protocol for the selection of the NEEs based on their electrochemical behaviour was developed.

3.2 Optimization of the Au electroless deposition

Electroless metal deposition involves the use of chemical reducing agents to plate a metal from a solution onto a surface. The key requirement for this process is to control the chemistry so that the kinetics of homogeneous electron transfer from the reducing agent to the metal ion is very slow. A catalyst that accelerates the rate of metal ion reduction is indeed applied to the surface to be coated. As a consequence the metal ion is reduced preferentially at the surface incorporating the catalyst so that only this surface is coated with the desired metal.

The steps involved in the process, described in details in *Chapter 2,* involve: – application of a sensitizer (Sn^{2+}) to the membrane surfaces (pore walls and faces), – activation of the sensitized membrane by exposure to Ag^{+} resulting in the formation of discrete nanoscopic Ag particles, –displacement of the Ag nuclei by gold nanoparticles when the membrane is immersed into the gold plating bath –these gold nanoparticles act as catalytic system for the further gold reduction obtained by adding a suitable reducing agent (formaldehyde).

Analyzing this procedure, we thought that two points could be changed and hopefully, improved with respect to the known procedure. They are: 1) the formation of Au nuclei which act as catalyst for the following chemical reaction; 2) the pH of the electroless bath.

Concerning the first point, note that, previously formaldehyde was added to the Au plating bath immediately after the transfer of the membrane from the Ag^{+} solution. By this way, the Au nuclei grow as soon as they are formed. This can cause a fast growth which can be too fast in the most accessible parts of the pores, i.e closer to the outer faces of the membrane. If this process is too fast it can cause the plugging of the pore entrance, so inhibiting gold nucleation and growth of the deposit in the inner parts of the pores. In order to avoid this, we though to separate the nuclei formation step from their growth (by formaldehyde adding) by introducing a delay between these two steps.

In this way the first gold nuclei have the time to be formed on the whole surface of the pores, avoiding that an anticipated massive reduction of gold could lead to an only partial deposition.

The introduction of a delay time of 30 minutes between addition of the Au plating bath and formaldehyde addition gave, indeed, satisfactory results. The percentage of well-working electrodes (selected as described below) was increased indeed to approximately 80%, thus confirming that this modification leads to the more homogeneous filling of all the pores.

The other aspect investigated was the role of pH of the electroless bath on gold deposition. On the basis of Eq. (2.3), high (alkaline) pH value should favour Au deposition with respect to lower pH (closer to neutrality). In the literature it has been reported that the electroless plating procedure can be used to deposit not only nanofibres (as required for producing NEEs) but also gold nanotubes [6,7].

In the latter case, the length of the nanotubes corresponds to the thickness of the template membrane and the thickness of the Au nanotubes walls depends on the plating time; for filling completely the pores to obtain nanowires, the electroless plating must be extended up to 24 hours.

In the electroless method, the growth of the metal layer starts from the sensitised/activated sites located on the pore walls (and outer faces of the membrane), so that in the pores the deposition proceeds from the walls to the centre.

In our laboratory, attempts to prepare Au nanotubes in 30 nm PC membranes, were unsuccessful, even using deposition time as short as 10-30 min. HR-TEM analyses of the template indicated that a series of interconnected gold particles were obtained instead (see Fig. 3.1).

This prompted us to examine carefully the factors behind such a difference with respect to what was reported in the literature. We noted that, in the fabrication of Au nanotubes (apart the first paper by Menon & Martin), the pH of the electroless bath was lowered from ~ pH 12 (pH of the electroless commercial bath) to ~ pH 10 [8]. For this reason, we focused on the effect of pH on the template electroless deposition.

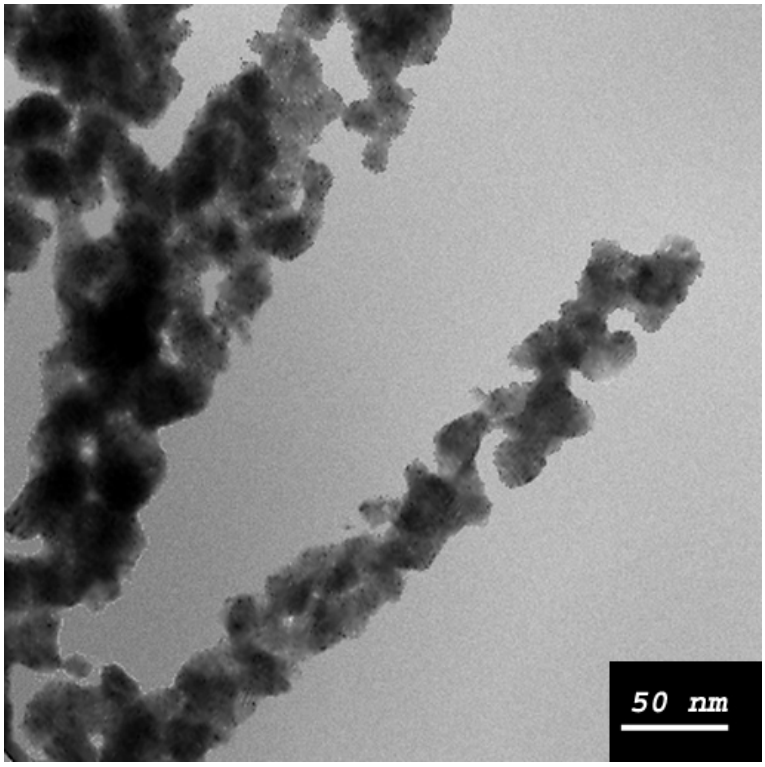

Figure 3.1
Nanowires formation: TEM image of the template after gold electroless deposition and dissolving the polycarbonate membrane. Pore diameters of 30nm, deposition time of 20 minutes and pH value 12.

In a series of experiments, we performed the electroless deposition of Au in polycarbonate membranes with pore diameters of 200 nm changing either the plating time or the pH values. Fig. 3.2 shows the macroscopic aspect of PC membranes plated at pH 10 using different deposition time. Depending on the deposition time, the samples presented different colours ranging from transparent pink (10 min) to deep purple (2 hours) as long as gold particles were deposited mainly within the pores. After 3.5 h a thin massive gold layer deposited on the surface of the membrane was observed. The pink and purple colours were due to the size of the gold nanoparticles formed within the pores at short deposition time. These particles absorb light in the visible, with a maximum wavelength depending on the particle size [9,10]. Smaller particles absorb mainly at 520 nm and appear pink, while the increase of the particle diameter is reflected in a blue shift.

Figure 3.2
Photograph of the membranes plated at pH 10 using different deposition time: 10, 20, 30, 40, 60, 90, 120, 210, 240 minutes in clockwise direction from the arrow.
Membranes 200 nm pore diameter.

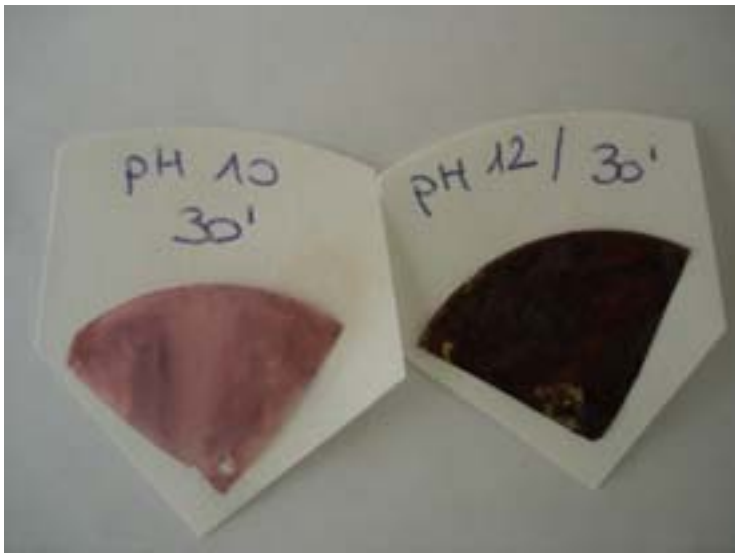

Figure 3.3
Comparison between membranes plated at pH 10 and pH 12 for 30 minutes. Membranes 200 nm pore diameter.

The same experiment was carried out keeping the pH of the electroless bath at 12, Fig. 3.3 shows the comparison between two membranes withdrawn at the same time but obtained from solutions with different pH. This figure shows that, after the same deposition time, a larger amount of Au was deposited in the bath with higher pH. The results of SEM analysis obtained on membranes plated for 40 minutes at pH 10 are reported in Fig. 3.4. They show that gold is deposited only on the pore walls, as indicated by the formation of golden rings all around each pore, suggesting the presence of gold nanotubes. At pH 12 these structures were not observed.

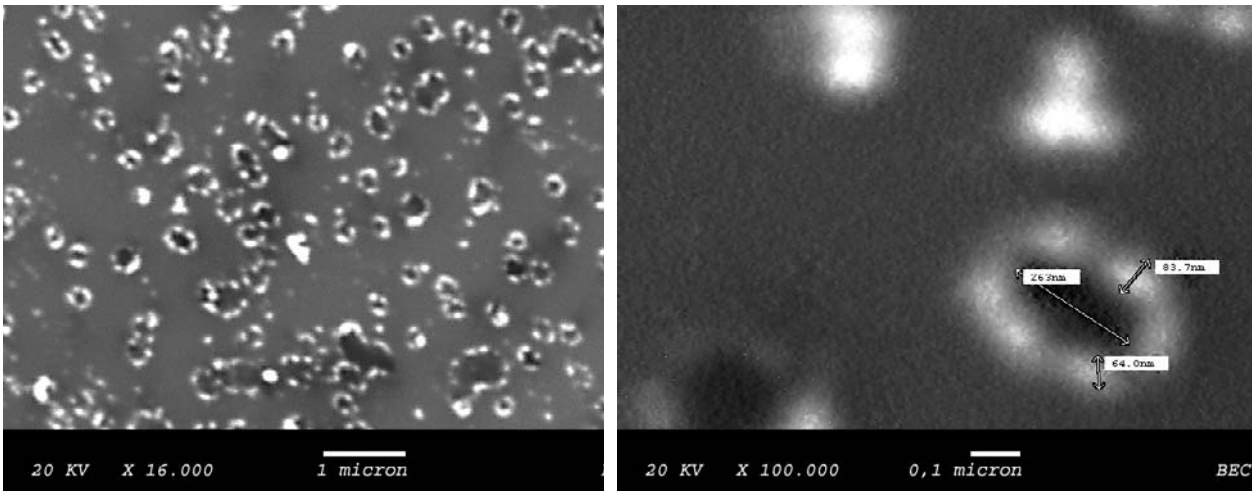

Figure 3.4
A) Nanotubes formation: SEM imagine of the template after gold electroless deposition. Pore diameters of 220 nm, the deposition time of 40 minutes and pH 10. B) Magnification

AFM was used to analyse the morphology of the gold surface deposited on the outer face of the template; plating was carried out for 40 h at pH 7, 9 and 10. AFM images Fig. 3.5 and data reported in Tab. 3.1 indicate that grain size and surface roughness increases with the pH of the deposition bath. Note that all images have the same scale in order to allow an easy comparison between the surface roughness.

All these evidences confirm that the deposition kinetics becomes progressively faster increasing the pH of the bath. This is reflected by a larger grain size and higher roughness of the deposit obtained at more alkaline pH.

pH	S_{ds} [μm^{-2}]
7	168
9	159
10	131

Table 3.1
Dependence of the surface roughness on pH values
S_{ds}, the density of the summits, is the number of the local maximums per area

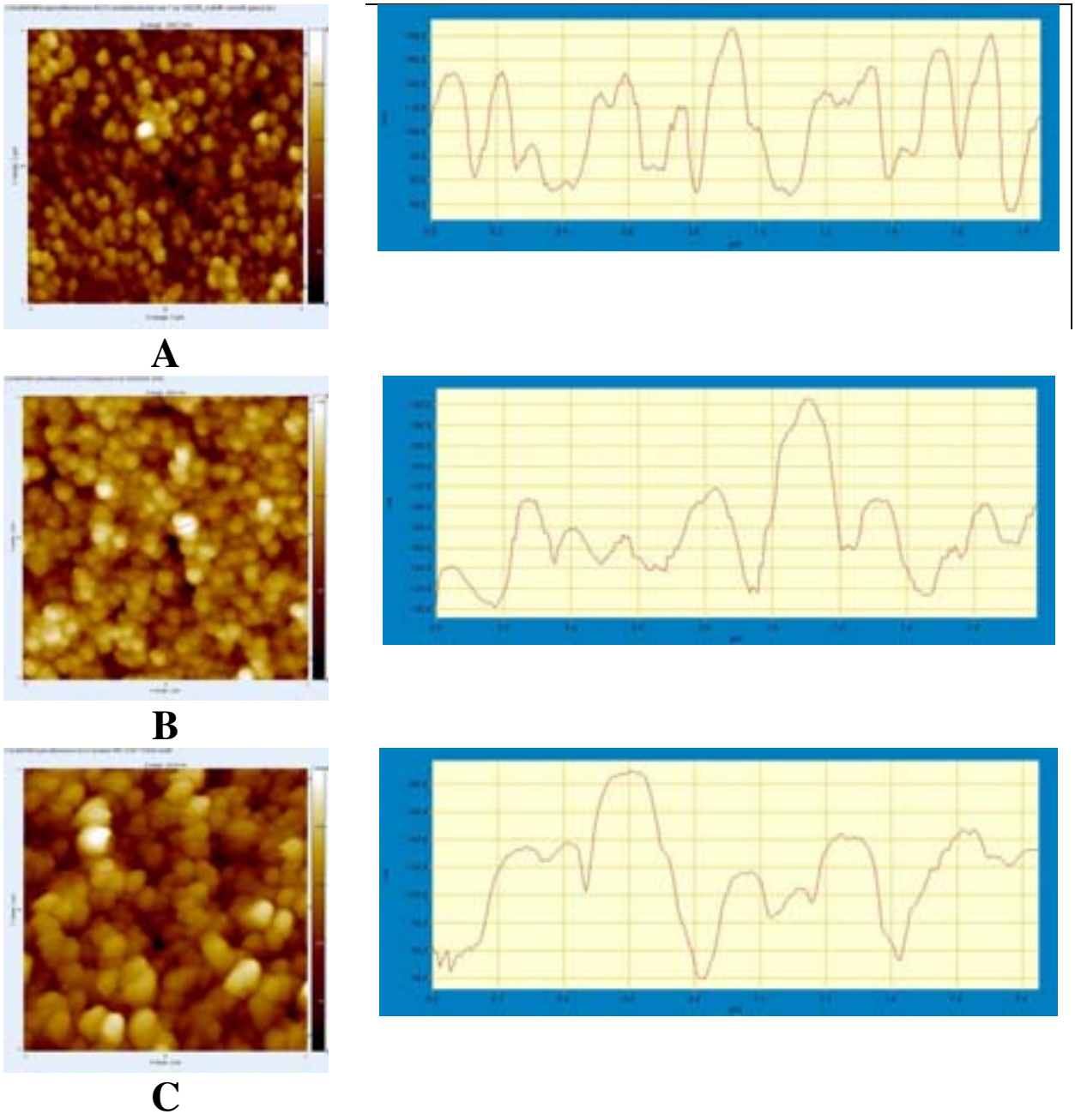

Figure 3.5
Surface roughness dependence on pH values: AFM imagine of the template after gold electroless deposition performed at A) pH 7, B) pH 9, C) pH 10. Pore diameters of 30nm, the deposition time of 40 hours. On the right side, the surface roughness trend is reported (see table 3.1).

The influence of pH on the structure of the gold deposited within the pores template is sketched here below in Fig. 3.6.

At low pH (8-10), smaller grain size and smaller roughness indicate a slower nucleation/growth of the gold nanoparticles. A larger number of nuclei is formed per unity of length along the pore walls before they start enlarging. Note that the growth process of each nucleus is slowed down by the presence of a large number of nuclei which all consume the slowly diffusing Au (I) ions. This explains why at short time, nanotubes can be formed (see Fig. 3.4).

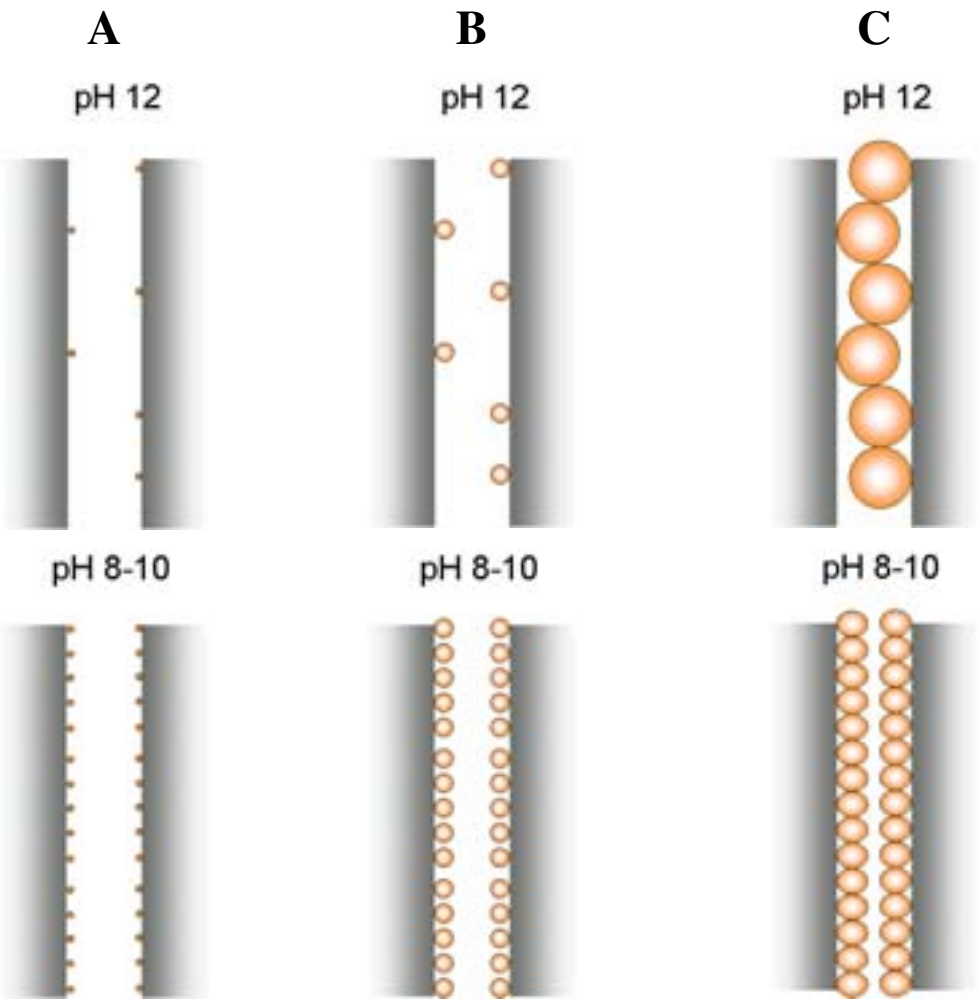

Figure 3.6
Influence of the pH on the electroless deposition. Sketches of particles growth: comparison of the situation at pH 8-10 and pH 12 after A) a few minutes, B) 1-2 hours and C) several hours of deposition time.

On the contrary, at high pH values all the kinetics are accelerated, both the nuclei formation as well as their growth. This reflects in the fast formation of a smaller number of relatively large nuclei, which quickly grow to connect together producing (under small pore diameter constrains) nanofibres composed, however, by linear aggregates of Au particles. This agrees with TEM observations reported in Fig. 3.1.

On the basis of the above reported experimental observations and the simplified qualitative model, we can conclude that pH 10, or even lower, is to be preferred when nanotubes are the desired final product of the template deposition, while pH 12 is the right choice when one wishes to obtain continuous (and not porous) nanofibres. Obviously, in the case of the NEEs the latter situation is the best one.

Fig. 3.7 shows a cross-section of the PC membrane after gold deposition, which was performed at pH 12.

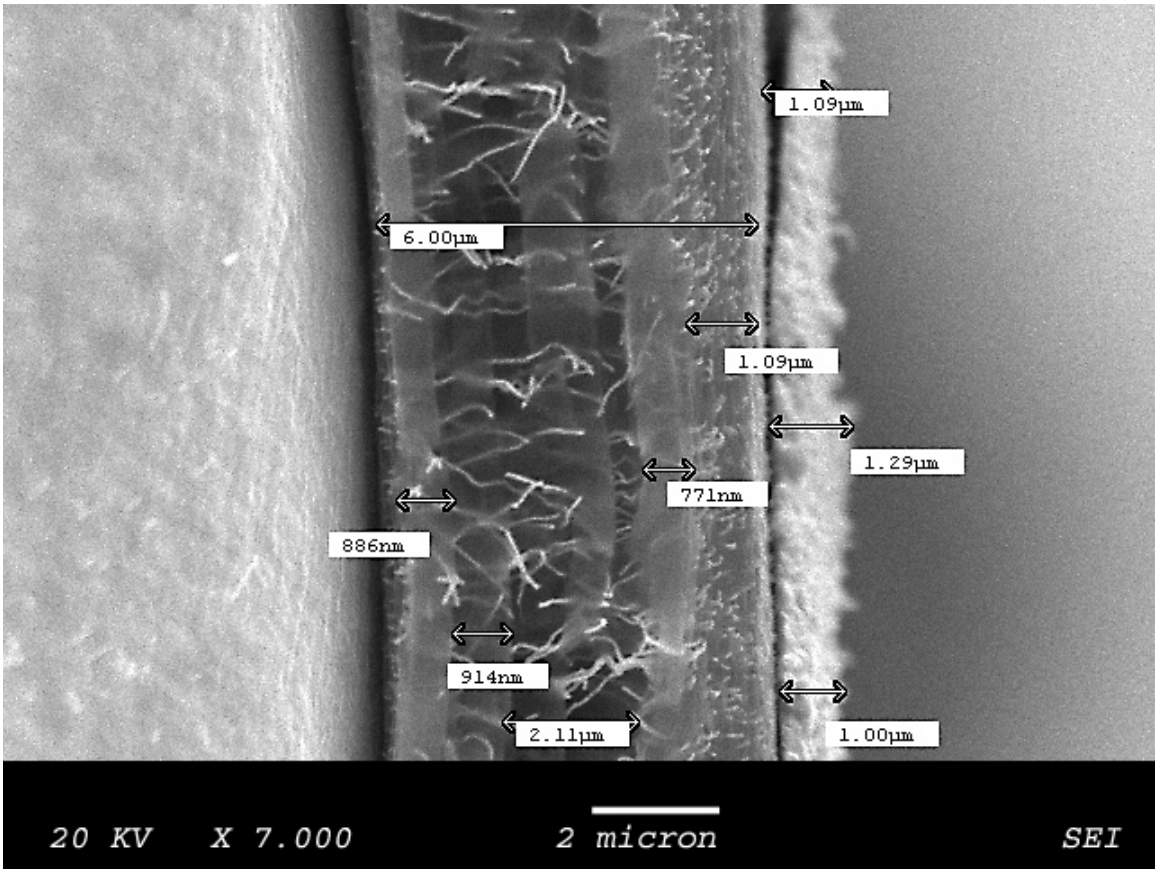

Figure 3.7
SEM imagine of the cross section of the template after gold electroless deposition. Pore diameters of 30nm, the deposition time of 24 hours and pH 12.

This particular view allows us to see the Au-filled pores as well as the two layers of gold on both sides of the membrane, without dissolving the guest membrane. This image clearly shows the nanofibres, grown inside the membrane, are not aligned parallel, but have a considerable angular distribution. This is a consequence of the angles of the original trajectories of the tracks used to sensitise the membrane before etching of the pores. However, in this case, some distortion and artefacts cause apparent whirling and bending of the fibres; this is attributable to possible interactions between the e-beam and the polymer. In fact, after removing the PC guest membrane by dissolution with CH_2Cl_2, straight nanofibres were observed.

3.3 Electrochemical deposition

Electrochemical deposition within a porous membrane requires the pre-coating of one face of the membrane with a metal film (usually *via* ion sputtering or thermal evaporation) and using this metal film as cathode for electroplating. The electrodeposition solution is confined to the bare side of the membrane so that deposition is initiated on the metal film through the pores by applying a constant potential (potentiostatic conditions) or a constant current (galvanostatic conditions). We chose potentiostatic control since it allows a better control of experimental conditions, avoiding undesired processes (e.g hydrogen evolution). For details on the assembly of the electrochemical cell, used by us, see *Chapter 2*.
The filling of the pores by electrochemical deposition of gold, was studied by chronoamperometry (I-t curves). The change in current response during the reduction of Au ions (at a constant applied potential of -1.1 V) is shown in Fig. 3.8.
The deposition current depends on the mass transport conditions and effective surface area of the electrode. The trend of the I-t curves reveals four different steps: I) double layer charging current (stretch A in Fig. 3.8); II) a small, almost constant, current which corresponds to the deposition of gold within the pores; note that this current slightly increases with time as the distance to the pore opening becomes smaller (stretch B in Fig. 3.8); III) a steep current increase characterizes

the 3rd step; this happens when the pores are completely filled so that three-dimensional deposition, on the outer surface, starts. The formation of hemispheric caps on the outer face of the membrane originating from each nanowire (stretch C in Fig.3.8) can indeed be observed; IV) a constant current is finally achieved, which corresponds to the formation of a coherent, planar layer on the entire surface of the membrane: the gold layer can grow only in thickness so that the effective cathode area does not change, and therefore the current tends to a constant value (stretch D in Fig. 3.8).

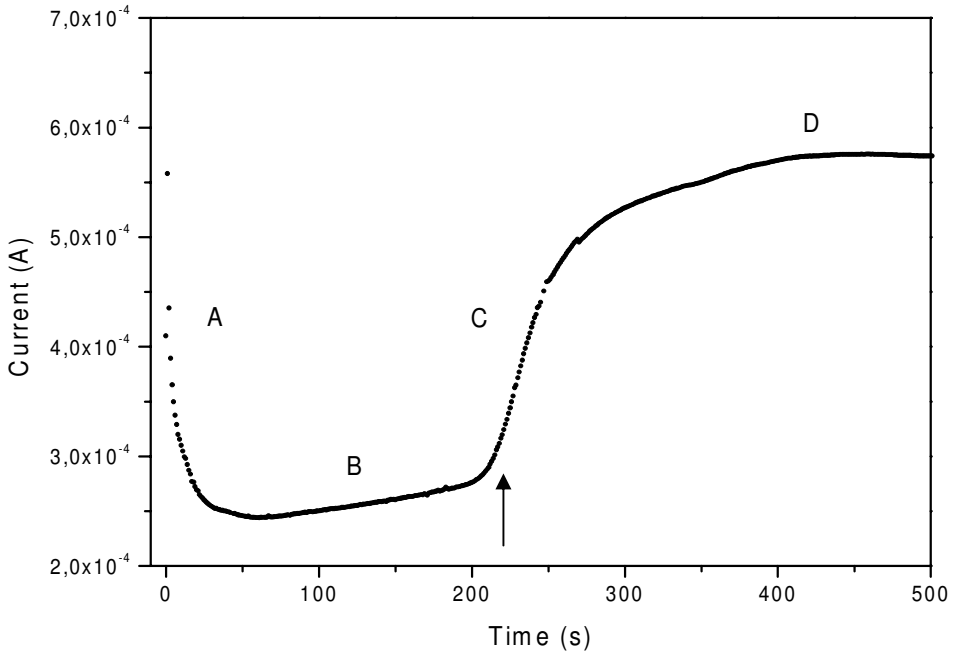

Figure 3.8
Dependence of the electrochemical reduction current on time for the potentiostatic deposition of a metal in a nanoporous membrane. In this current vs time curve four steps are observed: A) double layer charging current; B) slight current increase which corresponds to the pores' filling with gold; C) steep current increase which corresponds to the formation of hemispheric caps; D) constant current which correspond to the formation of a planar layer.

For the present application, that is obtaining NEEs, the electrodeposition process can be stopped when the current reaches a point in the curve (see arrow in Fig.3.8), which indicates that the pores are completely filled but the outer face of the membrane only starts to be coated by an Au-layer.

By stopping the process at this stage and removing mechanically the caps at the top of the nanowires, one should end the preparation thus obtaining the desiderated ensemble of nanodisks.

One problem that was observed by comparing NEEs from different batches as was the scarce reproducibility obtained by this method.

A possible explanation of this observation is that the pores in the membranes are not aligned parallel but have a considerable angular distribution (± 20°) which results in a large length distribution of the pores, so that the pores with different lengths fill up with nanowires at different time. Another possible reason is inhomogeneous growth rates in different pores, due to different degrees of wetting of the pores. The wetting problem tends to be more severe for membranes with smaller pores because of the increased difficulty to wet all the pores before electrodeposition. This can be solved by adding some gelatine to the electroplating solution [11,12]. The process in the presence of gelatine was optimised by us using Cu^{2+} as a model metal ion to be reduced electrochemically. Fig. 3.9 shows that continuous Cu fibres are obtained.

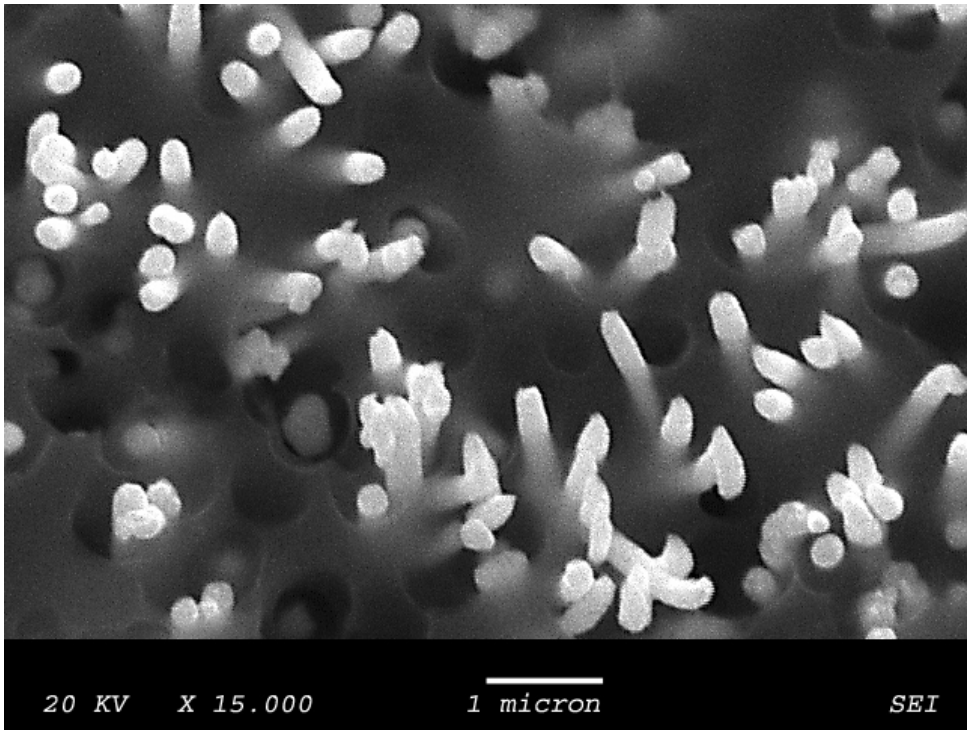

Figure 3.9
SEM images of copper nanowires electrodeposited into the polycarbonate membrane with pores diameter of 200nm. Electrodeposition is stopped between steps B and C (see Fig. 3.8).

However, we found again some difficulties in controlling the surface of the outer face of the plated membrane. If the electrodeposition is continued up to coating the outer face of the template (stretch D in Fig. 3.8), the surface of the metal deposit is so sticky that it is very difficult to remove it by usual methods (peeling with adhesive tape and/or cleaning with ethanol). If the deposition is stopped at the end of the stretch C, beginning of the stretch D in Fig. 3.8, (so avoiding the formation of the outer metal layer) because of the above mentioned different lengths of the pores (related to their wide angular distribution) the extent of filling is too broadly distributed between the different pores. In fact, SEM observations (Fig. 3.10) indicated that some pores are completely filled, others are filled only partially and others present the deposit coming out of the pore-end. This reflects in a complex electrochemical behaviour of these structures when one tries to use them as NEEs.

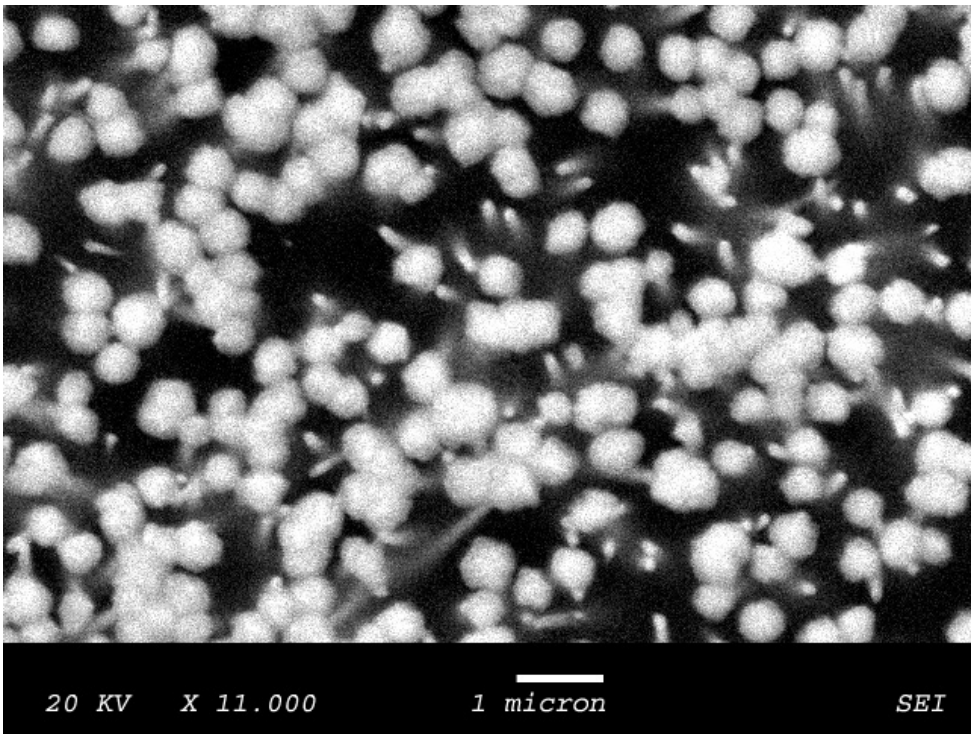

Figure 3.10
SEM imagine of copper nanowires electrodeposited into the polycarbonate membrane with pores diameter of 200nm. Electrodeposition is stopped between steps C and D (see Fig. 3.8)

Fig. 3.11 reports SEM images obtained, again, for gold deposition; in particular, Fig. 3.11/A shows the outer gold coating at the end of the electrodeposition (stretch D in Fig. 3.8). Fig. 3.11/B shows the surface after the removal of the outer Au layers: the surface of the nanodisks emerging from the polycarbonate template, whereas the fading lines behind the nanodisks represent the traces of the nanofibres that grew inside the membrane.

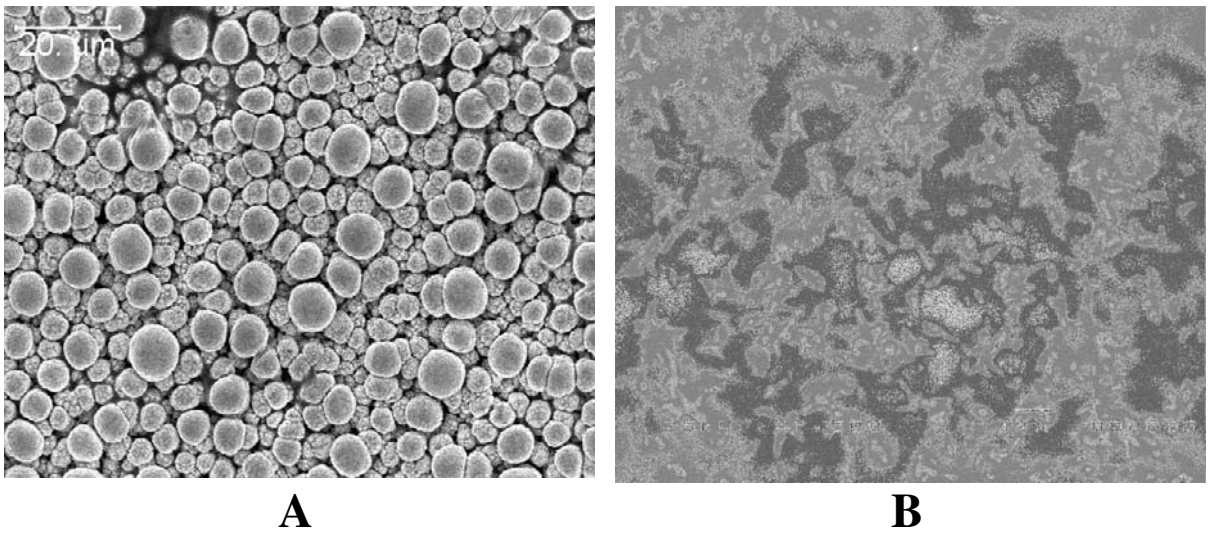

Figure 3.11
SEM images of the template after gold electrochemical deposition before A) removing the outer layer of Au and after B).

The observation of such traces is related to the partial transparency of the polycarbonate template to the electron beam. The electrochemical behaviour of NEEs, obtained by electrochemical deposition, was studied by cyclic voltammetry using as a redox probe, the ferrocene derivative FA^+. However, again, the percentage of NEEs which showed satisfactory behaviour was too low and reproducibility was scarce.

In conclusion, the electrochemical procedure can be considered as a good deposition tool for preparing isolated nanostructures (e.g many fibres), but it does not allow to achieve a reproducibility good enough as the one required for NEEs.

3.4 Protocol for the selection of the NEEs

Obviously to select "good" working NEEs from "bad" working NEEs, it was required to develop a protocol for their selection. This protocol as well as its theoretical basis are described below.

The Faradaic peak current at a NEE operating in the total overlap regime for a reversible redox system obeys the Randles–Sevcik equation [1]:

$$I_p = 2.69 \times 10^5 \, n^{3/2} \, A_{geom} \, D^{1/2} \, C^* \, v^{1/2} \tag{3.1}$$

where I_p is the peak current (A), A_{geom} the overall (nanoelectrodes + insulator between them) geometric area of the ensemble (cm^2), D the diffusion coefficient ($cm^2\ s^{-1}$), C^* the redox species bulk concentration (mol cm^{-3}) and v is the scan rate ($V\ s^{-1}$).

At the same NEE, the double layer charging current (I_c) is proportional only to the area of the electrode elements (active area, A_{act}) [12,13]:

$$I_c = v \, C_{dl} \, A_{act} \tag{3.2}$$

where C_{dl} is the double layer capacitance of the metal nanodisks of the NEE. Typical I_c values for the NEEs used in this work should be around 1 nA (based on a C_{dl} value between 20 and 40μF cm^{-2} [14], a gold NEE with A_{geom} = 0.079 cm^2, pore density = 6×10^8 pore cm^{-2}, average pore radius = 2×10^{-6} cm, scan rate (v) = 0.05 V s^{-1}). From a practical viewpoint, the values given for the Faradaic peak currents and for the double layer charging currents calculated by Eqs. (3.1) and (3.2) can be used to discriminate between "good" and "bad" NEEs, the latter being NEEs with some defect which causes their voltammetric signals to differ from the expected ones. In our laboratory, from a commercial PC microporous membrane of 47 mm diameter, we prepare a rather large number (typically around 30) of NEEs, which are then selected on the basis of the agreement between theoretical and experimental I_p and I_c values.

The latter can be obtained from the cyclic voltammogram recorded in supporting electrolyte alone [1,12] and the former by recording the CV in solution containing a known concentration of a reversible redox probe of known diffusion coefficient. From the CVs with and without the redox probe we select as "good NEEs" those that are characterized by I_p(exp) = I_p(theor) (1±0.2) and I_c(exp) = I_c(theor) (1±0.5), where I_p(exp) and I_c(exp) are the Faradaic peak currents and double layer charging currents measured experimentally, I_p(theor) and I_c(theor) are values calculated by Eqs. (3.1) and (3.2), respectively.

An even more practical way to rapidly distinguish good ensembles from bad ones is the comparison between experimental and digitally simulated CVs. Fig. 3.12 compares experimental voltammograms (dotted and dashed lines) recorded at "good" (part A) and "bad" NEEs (part B) with simulated ones (full line); the redox probe used is (ferrocenylmethyl)-trimethylammonium hexafluorophosphate ($FA^+PF_6^-$), which is characterized by a known reversible electrochemical behaviour [1,15]. For the digital simulations the following parameters were used: E^0 = 0.44 V, k^0 = 0.008 and D =4×10^{-6} cm^2 s^{-1} [16]. Note that k_0 is really the apparent rate constant k^0_{app}; NEEs behave, in fact, as electrodes with a partially blocked surface (PBE). According to the model developed by Amatore et al. [17], the current response at a PBE is identical to that at a bare electrode of the same overall geometric area but with a smaller apparent standard rate constant for the electron transfer which decreases with the porosity of the template membrane. Such an apparent rate constant (k^0_{app}) is related to the true standard charge transfer rate constant (k^0) and the fraction of blocked surface (θ) by the following relationship [17]:

$$k^0_{app} = k^0(1 - \theta) \tag{3.3}$$

Considering that $\theta = (A_{geo} - A_{active})/A_{geo}$ [1], then Eq.(3.3) can be easily converted into

$$k^0_{app} = k^0 f \tag{3.4}$$

For the FA^+ case, k^0 = 0.56 [16] and f = 1.5×10^{-2} [18].

"Good" NEEs should indeed display a satisfactory agreement between experimental and simulated CVs, as shown typically in Fig.3.12/A. The number of NEEs that satisfy this criterion ranges typically from 40 to 70% in a batch of NEEs obtained from just one PC membrane. On the other hand (see Fig. 3.12/B), experimental CVs at "bad" NEEs will differ significantly from the simulated curves. Note that the experimental CVs in this latter figure show the features typical for two kinds of defects which can be produced during the preparation of NEEs. The dotted line voltammogram indicates that this NEE is affected by a large capacitive current, which was probably produced by poor sealing between the nanowires and the surrounding PC insulator and/or by heavy scratches or abrasions of the PC membrane caused by improper handling of the NEE. The poor sealing problem can be solved by heating the NEEs at 150 °C for 30 min [1]. The dashed line voltammogram shows a radial diffusive contribution to the overall signal and a current smaller than the theoretical one. This suggests larger distances between and a smaller number of nanoelectrode elements with respect to expected values, possibly as a consequence of the fact that not all the pores are filled by gold in the final NEE.

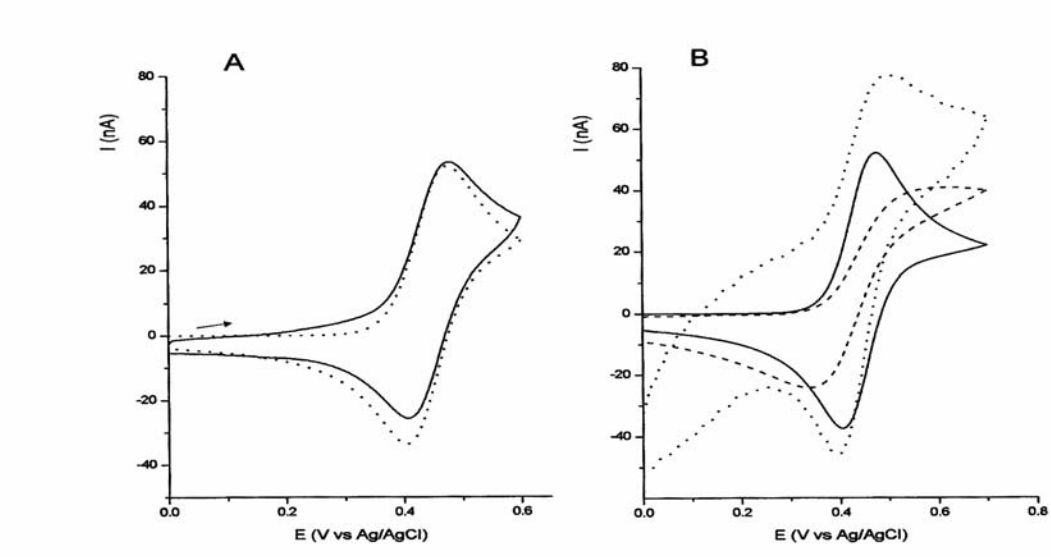

Figure 3.12
Comparison between digital simulations (—) and experimental cyclic voltammograms; the experimental curves refer to: (A) (···) a "good" NEE; (B) (··· and ---) "bad" NEE (for "good" and "bad" definition, see text). Experimental conditions: 10^{-2} M $NaNO_3$, 6 μM (ferrocenylmethyl)-trimethylammonium hexafluorophosphate, A_{geom} = 0.079 cm^2, scan rate 50 mV s^{-1}. Additional parameters used for the digital simulation: E^0 = 0.44 V, k^0 = 0.008 (see text), D = 4x10^{-6} cm^2 s^{-1}

3.5 NEE/SPS as flow detectors

The NEE/SPS are an interesting alternative to the traditional NEE assembly, described above. The NEE/SPS [19, 20] has the advantages of the screen printed electrodes that are low-cost with the possibility to include on the same devices also reference and counter electrode and suitability for analysis of small volume samples and thin layer flow-cells.

In this section, some preliminary results with respect to the use of NEE/SPS as electrochemical detector in flow cells are presented.

At first, tests with a flowing solution containing 10^{-3} M FA^+ as the electroactive probe analyte, were carried out. The analyte solution was constantly pumped through the flow cell by using a syringe pump at a flow rate of 50 μL/min. Fig. 3.13 shows the current signals recorded with time when steps at different potentials were applied to the WE.

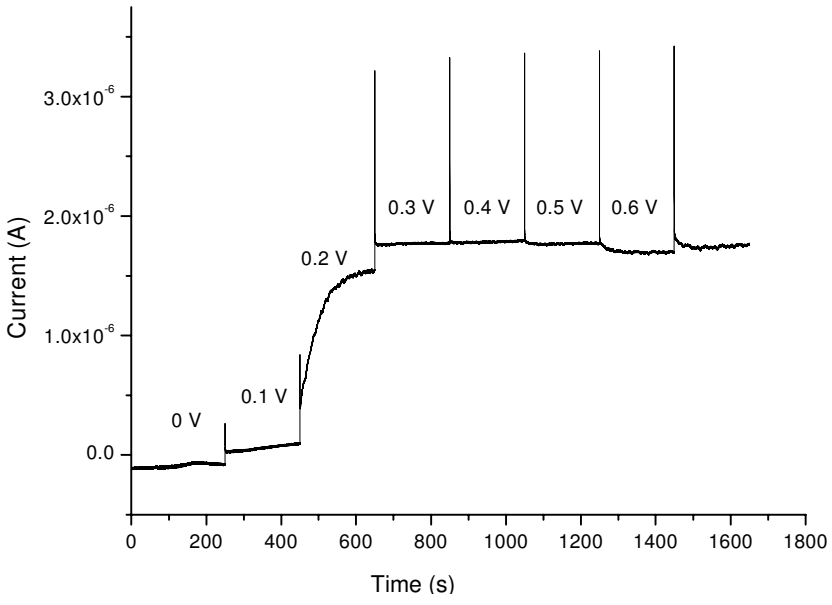

Figure 3.13
Current signal at increasing step potential recorded at a NEE/SPS in a flow cell. Analyte employed was a solution of FA^+ 10^{-4}M in KNO_3 10^{-2}M as supporting electrolyte. Flow rate was 50 μL/min.

At low applied potential only the background current is detected, while for E>0.3 V an almost constant current is detected, which corresponds to the oxidation $FA^{+} \rightarrow FA^{2+} + e^{-}$ under controlled hydrodynamic conditions.

Note that the analyte current is well resolved from the background and also the noise is quite low. This is evidenced by the comparison with Fig. 3.14 obtained under the same experimental conditions using a commercial GC detector.

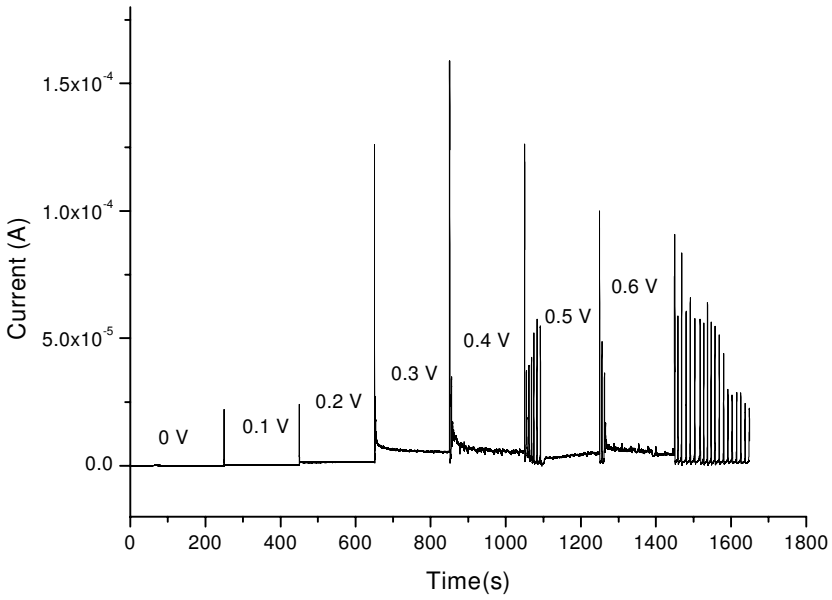

Figure 3.14
Current signal at increasing step potential recorded at a GC macroelectrode in a flow cell. Analyte employed was a solution of FA^{+} 10^{-4}M in KNO_3 10^{-2}M as supporting electrolyte. Flow rate was 50 µL/min.

After these first encouraging results, a more complex detection was used in which the NEE/SPS was functionalised with glucose oxidase. GOx immobilization was used as a model system to test the feasibility of NEE/SPS as flow biosensor. The functionalization of the Au-nanoelectrodes of the NEE/SPS was achieved by producing a thiol SAM on the gold surface followed by covalent attachment of the enzyme.

In particular, the following steps were used:

a) cysteamine (CYS) was assembled on the surface of the Au nanodisks either electrochemically (20 s of 21 mM CYS adsorption at +700 mV vs. RE) or chemically (immersion for 16 hours of the NEE/SPS in a solution of 21 mM CYS);

b) glutaraldehyde (GA) was chosen as a coupling agent; SAM/NEE/SPS was immersed for 1 hour in a 12.5 % v/v solution of GA;

c) a buffered GOx solution (6 mg mL^{-1}) was dropped on GA/SAM/NEE/SPS and left to be covalently attached thanks to the primary amine groups of the enzyme. The non-covalently bound enzyme as well as the excess of GA was easily removed by three-times washing with buffer solution.

The NEE/SPS based biosensors was used as glucose detector in a thin layer flow cell (see Fig. 2.1) exploiting the following reaction sequence:

$$\text{Glucose} + O_2 + GOx_{ox} \rightarrow \text{Glucolactone} + H_2O_2 + GOx_{red} \qquad (3.5)$$

The analyte detected was H_2O_2, which was determined by its electrochemical oxidation at Au-nanoelectrodes. Note that the amount of H_2O_2 generated is directly proportional to the glucose concentration in the sample.

Figure 3.15 shows the response of analyte (circles) and signal/background ratio (squares) at different applied potentials. Each point of the plot corresponds to the injection in a FIA system of 1.0 10^{-3} M glucose. The unmodified NEE/SPS did not respond to glucose, confirming that non-specific oxidation of glucose at the Au surface does not take place. The best signal / noise ratio was achieved for applied potentials between +500 and +600 mV.

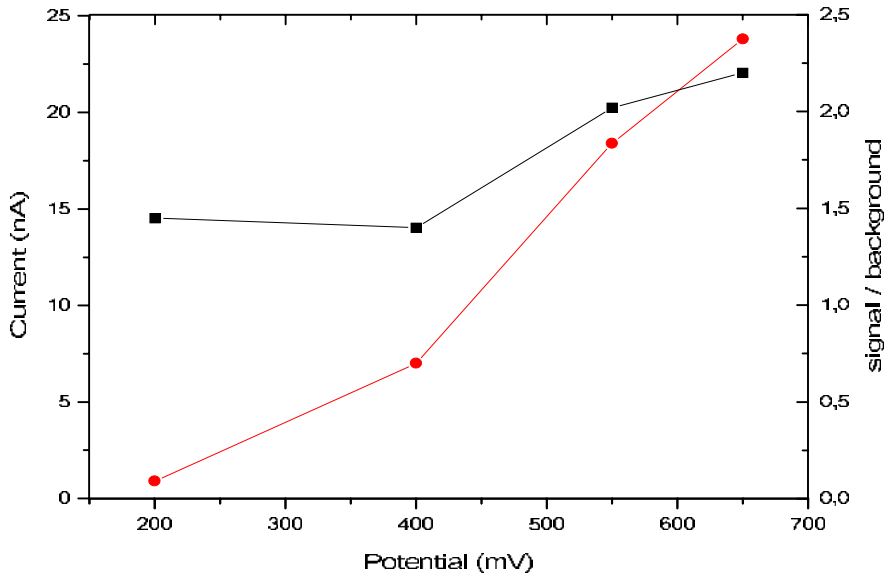

Figure 3.15
Signal to background ratio (black, right Y axis), current (red, left Y axis) as a function of the applied potential; injections of 10^{-3} M glucose in PB solution at pH 6.8 on GOx /SAM/NEE/SPS biosensor; sample loop: 115 µL, flow rate: 0.4 mL min^{-1}

3.5.1 Summary on NEE/SPS

NEE/SPS represent a valid alternative to conventionally assembled NEE and display interesting characteristics when used as flow detectors, in particular with respect to improved resolution of signals. The microscopic reasons behind such improvement in thin layer flow cells cannot be attributed to the lowering of the double layer charging currents as in CV experiments, since here we operated under constant potential. Probably, they are related to a combination of diffusion pathways at the NEE and flow lines under the constrained geometry of a thin layer flow cell .

It is not easy to elucidate this behavior and it would require a specially devoted study of electrochemical hydrodynamics. At the present state of research what is interesting is the experimental observation of such effects and the possibility to exploit them for analytical applications.

3.7 Conclusions

This careful study of the steps involved in the electroless template deposition of gold allowed us to improve the overall process, in particular as far as the reproducibility in the electrochemical behaviour of NEEs is concerned.

Electrochemical deposition can also be used to prepare NEE. In comparison with the electroless method, it has the advantage of being faster, but it has the drawback of requiring a preliminary deposition of a gold layer to make one face of the membrane conductive. This is a critical step which probably determines the rather scarce reproducibility found so far by us with the electrochemical method. For these reasons, in the following of this research, we will use NEEs prepared by the optimised electroless deposition method.

When trying to improve also the steps involved in the final assembly of NEEs, we explored the possibility to assemble the NEE on screen printed substrates. The obtained NEE/SPS seems to represent a valid alternative to NEEs assembled with previous methods, allowing one to include on the same substrate in addition to the NEE also the working and reference electrode.

This assembly has been demonstrated to be useful as electrochemical detectors in flow cells. Actually, in order to explain some peculiarities of the electrochemical responses obtained at NEEs in flow systems deeper investigations are still required. However, from a practical viewpoint it is interesting to note that NEEs lead to improved signals with respect to conventional detectors even under flow conditions.

References

[1] V.P.Menon, C.R.Martin, *Anal. Chem.* **1995**, 67, 1920.

[2] J.D.Klein et al., *Chem. Mater.* **1993**, 5, 902.

[3] C.G.Wu, T.Bein, *Science* **1994**, 264, 1757.

[4] C.R.Martin, *Science* **1994**, 266, 1994.

[5] R.Parthasarathy, C.R:Martin, *Nature* **1994**, 369, 298.

[6] M.Nishizawa, V.P.Menon, C.R.Martin, *Science* **1995**, 268, 1920.

[7] C.J.Brumlik, *V.*P.Menon, C.R.Martin, J.*Mater. Res.* **1994**, 9, 1175.

[8] K.B.Jirage, J.C.Hulteen, C.R.Martin, *Science* **1997***,* 278, 655.

[9] C.A.Foss Jr., G.L.Hornyak, J.A.Stockert, C.R.Martin, *J.Phys.Chem.* **1992***,* 98, 7497.

[10] M.L.Tian, J.Wang, J.Kurtz, T.E.Mallouk, M.H.W.Chan, *Nano Lett.* **2003**, 3, 919.

[11] M.L.Tian, J.Wang, J.Snyder, J.Kurtz, Y.Liu, P.Schiffer, T.E.Mallouk, M.H.W.Chan, *Appl. Phys. Lett.* **2003**, 83, 1620.

[12] A.J.Bard, L.Faulkner, *Electrochemical Methods*, Wiley, New York, **2000**.

[13] R.Greef, R.Peat, L.M.Peter, D.Pletcher, J.Robinson, *Instrumental Methods in Electrochemistry*, Ellis Horwood, Chichester, UK, **1985**.

[14] A.Lombardo, T.I.Bieber, *J. Chem. Educ.* **1983**, 60,1080.

[15] P.Ugo, L.M.Moretto, S.Bellomi, V.P.Menon, C.R.Martin, Anal. Chem. **1996**, 68, 4160.

[16] E.Sabatani, J.Rubinstein, J. *Phys.Chem. B* **1987** 91 6663.

[17] C.Amatore, J.M.Saveant, D.Tessier, *J. Electroanal. Chem*. **1983**, 147, 39.

[18] P.Ugo, N.Pepe, L.M.Moretto, M.Battagliarin, *J. Electroanal. Chem.* **2003**, 51, 560.

[19] *S.*Timur; L.Della Seta, N.Pazarlioglu, R.Pilloton, A.Telefoncu, *Proc. Biochem*. **2004**, 39, 1325.

[20] *MR.*Montereali, W.Vastarella, L.Della Seta, R.Pilloton, *Int. J. Env. Anal. Chem.* **2005**, 85, 795.

4 NEEs for direct trace analysis of iodide

4.1 Introduction

Iodine is a trace element present in seawater and sea products mainly in the form of iodide or iodate anions. For human beings, iodine is an essential component. It is required by the thyroid gland to produce two iodized hormones, thyroxine and triiodothyronine, which are used by the body during metabolism. The most common sources of iodine intake are table salt and seafood, but also other food can contain iodine, such as plants grown in iodine rich soils. However, in certain parts of the world the soil and hence the plants contain no iodine and such a deficiency in the diet can cause health problems [1,2]. Iodine enriched food products, in particular edible salt, are indeed commercialized to complete iodine supply and to avoid dangerous deficiencies. Iodized table salt is, typically, produced by the addition of potassium iodide or iodate to common table salt.

The amount of iodine added to table salt or to other enriched food should be monitored carefully since also excess iodine can be a source of serious health problems [3]. This caution extends also to pharmaceutical products, such as some iodide containing ophthalmic drugs used to contrast cataract [4,5].

The availability of reliable analytical methods to monitor the iodide content in food and drugs plays therefore a key role.

Methods to be applied for such analyses should be characterized by low detection limits, a wide dynamic range and a short response time. Various methods have been proposed to this aim such as spectrophotometry [6], ICP-MS [7], capillary electrophoresis [8,9], ion-chromatography and HPLC [10,11], the latter being probably the most widely used. By taking advantage of the electroactivity of iodide, electrochemical methods have been often applied to this goal. In order to reach low enough detection limits, the preconcentration of the analyte in the form of insoluble salts such as HgI/Hg_2I_2 or AgI was exploited for developing cathodic stripping methods [12–17].

In particular, silver electrodes were applied both for cathodic stripping analyses [18–20] and as electrochemical detector for iodide by ion-chromatography [11,21,22]. More recently, methods based on adsorptive accumulation [23], ion-pairing [24], ion-exchange at electrodes coated with clays [25] and polylysine [26], have been proposed. From the viewpoint of quick analytical control, e.g. in the environment or in foodstuff, direct methods (which could avoid a preconcentration step) might be preferable. It was shown that at low pH values, the electrochemical oxidation of dilute solutions of iodide at Pt [27–30] or Au [31,32] electrodes is reversible, however, at iodide concentrations equal or higher than 1 mM the process is complicated by the formation of adsorbed iodine films. The structure of the adsorbate layer was studied by surface-enhanced Raman spectroscopy on gold electrodes by Weaver and coworkers [33,34]. It was also shown [32] that iodide voltammetric patterns are improved when gold ultramicroelectrodes are used instead of "conventional" millimeter sized electrodes. Further improvements could be expected by an additional miniaturization of the electrode system.

Recent studies [35–39] showed that the use of the so called nanoelectrode ensembles (NEEs) can improve the performances of electrochemical determinations thanks to dramatically improved signal to background current ratios with respect to other electrode systems [39]. NEEs are useful electrochemical tools for biosensor development [40,41], for the measurement of (high) charge transfer rate constants [35] and for solving adsorption related problems [36]. With respect to the latter issue, it was shown that operating in very diluted solutions of the analytes (thanks to the very low detection limits achievable at NEEs) it was possible to obtain diffusion-controlled responses even for molecules such as some phenothiazines [35] or redox proteins such as cytochrome *c* [36], which can adsorb on electrode surfaces.

In the present chapter we examine the use of NEEs for the direct electroanalysis of iodide, focusing in particular on the possibility of performing the direct determination of trace amounts (<1μM) without preconcentration of the analyte. The method developed is applied finally to analyses in real samples such as iodized table salt and iodide containing drugs.

4.2 Cyclic voltammetry of iodide

Fig. 4.1 compares the cyclic voltammograms recorded in sulphuric acid, pH 1.0, at an Au-macro electrode at iodide concentrations in the 50–70 μM range and at a NEE in the 5–7 μM range. The CVs are characterized by an oxidation peak with associated return peak both at the Au-macro and at the NEE. $E_{1/2}$ values, calculated as $(E_{pf} + E_{pb})/2$, where the *f* and *b* subscripts indicate the forward and backward peaks, respectively, were 0.548V at the NEE and 0.524V at the Au-macro; ΔEp values were of the order of 158mV at the NEE and 81mV at the Au-macro (both at 20 mVs^{-1}). The observed peak system corresponds to the electrochemical oxidation of iodide [34] and the following re-reduction in the reverse scan. By lowering the solution pH to 0 (H_2SO_4 1M) at both electrode systems, $E_{1/2}$ values shift slightly to less positive values being $E_{1/2}$ = 0.520 V at the NEE and 0.490 V at the Au-macro, respectively.

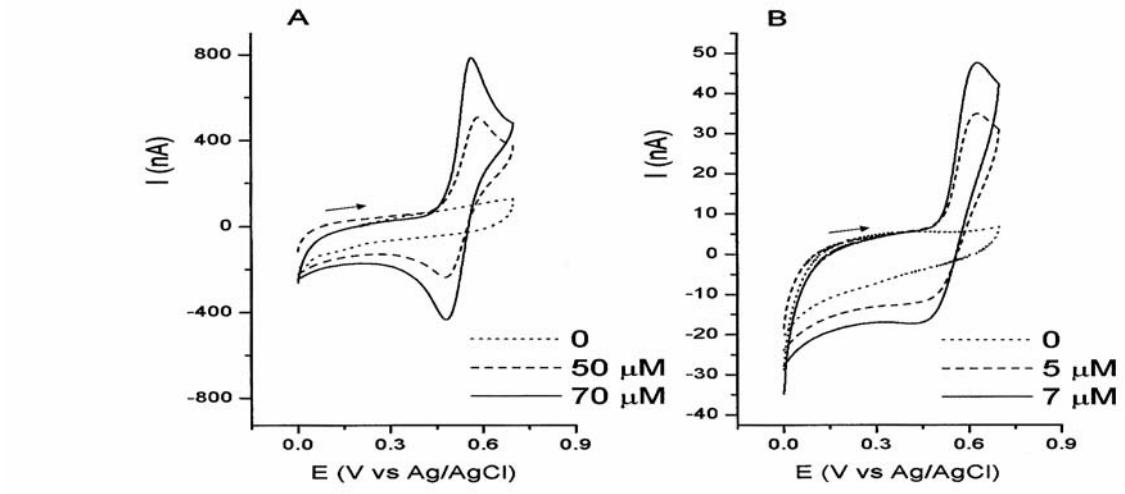

Figure 4.1
Cyclic voltammograms recorded at different KI concentrations in sulphuric acid, pH 1.0: (A) at Au-macro electrode; (B) at a NEE. KI concentrations as indicated in the figure; scan rate 20 mV s^{-1}, initial potential 0 V, vertex potential 0.7 V.

As shown in Fig. 4.1, even if the I^- concentration for the NEE measurements is one order of magnitude lower than at the Au-macro, the ratio between Faradaic (peak) currents and background currents is roughly comparable, in agreement with the

lowering of capacitive (background) current which characterizes NEEs' responses [38,39]. At NEEs operating under total overlap diffusion conditions, capacitive currents scale with the active area (metal surface of the nanodisks electrodes) while the Faradaic current scales with the overall geometric area of the ensemble [37]; at the Au-macro both currents increase linearly with the geometric area [42].

As shown in Fig. 4.2, at the NEE, peak currents depend linearly on the square root of the scan rate, thus indicating a process controlled by semi-infinite linear diffusion (typical for a NEE operating under total overlap conditions [39]). The same trend is observed at the Au-macro (not shown).

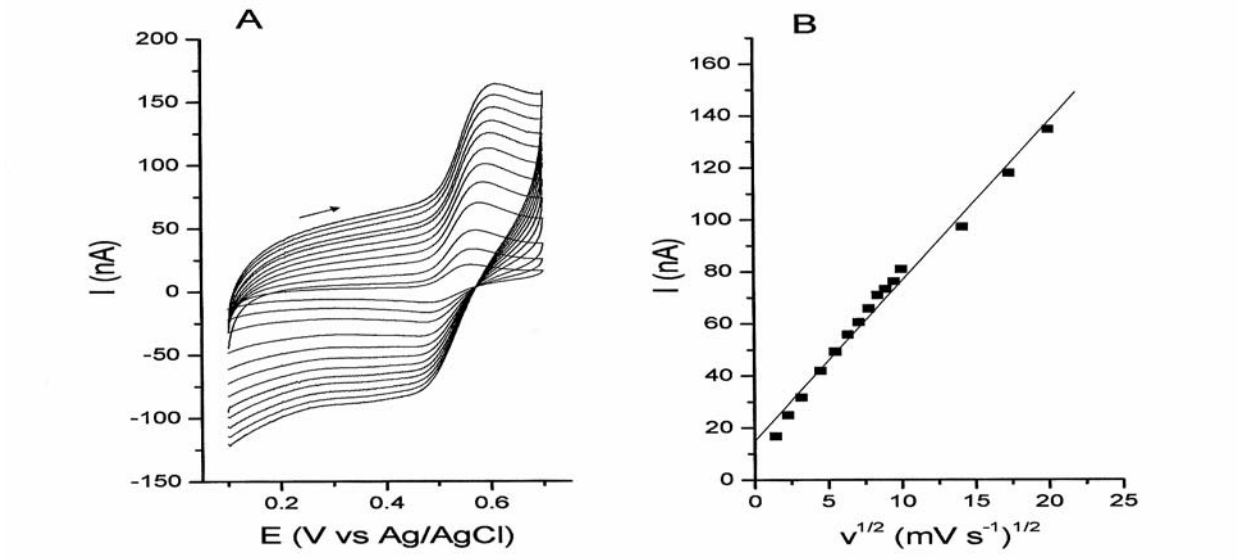

Figure 4.2
(A) Cyclic voltammograms recorded at different scan rates (from 2 to 100 mV s^{-1}) at a NEE in 5 µM KI; (B) peak current dependence on the square root of the scan rate. Other conditions as in Fig. 4.1

Relevant voltammetric parameters measured at different scan rates at both kinds of electrodes in 1M H_2SO_4, are listed in Table 4.1. These data show that, at both kinds of electrodes, ΔEp values increase with the scan rate. This might indicate a quasi-reversible electron transfer process, however, $E_{1/2}$ values shift towards more positive potentials with increasing scan rate thus indicating the involvement of a more complex mechanism. Similar trends, however with proper adjustment in $E_{1/2}$ values (see above), are observed in 0.1M H_2SO_4.

It is known, indeed, that iodide oxidation occurs via many steps in which adsorption–desorption processes are involved; this was studied in detail for Pt electrodes [27–30] and for gold electrodes as well [31–34]. For the latter case, it was shown by Weaver and coworkers [34] that iodide electroxidation follows the pathway (where "*ads*" refers to an adsorbed species):

$$2I^- (sol) + I^- (ads) \rightarrow I_3^- (ads) + 2e \quad (4.1)$$

$$2I^- (sol) + I_3^- (ads) \rightarrow I_5^- (ads) + 2e \quad (4.2)$$

and/or

$$2I^- (sol) + I^- (ads) \rightarrow I_2 \cdots I^- (ads) + 2e \quad (4.3)$$

followed by

$$I_5^- (ads) \rightarrow I_2 (sol) + I_3^- (ads) \quad (4.4)$$

and/or

$$I_2 \cdots I^- (ads) \rightarrow I_2 (sol) + I^- (ads) \quad (4.5)$$

The electron transfer is indeed coupled with a series of chemical reactions involving both adsorbed and solution species. Increasing the scan rate causes a shift towards more positive potentials which could be related to the lower effect of the kinetics of the following chemical reactions (4.4) and (4.5) [42].

	E_{pf} (mV)		E_{pb} (mV)		ΔE_p (mV)		$E_{1/2}$ (mV)	
V (mVs^{-1})	NEE	Au-macro	NEE	Au-macro	NEE	Au-macro	NEE	Au-macro
5	564	528	489	460	75	68	526	494
10	569	531	487	461	82	70	528	496
20	576	536	483	454	93	82	530	495
50	590	546	480	450	110	96	535	498
100	606	556	473	443	133	113	540	500
200	620	571	470	431	150	140	545	501
500	616	597	468	418	148	179	542	508

Table 4.1
Cyclic voltammetric parameters at different scan rates (v) at a NEE in 5 µM KI, and at an Au-macro in 100 µM KI; supporting electrolyte 1M H_2SO_4

The slightly larger ΔEp values observed at NEEs, correspond anyway to the fact that the charge transfer at such nanoelectrode systems becomes apparently slower than at the Au-macro, since they behave like PBE (see Chapter 3).

Fig. 4.3 reports the concentration dependence and relevant calibration plot for the CVs recorded at NEEs at 20 mVs^{-1}. The dynamic range extends over two orders of magnitude with a sensitivity (m, slope of the calibration plot) of 30 nA cm^{-2} μM.

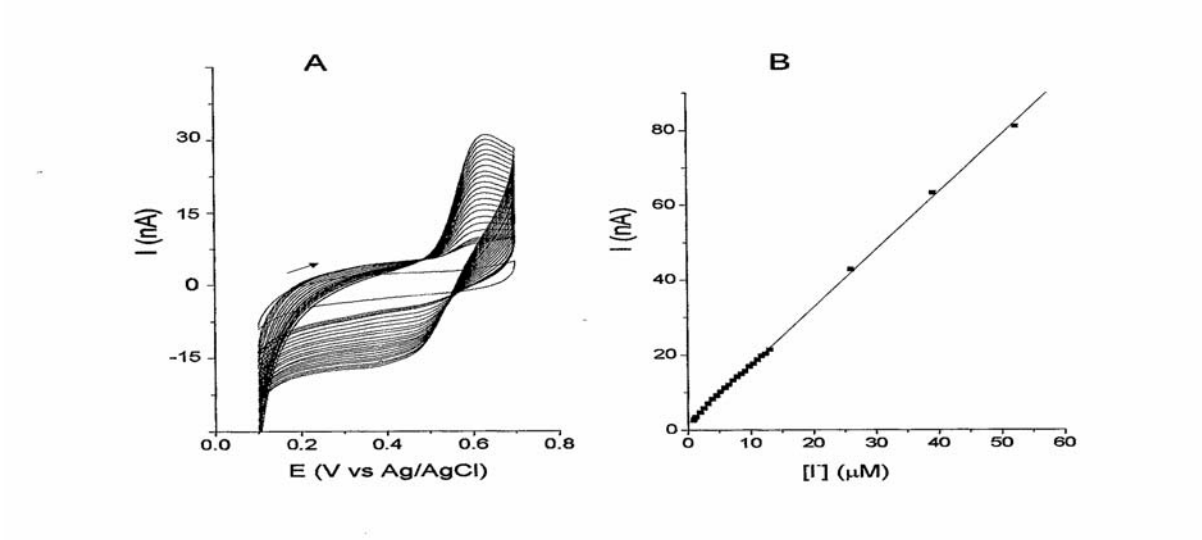

Figure 4.3
(A) Cyclic voltammograms recorded at 20 mV s^{-1} at a NEE in sulphuric acid, pH 1.0, at increasing KI concentrations (blank and then from 0.7 to 10 μM); (B) calibration plot

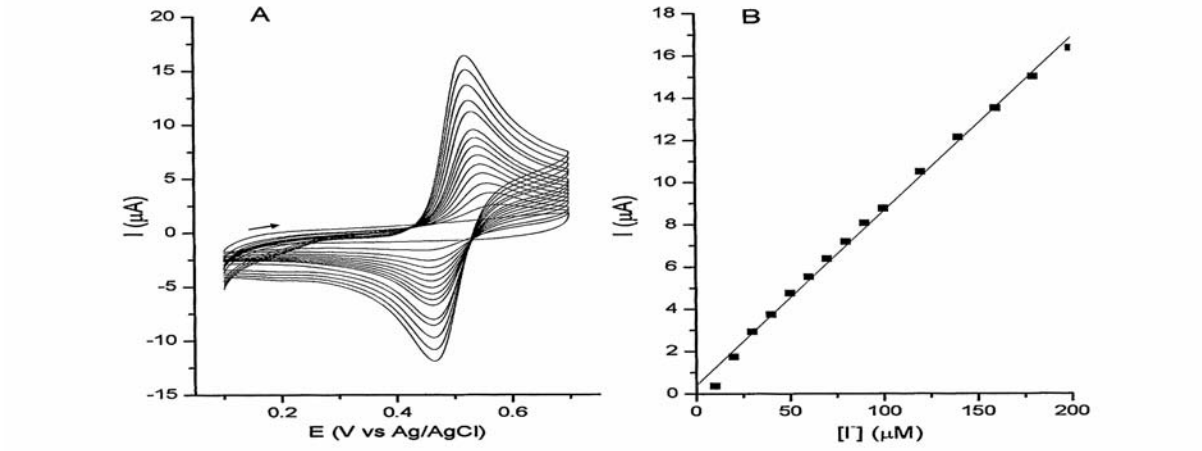

Figure 4.4
(A) Cyclic voltammograms recorded at 20 mV s^{-1} at an Au-macro electrode in sulphuric acid, pH 1.0, at increasing KI concentrations (blank and then from 20 to 200 μM); (B) calibration plot

Replicate measurements of the blank current at 570mV gave a blank standard deviation σ_b of 0.03 nA, from which a detection limit (DL = $3\sigma_b/m$) of 0.3 μM was obtained. Such a DL is almost one order of magnitude lower than the best literature value at gold ultramicroelectrodes [32]. Note also that data obtained by us at the Au-macro (see Fig. 4.4) is 4 μM, which is more than one order of magnitude higher than the DL at NEEs. A relative precision of ±2% was evaluated from the standard deviation of 15 repeated measurements at the same NEE dipped in a 5 μM KI solution in sulphuric acid, pH 1.0 and the reproducibility of voltammetric signals (in the same solution) within a batch of 10 different NEEs was ±10%. No preconcentration of iodide was employed in all these analyses.

4.3 Electroanalysis in real samples

The above-developed method was tested for direct determination of iodide in two kinds of real samples: ophthalmic drugs and edible salt. For the first application, the iodide content in two pharmaceutical preparations, namely Facovit and Rubjovit which are used for cataract therapy, was determined. To this aim, after recording a blank in sulphuric acid, pH 1.0, a small volume (see Chapter 2) of the Facovit drug was added and the voltammetric scan performed.

As shown in Fig. 4.5/A, a peak is observed at approximately 0.620 V, whose current increases with standard additions of KI. From the standard additions plot (see Fig. 4.5/B), the concentration of iodide in the electrochemical cell (before the standard additions) was determined to be 1.9 μM. Three repeated analyses of the sample indicate that the average iodide concentration determined with the NEE was 1.9±0.1 μM; by taking into account sample dilution this agreed within 94.6% with the value expected on the basis of the iodide content declared by the producer, and within 98.4% with the result of a Volhard titration [43] performed in an undiluted sample of the drug. Fully comparable results (not shown) with similar agreement between measured and declared iodide contents were obtained also for the other drug examined, namely Rubjovit, notwithstanding the different compositions of the two drugs examined.

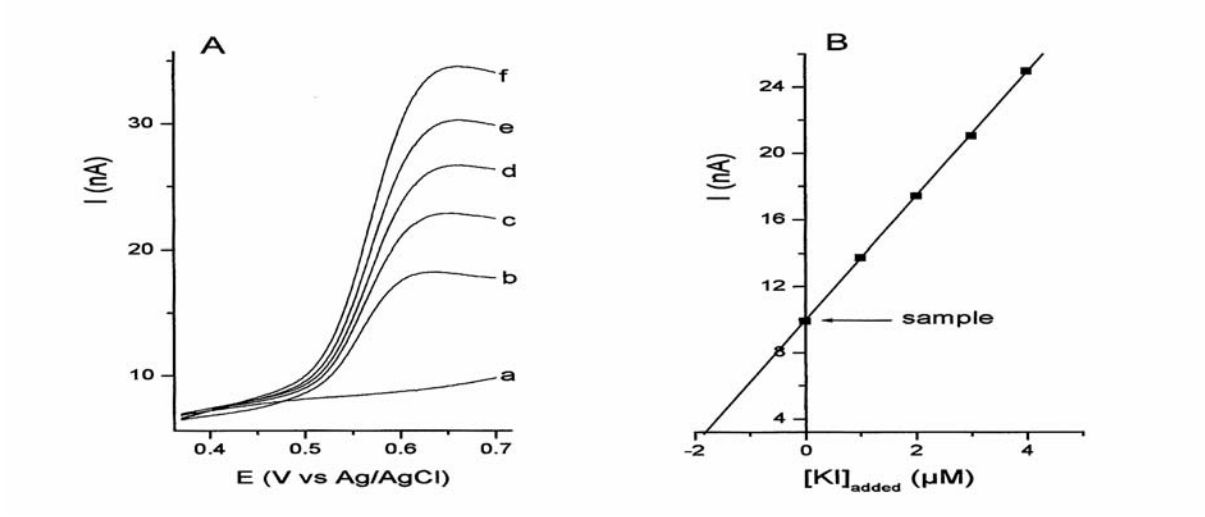

•

Figure 4.5
(A) Linear sweep voltammograms recorded at 20 mV s^{-1} at a NEE in: a) sulphuric acid, pH 1.0 (blank, 20mL); b) spiked with 35 µL of Facovit (pre-diluted 1:10) and after standard additions of KI: (c) 1 µM; (d) 2 µM; (e) 3 µM; (f) 4 µM. (B) Standard additions plot.

The second application concerned the determination of iodide in iodized table salt. As shown by the CVs in Fig. 4.6/A, the voltammetric oxidation of I^- in this kind of sample is slightly less reversible than in the previous ones (synthetic as well as pharmaceutical samples), however an oxidation peak is detected, whose current is proportional to the overall iodide content in the sample (see standard addition plot in Fig. 4.6/B). At the dilution value used by us (namely, [NaCl] ~0.08 M) no interference from chloride was observed.

The iodide concentration in the electrochemical cell, determined from triplicate analyses, was 1.6±0.3 µM. This value is smaller, but in acceptable agreement with the values of 2.1 µM calculated from the iodide contents declared by the producer.

Note that the iodine content declared for this kind of products is rather indicative; the initial amount of added iodide can, in fact, be lowered during storage as a consequence of partial volatilization following spontaneous oxidation of iodide to iodine [4,44].

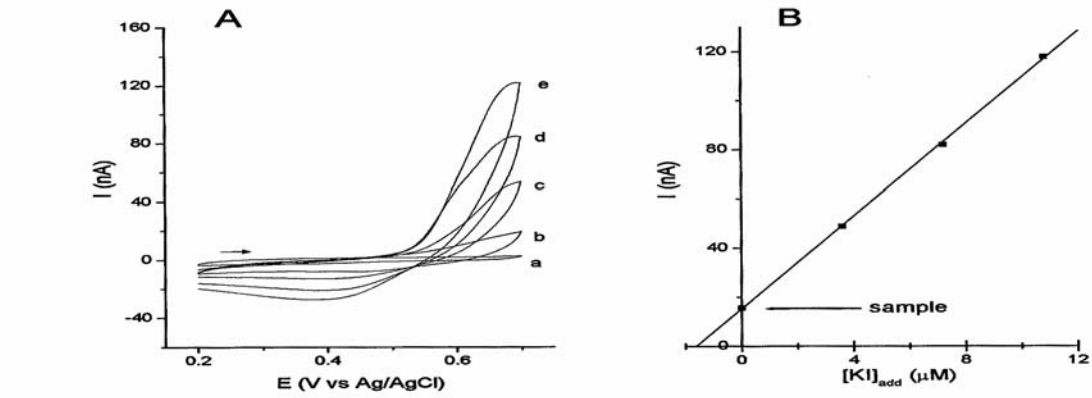

•

Figure 4.6
(A) Linear sweep voltammograms recorded at 20 mV s^{-1} at a NEE in: a) sulphuric acid, pH 1.0 (blank, 20mL); b) spiked with 400 µL of iodized table salt solution (234 g L^{-1}) and after standard additions of KI: (c) 3.5 µM; (d) 7.0 µM; (e) 10.5 µM. (B) Standard additions plot.

The lower electrochemical reversibility of the CVs in these salt samples is probably due to other components, such as anticaking agents [45], which can be present in this rather complex sample. Anyway, the slight flattening of the peak currents does not prevent from performing quantitative determinations, if the standard additions method is used.

4.4 Conclusions

Iodide is oxidised electrochemically both at gold macroelectrodes and at ensembles of gold nanodisk electrodes. The detection limits are 0.3 μM at NEEs and 4 μM at Au-macro electrodes. Such an improvement in detection limits at NEEs, although relevant, is not as dramatic as in other applications, described previously [36,37,39]. This is related to the fact that iodide is an analyte difficult to determine at NEEs, since its oxidation takes place at potential values quite close to the oxidation limit of the potential window accessible with this kind of nanoelectrodes [39]. Note that such an increase in DL for species which are electroactive at potentials approaching the limit of the accessible potential window, was observed before, however for the case of reduction processes [35].

In any case, the results presented here show that the use of gold NEEs allows the direct determination of micromolar and even submicromolar concentrations of iodide by simple cyclic voltammetry, without requiring any preceding preconcentration of the analyte. This direct method of analysis can be applied successfully to the determination of iodide in pharmaceutical products and iodized edible salt.

References

[1] P.Pongpaew, S.Saowakontha, R.Tungtrongchitr, U.Mahaweerawat, F.P.Schelp, *Nutr. Res.* **2002**, 22, 137.

[2] F.Delange, B.de Benoist, D.Alnwick, *Thyroid* **2001**, 11, 437.

[3] F.Delange, B.de Benoist, D.Alnwick, *Thyroid* **1999**, 9, 545.

[4] K.Muranov, N.Poliansky, R.Winkler, G.Riegerm, O.Schmut, J.Horwat-Winter, *Graefes Arch. Clin. Exp. Ophthalmol.* **2004**, 242, 146.

[5] E.F.Elstner, R.Adamczyk, A.Furch, R.Kroner, *Ophthalmic Res.* **1985**, 17, 302.

[6] J.L.Lambert, G.L.Hatch, B.Mosier, *Anal. Chem.* **1975**, 47, 915.

[7] M.Haldimann, B.Zimmerh, C.Als, H.Gerber, *Clin. Chem.* **1998**, 44, 817.

[8] K.Ito, T.Ichihara, H.Zhuo, K.Kumamoto, A.R.Timerbaev, T.Hirokawa, *Anal. Chim. Acta* **2003**, 497, 67.

[9] K.Yokota, K.Fukushi, S.Takeda, S.I.Wakida, *J. Chromatogr.* A **2004**, 1005, 145.

[10] G.T.Wong, P.G.Brewer, *Anal. Chim. Acta* **1976**, 81, 81.

[11] K.Ito, *J. Chromatogr. A* **1999**, 830, 211.

[12] W.Kemula, Z.Kublik, J.Taranszewski, *Microchem. J. Symp. Ser.* **1962**, 2.

[13] J.Perchard, M.Buvet, R.Molina, *J.Electroanal. Chem.* **1967**, 14, 57.

[14] R.C.Propst, *Anal. Chem.* **1977**, 49, 1199.

[15] K.Z.Brainina, Fresenius Z. *Anal. Chem.* **1982**, 312, 428.

[16] G.W.Luther, C.B.Swartz, W.J.Ullman, *Anal. Chem.* **1988**, 60, 1721.

[17] L.Rong, T.Takeuchi, *J. Chromotogr.* A **2004**, 1042, 131.

[18] I.Shain, S.P.Perone, *Anal. Chem.* **1961**, 33, 325.

[19] T.Nomura, T.Mimatsu, *Anal. Chim. Acta* **1982**, 143, 237.

[20] T.Nomura, M.Watanabe, T.S.West, *Anal. Chim. Acta* **1985**, 175, 107.

[21] R.D.Rocklin, E.J.Johnson, *Anal. Chem.* **1983**, 55, 4.

[22] L.Liang, Y.Cai, S.Mou, J.Cheng, *J. Chromatogr. A* **2005**, 1085, 37.

[23] L.Guangam, Y.Min, Z.Qifang, W.Ailan, J.Zexiang, *Electroanalysis* **1995**, 7, 591.

[24] I.Svancara, J.Konvalina, K.Schachl, K.Kalcher, K.Vytras, *Electroanalysis* **1998**, 10, 435.

[25] A.Walcarius, G.Lefevre, J.-P.Rapin, G.Renaudin, M.Francois, *Electroanalysis* **2001**, 13, 313.

[26] F.C.Pereira, A.G.Fogg, P.Ugo, E.P.Bergamo, N.R.Stradiotto, M.V.B.Zanoni, *Electroanalysis* **2005**, 17, 1309.

[27] CR.A.Osteryoung, F.C.Anson, *Anal. Chem*. **1964**, 36, 975.

[28] A.T.Hubbard, R.A.Osteryoung, F.C. Anson, *Anal. Chem*. **1966**, 38, 692.

[29] E.C.Toren, C.P.Driscoll, *Anal. Chem*. **1966**, 38, 873.

[30] S.Swathirajan, S.Bruckenstein, *J. Electroanal. Chem*. **1980**,112, 25.

[31] T.Bejerano, E.Gileadi, J. *Electroanal. Chem*. **1977**, 82, 209.

[32] W.Zhang, H.Zha, B.Yao, C.Zhang, X.Zhou, S.Zhong, *Talanta* **1998**, 46, 711.

[33] P.Gao, M.J.Weaver, *J. Phys. Chem*. **1986**, 90, 4057.

[34] M.A.Tadayyoni, P.Gao, M.J.Weaver, *J. Electroanal. Chem*. **1986**, 198, 125.

[35] B.Brunetti, P.Ugo, L.M.Moretto, C.R.Martin, *J. Electroanal. Chem*. **2000**, 491, 166.

[36] P.Ugo, N.Pepe, L.M.Moretto, M.Battagliarin, *J. Electroanal. Chem*. **2003**, 560, 51.

[37] L.M.Moretto, N.Pepe, P.Ugo, *Talanta* **2003**, 62, 1055.

[38] P.Ugo, L.M.Moretto, F.Vezzà, *Chemphyschem* **2002**, 3, 917.

[39] V.P.Menon, C.R.Martin, *Anal. Chem*. **1995**, 67, 1920.

[40] M.Delvaux, S.Demoustier-Champagne, A.Walcarius, *Electroanalysis* **2004**, 16, 190.

[41] M.Delvaux, A.Walcarius, S.Demoustier-Champagne, *Biosens. Bioelectron*. **2005**, 20, 1587.

[42] A.J.Bard, L.Faulkner, *Electrochemical Methods*, Wiley, New York, **2000**.

[43] A.I.Vogel, *A Textbook of Quantitative Inorganic Analysis*, 3rd ed., Longman, London, UK, **1961**, p. 267.

[44] I.Svancara, B.Ogorevc, K.Vytras, *Anal.Bioanal.Chem*. **2002**, 372, 795.

[45] J.Holman, *Boletin de la Oficina Sanitaria Panamericana*, Febrero **1966**, 139.

5 3D-ensembles of gold nanowires

5.1 Introduction

In the present chapter, we examine in detail the use of NEEs as electrochemical detectors for mediated biosensors. From this viewpoint, NEEs made of ensembles of nanodisk electrodes suffer from the fact that the electrode surface useful for immobilizing mediators and/or enzymes (i.e. the active area) is very limited. For this reason, a different NEE fabrication procedure in which the nanodisk electrode elements are substituted by short nanofibre elements is proposed. To this aim, the surface of "classical" NEEs, made of gold nanodisks imbedded in the polycarbonate template, is treated with oxygen plasma or with solvent mixtures in order to achieve controlled etching of part of the polycarbonate of the template membrane. This causes the structure of the final ensemble to change from a 2-D flat structure into a 3-D one, in which a "forest" of gold nanowires protrudes from the polycarbonate insulating layer.

In order to investigate the electrochemical behavior at 3D-NEEs, cyclic voltammetric analysis of diffusing redox species, characterized by fast or slow electron transfer kinetics, as well as of redox probes adsorbed on the gold surfaces, were performed. Finally, in order to get preliminary information about the possible use of 3D-NEEs for biosensors development, we studied voltammetric responses of an electrocatalytic chain composed by an adsorbed redox mediator, NADH and glucose dehydrogenase.

5.2 Etching process: 3D-NEEs

At first, we critically compared and optimized the two etching procedures, i.e. oxygen-plasma [6] vs. chemical etching [9]. Fig. 5.1 reports scanning electron micrographs (SEM) of the surface of the NEEs before (Fig. 5.1/A) and after controlled etching with O_2 plasma (Fig. 5.1/B) and with CH_2Cl_2/C_2H_5OH (Fig. 5.1/C).

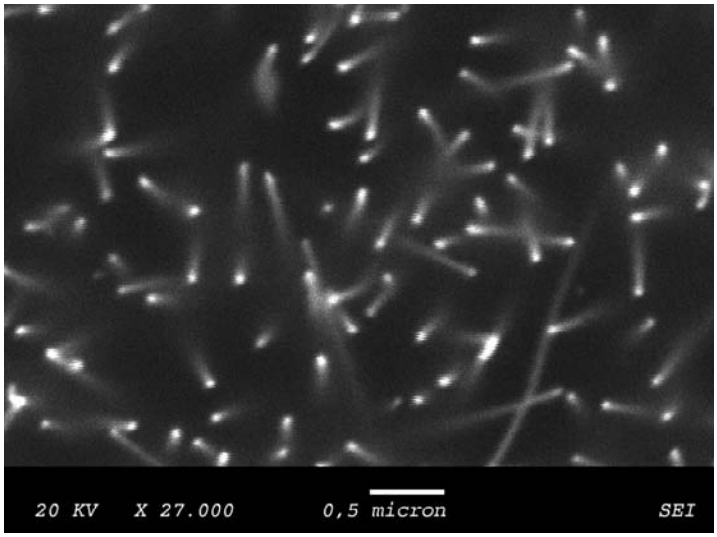

A

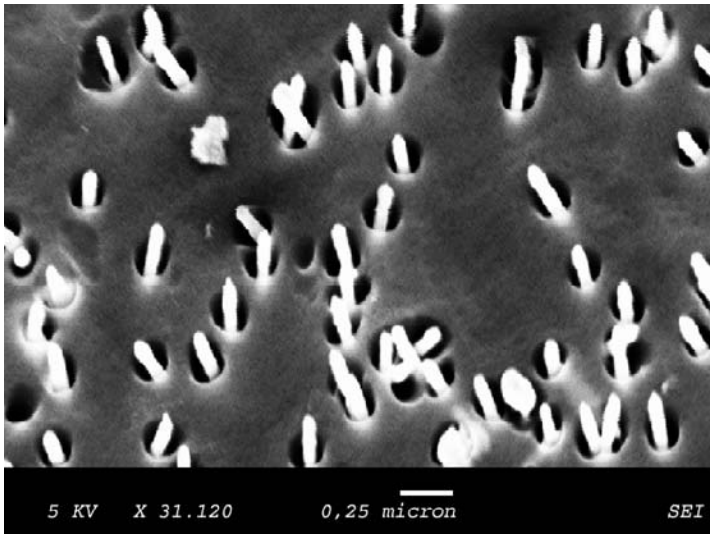

B

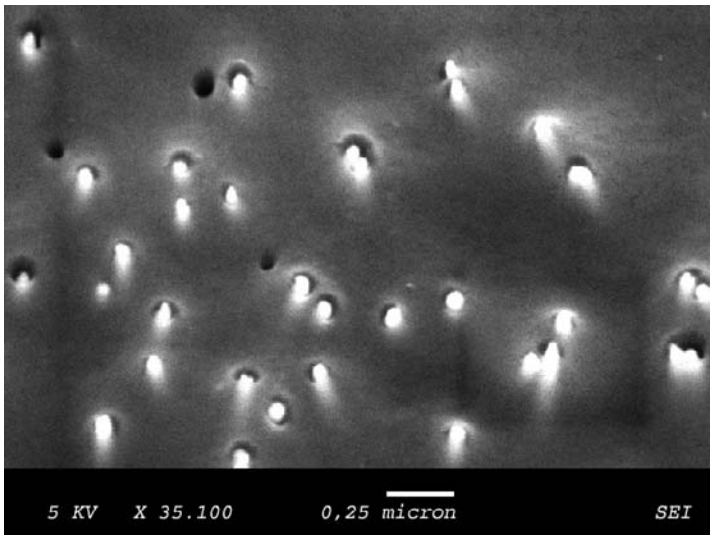

C

Figure 5.1
SEM (A) and FE-SEM (B,C) images of a NEE : A) after gold electroless deposition and peeling the gold from the outer face of the membrane; B) after etching with O_2/Ar plasma for 30 seconds; C) after chemical etching with 1:9 CH_2Cl_2/C_2H_5OH for 5 seconds.

The heads of the fibres, which appear in Fig. 5.1/B, indicate that the use of O_2 plasma leads to the successful removal of the external layer of the PC membrane.

Preliminary results indicated that 30 seconds etching time is enough for exposing the fibres to a length of about 200 nm, which is a length suitable for the fabrication of 3D-NEEs sensors.

However, SEM images show that rather large holes were created around the gold nanowires, probably caused by high local heating of the fibres during the plasma etching process. This has been described previously by Martin et al. [6] who reported also the progressive shrinking of the NEE with increasing etching time as a consequence of plasma–induced heating of the membrane.

The presence of the holes around the fibres is undesirable from an electrochemical viewpoint, since it breaks the sealing between the gold nanofibres and the PC membrane. This limits dramatically the possibility to use plasma etched NEEs for electrochemical studies because of the big uncertainty and difficulty in controlling the total active area of the ensemble.

Typical 3D-NEEs obtained after the chemical etching are shown in Fig. 5.1/C. The removal of the outer PC layers by dilute CH_2Cl_2 is quite homogenous, equally affecting the whole observed surface. Some slits are still present around the fibres, however, they are much smaller compared to those observed after plasma etching. Heating of the chemically etched 3D-NEEs at temperatures higher than the PC glass transition temperature (150°C) further decreased the dimensions of these small slits below the resolution limit of the SEM images.

Fig. 5.2 shows the cyclic voltammograms (CV) recorded in pure supporting electrolyte at 100 mV/s with NEEs before (curve A) and after chemical etching, using different etching times (curves B-D). From these voltammograms, increments in double layer charging currents due to etching can be easily calculated by known methods (see reference [13]).

Data listed in the first line of Table 5.1, show that these increments scale with the etching time, as expected on the basis of equation (5.1), which correlates double layer charging current with the active area of NEEs [1, 14]:

$$i_C = v \cdot C_{dl} \cdot A_{act} \qquad (5.1)$$

where C_{dl} is the double layer capacitance of gold and v is the scan rate.

Background CVs of plasma etched NEEs (not shown) point out a much larger increase in capacitive current, that is approximately 3-times larger than the value expected on the basis of the length of the Au nanofibres protruding out of the PC surface after etching (see Fig. 5.1/B). The large disagreement between experimental and expected data for plasma etched NEEs confirms the difficulty to achieve full control of the active area by this etching method. For this reason, only chemical etching was used in the following experiments to prepare 3D-NEEs with well controlled active area.

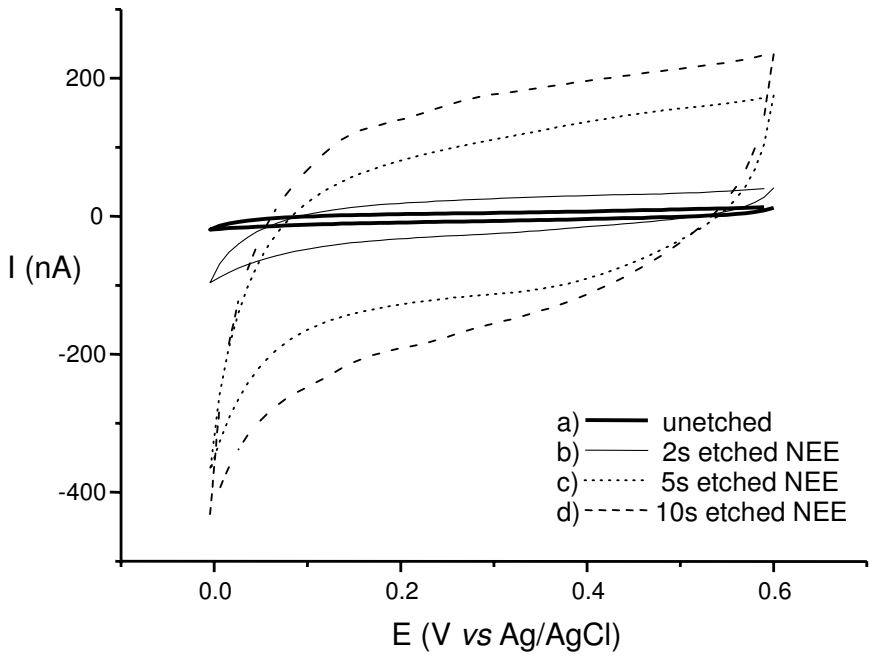

Figure 5.2
Background CVs in 1 mM KNO_3 recorded at 100 mV/s: a) with an unetched NEE and with NEEs etched with 1:9 CH_2Cl_2/C_2H_5OH for 2 seconds (b), 5 seconds (c), 10 seconds (d).

	ETCHING TIME		
	2 seconds	**5 seconds**	**10 seconds**
Increase of capacitive current (i_C)	8 times	25 times	45 times
Increase of faradaic current (i_F)	0.9 times	0.9 times	0.9 times

Table 5.1
Dependence on the etching time (in 1:9 CH_2Cl_2/C_2H_5OH) for the increase in double layer charging current and faradaic peak current, obtained from the CVs in Fig. 2 and 3, respectively, with respect to CVs recorded at unetched NEEs

5.2.1 Electrochemical behaviour at 3D-NEEs

Since the main goal of this work was the detailed understanding of the factors influencing voltammetric responses at 3D-NEEs, a comparison of signals obtained using redox species characterized by fast and slow heterogeneous electron transfer kinetics respectively was performed. FA^+ was chosen as a typical water soluble redox probe characterized by fast heterogeneous electron transfer kinetics [1, 2, 15]. Fig. 5.3/A shows the CVs recorded in the same 10 μM FA^+ solution, using three different NEEs before chemical etching.

Peak shaped voltammograms are obtained with features in agreement with previous CVs recorded at 2D-NEEs operating under total overlap conditions [1,2,16]; the similarity between the three CV patterns obtained at three different NEEs confirms a very satisfactory reproducibility in the preparation procedure. Fig. 5.3/B shows the CVs recorded in the same solution, but using 3D-NEEs etched in CH_2Cl_2-C_2H_5OH for 2, 5 and 10 seconds.

These CVs, together with the relevant data listed in Table 5.1, indicate that faradaic peak currents are practically uninfluenced by the etching process, while double layer capacitive currents are. Both at unetched and etched NEEs, peak currents for FA^+ oxidation increase linearly with the square root of the scan rate, the slopes of the plots (not shown) not depending on etching time.

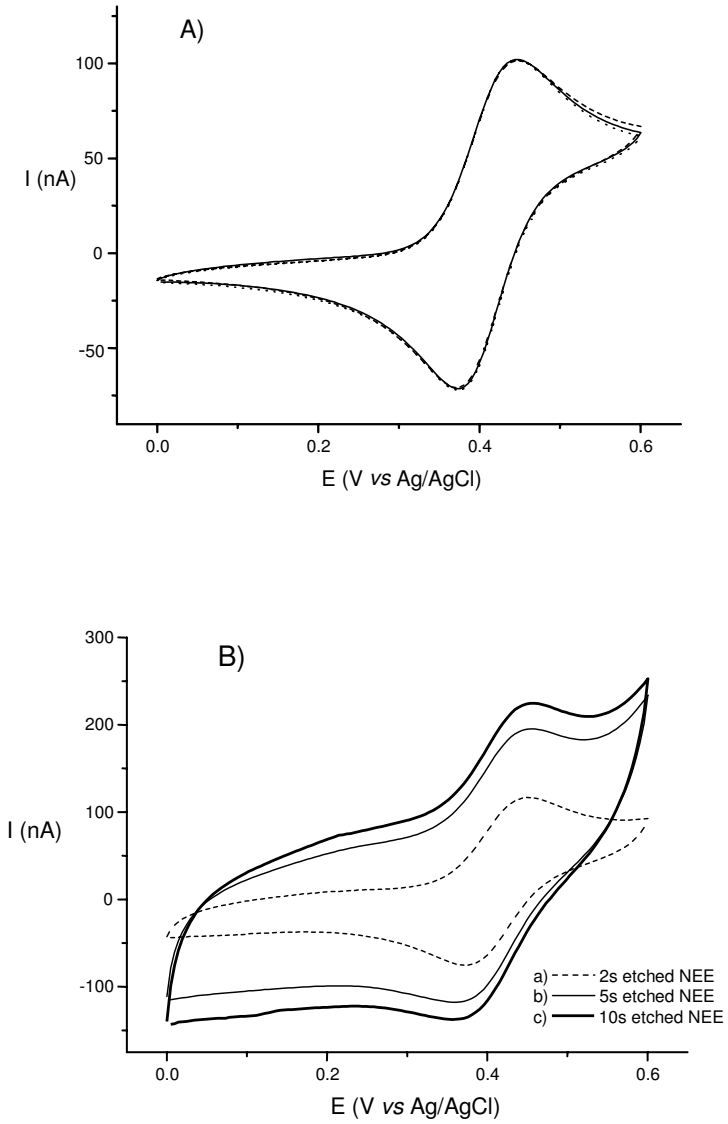

Figure 5.3
CVs of 10 µM FA^+ in 1 mM KNO_3 recorded at 50 mV/s: A) with three different unetched NEEs; B) with NEEs etched with 1:9 CH_2Cl_2/C_2H_5OH for 2 seconds (a), 5 seconds (b), 10 seconds (c).

The observation that the faradaic currents do not change significantly with the etching time can be explained taking into account that the redox species studied here undergo a fast electron transfer process, characterized by a quite high value for the true heterogeneous rate constant k^o=0.56 [15]. Since NEEs behave as PBE, one has to take into account that the true kinetic constant should be substituted by an apparent kinetic constant given by equation (1.3). However, for a fast redox couple such as FA^+, the influence of the change of $k°_{app}$ values by changing f cannot be appreciated experimentally at the scan rates used here (100 mV/s or lower) at 30 nm NEEs [1].

Under total overlap conditions, for a fast redox species, the faradaic current is indeed controlled by linear diffusion, so that it remains proportional to the overall geometric area of the ensemble [4, 17], whether the individual nanoelectrodes are etched or unetched.

5.2.2 Fast vs slow redox couples at 3D-NEEs

Following the guideline described above, the reduction of H_2O_2, occurring according to reaction (5.2):

$$H_2O_2 + 2H^+ + 2e^- \rightarrow 2H_2O \qquad (5.2)$$

was chosen as a typical electrochemical process characterised by a slow heterogeneous electron transfer kinetics. Note that it was theoretically predicted by Amatore [4, 17] that voltammetric responses at PBEs (and, therefore, at NEEs as well) should change dramatically when kinetic control, instead of simple diffusion is involved. This is because the heterogeneous kinetics limitation causes a considerable torsion of the lines of flux near each nanoelectrode element, thus imposing a local rate of diffusion considerably larger than the one far from each electrode [17]; under these conditions, each nanoelectrode should behave as an individual element, as far as heterogeneous kinetics is concerned.

Fig. 5.4 shows the CVs relevant to H_2O_2 reduction at unetched and etched NEEs. Note that in order to record the signals, a high H_2O_2 concentration and a slow scan rate had to be employed.

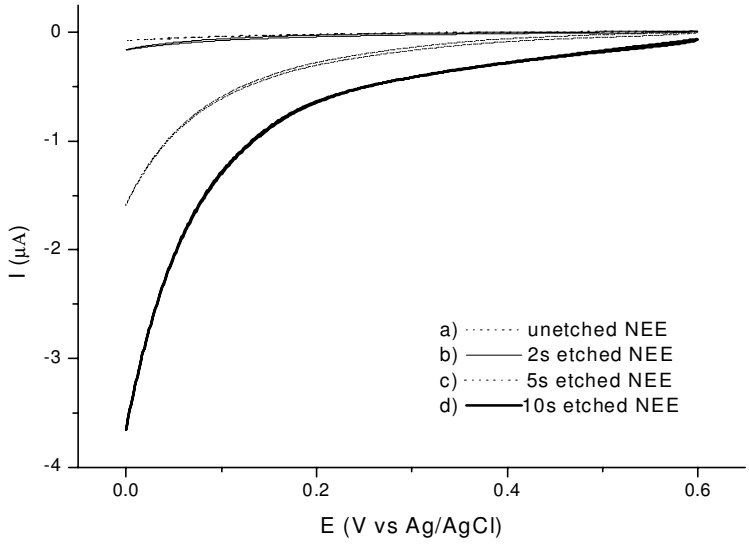

Figure 5.4
CVs recorded in 0.3 M H_2O_2, 0.5 M H_2SO_4 at 10 mV/s: a) with an unetched NEE and with NEEs etched with 1:9 CH_2Cl_2/C_2H_5OH for 2 seconds (b), 5 seconds (c), 10 seconds (d).

These data show that currents recorded at the cathodic limit of the explored potential window, depend strongly on the etching time of the NEE. At an unetched NEE a very small, almost neglectable, cathodic current is observed at 0 Volt, which increases gradually with NEEs etched for progressively longer time (see Fig. 5.4).
On the basis of equation (1.3), the etching reflects an increase of A_{act} and concomitantly of f and $k°_{app}$. This explains why the cathodic current for H_2O_2 reduction (slow process) increases when using progressively more etched NEEs; $k°_{app}$ increases, in fact, significantly with the active area and now, since the electron transfer process is kinetically controlled, such an effect causes dramatic changes in the CVs. The H_2O_2 cathodic current increases according to the ratio 1:10:25:55 for NEEs etched for 0, 2, 5 and 10 seconds, respectively, which reflects the increase in active area caused by the etching process (see increases in capacitive currents in Table 5.1).

Note that the difference in behaviour between fast and slow redox couples here discussed for NEEs is similar to what has been observed very recently for macroporous electrodes [18]. In the latter case, the key point was the possibility to control changes in surface area (surface roughness) on a micro-scale and to show that they can be detected only when using suitably slow redox couples.

5.2.3 Electrochemistry of adsorbed species at 3D-NEEs

For many electroanalytical applications the surface of electrodes in general, and NEEs in particular [19, 20] can be modified either with catalysts, mediators or molecular recognition elements. Therefore the electrochemical behaviour of surface-confined redox species was also examined here on the etched NEEs. With respect to the present study this is particularly interesting since, in contrast to diffusing species, signals of adsorbed redox probes, should always depend on the active area which means, for 3D.-NEEs, on the etching time.

Fig. 5.5 shows the CVs recorded at 50 mV/s for an unetched NEE and a 3D-NEE dipped in 5 mM phosphomolybdic acid (PMA), rinsed with water and transferred into pure supporting electrolyte. The voltammograms are characterized by two reversible processes which correspond to the following reactions:

$$PMo_{12}O_{40}^{3-} + 2e^- \Leftrightarrow PMo_{12}O_{40}^{5-} \quad (5.3)$$

$$PMo_{12}O_{40}^{5-} + 2e^- \Leftrightarrow PMo_{12}O_{40}^{7-} \quad (5.4)$$

The evidence that the electrochemical reduction of PMA is detected even after transfer to pure supporting electrolyte, agrees with literature reports [21] which indicate that PMA adsorbs on gold surfaces. Actually, the PMA signal at unetched NEEs is very small and barely distinguishable from the background current, while this signal increases dramatically for the etched NEE. This agrees with the presence of a surface confined process and with the increase in active area caused by the etching.

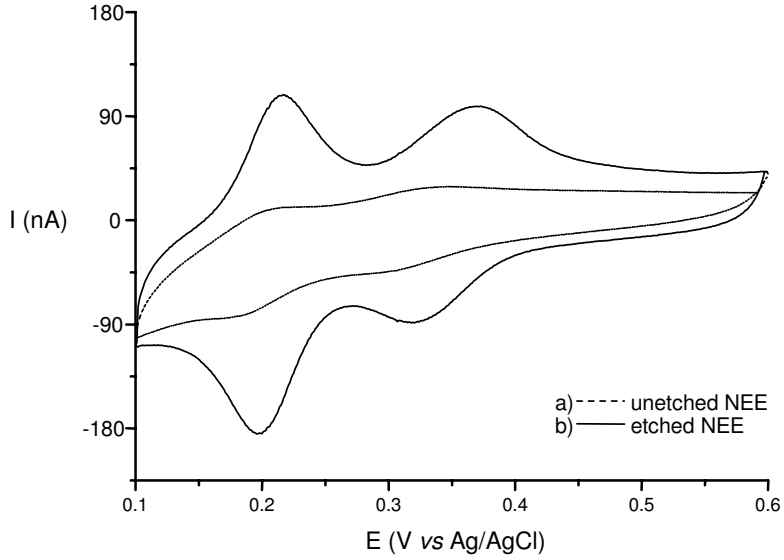

Figure 5.5
CVs recorded in 0.5 M H_2SO_4 at 50 mV/s after dipping the working electrode in 5mM $H_3PMo_{12}O_{40}$ for 1 hour, rinsing and transferring into pure supporting electrolyte for an unetched NEE and a NEE etched with 1:9 CH_2Cl_2/C_2H_5OH for 10 seconds.

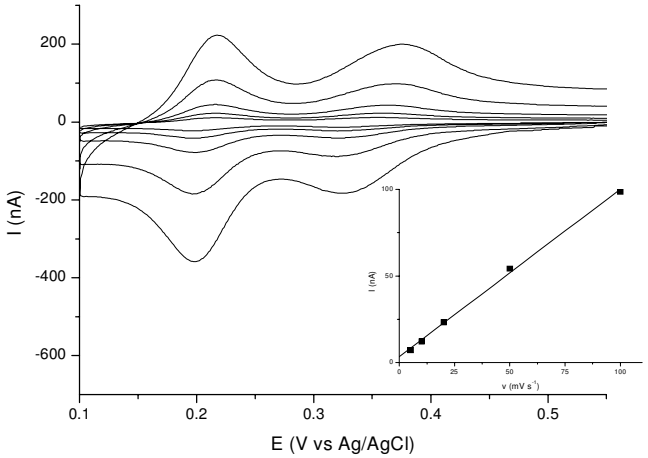

Figure 5.6
CVs recorded at different scan rates in 0.5 M H_2SO_4 at a NEE etched with 1:9 CH_2Cl_2/C_2H_5OH for 10 seconds; the working electrode was dipped in 5 mM $H_3PMo_{12}O_{40}$ for 1 hour, rinsed with water and transferred into pure supporting electrolyte; scan rates 5, 10, 20, 50 100 mV/s, from the smaller to the larger peak currents CVs. Insert: peak current vs scan rate plot, relevant to the first reduction peak.

Fig. 5.6 shows that at etched NEEs, reduction peak currents depend linearly on the scan rate, confirming once again that the signals refer to an adsorbed species [13].
The charge (Q) associated with the two reduction peaks can be obtained by integration of the peak area. Data obtained at NEEs chemically etched for different times, are listed in Tab. 5.2, together with the number of moles adsorbed (m) calculated by equation (5.5):

$$m = Q/nF \qquad (5.5)$$

where n is the number of electrons exchanged (in this case four) and F is the Faraday constant.

	ETCHING TIME		
	2 seconds	**5 seconds**	**10 seconds**
Q *(C)*	$1.5\ 10^{-8}$	$4.2\ 10^{-8}$	$6.9\ 10^{-8}$
m *(picomoles)*	$3.9\ 10^{-2}$	$1.08\ 10^{-1}$	$1.80\ 10^{-1}$

Table 5.2
Dependence on the etching time (in 1:9 CH_2Cl_2/C_2H_5OH) for the charge (Q) and number of moles adsorbed (m), obtained by integration of the reduction peak currents recorded at NEEs dipped in 5 mM $H_3PMo_{12}O_{40}$ for 1 hour, rinsed with water and transferred into 0.5 M H_2SO_4.

Both, charge and number of moles adsorbed scale with the etching time, once again confirming the possibility to control the active area of the NEE by controlling the etching time and, consequently, the amount of adsorbed redox probe.
Not only inorganic species, like PMA, can be easily immobilized on the surface of 3D NEEs but it was also possible to demonstrate the usefulness of 3D-NEEs for the adsorption of organic electroactive species suitable for example as mediators in electrochemical biosensors. As a model system the adsorption and electron shuttling capabilities of a nitrofluorenone derivative, namely 4-carboxy 2,5,7-trinitro-9-fluorenylidene-malononitrile (TNFM), has been examined.
The 3D-NEE was dipped in 1 mM TNFM solution and then transferred into pure supporting electrolyte. The adsorption and activation of TNFM proceeds via the two following steps [22]:

$$ArNO_2 + 4e^- + 4H^+ \rightarrow ArNHOH + H_2O \quad (5.6)$$

$$ArNHOH \Leftrightarrow ArNO + 2e^- + 2H^+ \quad (5.7)$$

with Ar as a symbol for the aromatic moiety of the molecule.

The first irreversible process (reaction (5.6)) proceeds at potentials more negative than approximately –350 mV, while the second reversible process takes place, at pH 7, with an $E_{1/2}$ of about –50 mV. Note that reaction (5.6) is required for the preactivation and assisted adsorption of the mediator, while reaction (5.7) is a process which can be exploited for the electrocatalytic oxidation of NADH [23].

The thin line pattern in Fig. 5.7-A shows the CV recorded in the potential range of reaction (5.7) for a 3D-NEE on which TNFM was adsorbed and preactivated. A small signal, relevant to reaction (5.7), is indeed detected, although it is not significantly resolved from the background current. Note that such a signal is undetectable at unetched NEEs (not shown).

As shown by the thick line in the CV of Fig. 5.7-A the CV pattern of the mediator modified 3D-NEE changes dramatically when NADH is added to the buffer solution. A well resolved wave is now observed, corresponding to the electrocatalytic oxidation of NADH caused by activated TNFM [23].

As expected, no electrocatalysis was observed for functionalised 3D-NEE when NAD^+ was used instead of NADH (not shown); moreover, the voltammetric pattern did not change after the addition of NAD^+ and GDH (see thin line in Fig. 5.7-B). However, as shown by the thick line of Fig. 5.7-B, the addition of glucose causes again a catalytic current. Under the latter experimental conditions, the following reaction sequence is operating [22]:

$$GDH_{ox} + Glucose \rightarrow P + GDH_{red} \quad (5.8)$$

$$GDH_{red} + NAD^+ \rightarrow GDH_{ox} + NADH \quad (5.9)$$

$$NADH + M_{ox} \rightarrow NAD^+ + M_{red} \quad (5.10)$$

$$M_{red} \rightarrow M_{ox} + 2e^- + 2H^+ \quad (5.11)$$

with P being the reaction product and M the mediator.

Under such conditions, NADH is produced at the electrode/solution interface by reaction (5.9), thus triggering indirectly the electrochemical signal of the mediator by reaction (5.10).

These preliminary results confirm the effective adsorption of the mediator on the nanowires and the possibility to apply 3D-NEEs in electrochemical biosensors which employ surface confined redox mediators with the perspective to benefit from an improved signal/background current ratio.

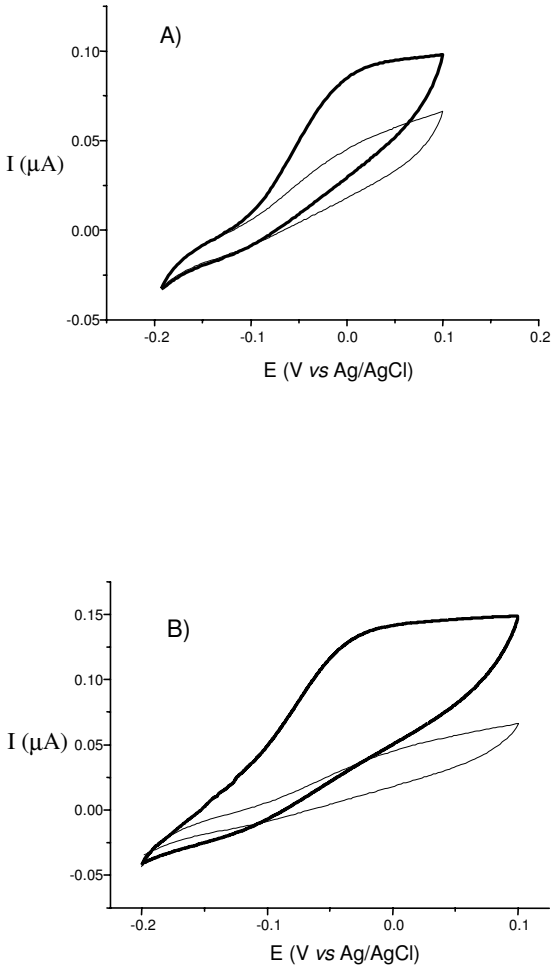

Figure 5.7
CVs recorded at 100 mV/s with a NEE etched in 1:9 CH_2Cl_2/C_2H_5OH, dipped for 2 hours in 1 mM 4-carboxy-2,5,7-trinitro-9-fluorenylidene-malononitrile, rinsed with water and transferred into 0.2 M $CaCl_2$, 0.1 M TRIS buffer solution (pH 8): A) before (thin line), and after the addition of 0.5 mM NADH (thick line); B) after the addition of 3.2 mM NAD^+ and 3 units of GDH (thin line), and 0.2 mM glucose (thick line).

5.3 Conclusions

3D-NEEs are powerful electrode systems with a high active surface suitable for functionalization and miniaturization. In contrast to previous preliminary observations reported in very recent literature [8-9], the results of the present study demonstrated that the etching really causes an increase in capacitive current, which is proportional to the increase in active area. Faradaic peak currents at 3D-NEEs can change dramatically with the heterogeneous electron transfer kinetics. For fast redox couples, Faradaic currents depend on the overall geometric area of the ensemble (nanoelectrodes and insulator between them), so that voltammetric peak currents remain almost unaffected by the partial etching of the template membrane causing a negligible increase of A_{gco}; this is not true for slow redox probes for which Faradaic currents are significantly dependent on changes of the active area (area of the nanoelectrodes alone). Electrochemical responses at 3D-NEEs agree, indeed, with the theoretical model developed some years ago for PBEs by Amatore et al. [4]. For very fast redox couples, such as FA^+, faradaic currents are insensitive to the etching since the heterogeneous kinetics is always very fast and total overlap conditions remain always operative. On the other hand, for redox couples characterized by slow heterogeneous kinetics, each nanoelectrode behaves individually and, because of strong kinetic limitations, Faradaic currents depend significantly on the increase in active area caused by the etching. This is true for diffusing electroactive species and in the case of the redox probes adsorbed on the nanoelectrode surface, the voltammetric signal depends always on the active area. These evidences indicate that the high surface area of 3D-NEEs can be best exploited to increase the voltammetric signals for electroactive species: i) that are adsorbed on the nanoelectrodes; ii) that diffuse from the bulk solution, but are characterized by slow heterogeneous electron transfer kinetics.

These aspects, for the first time demonstrated here, must be taken into proper account when thinking about using 3D-NEEs in electroanalysis and for the development and optimization of new electrochemical sensors.

References

[1] V.P. Menon, C.R. Martin, *Anal. Chem*. **1995,** *67*, 1920.

[2] P.Ugo, L.M.Moretto, S.Bellomi, V.P.Menon, C.R.Martin, *Anal. Chem*. **1996**, *68*, 4169.

[3] B. Brunetti, P.Ugo, L.M.Moretto, C.R.Martin, *J. Electroanal. Chem*. **2000**, *491*, 166.

[4] C.Amatore, J.M.Saveant, D.Tessier, *J. Electroanal. Chem*. **1983,** *147*, 39.

[5] P.Ugo, L.M.Moretto, F.Vezzà, *ChemPhysChem* **2002**, *3*, 917.

[6] S.Yu, N.Li, J.Wharton, C.R.Martin, *Nano Lett*. **2003**, *3*, 815.

[7] R.Gasparac, B.J.Taft, M.A.Lapierre-Devlin, A.D.Lazareck, J.M.Xu, and S.O.Kelly, *J. Am. Chem. Soc.* **2004**, *126*, 12270.

[8] M.A.Lapierre-Devlin, C.L.Asher, B.J.Taft, R.Gasparac, M.A.Roberts, S.O.Kelley, Nano Lett. **2005**, *5*, 1051.

[9] K. Krishnamoorthy, C.G.Zoski, *Anal. Chem*. **2005**, *77*, 5068.

[10] A.Lombardo, T.I.Bieber, *J. Chem. Edu.* **1983**, *60*, 1080.

[11] N.Mano, A.Kuhn, *J. Electroanal. Chem*. **1999,** *477*, 79.

[12] P.Ugo, N.Pepe, L.M.Moretto, M.Battagliarin, *J. Electroanal. Chem*. **2003**, *560*, 51.

[13] A.J.Bard and L.Faulkner, *Electrochemical Methods* Wiley, New York **2000**.

[14] F.C.Pereira, L.M.Moretto, M.DeLeo, M.V.Boldrin Zanoni, P. Ugo, *Anal Chim. Acta* **2006**, *575*, 16.

[15] L.M.Moretto, N.Pepe, P.Ugo, *Talanta* **2003**, *62*, 1055.

[16] E.Sabatani, J.Rubinstein, *J. Phys. Chem. B* **1987**, *91*, 6663.

[17] C.Amatore, in *Physical Electrochemistry*, (Ed. I. Rubinstein), Marcel Dekker, New York **1995**.

[18] R.Szamocki, S.Reculusa, S.Ravaine, P.N.Bartlett, A.Kuhn, R.Hempelmann, *Angew. Chem. Int. Ed.* **2006**, *45*, 1.

[19] M.Delvaux, S.Demoustier-Champagne, A.Walcarius, *Electroanalysis* **2004**, *16*, 190.

[20] M.Delvaux, A.Walcarius, S.Demoustier-Champagne, *Biosens. Bioelectron.* **2005**, *20*, 1587.

[21] A.Kuhn, F.C.Anson, *Langmuir* **1996**, *12*, 5841.

[22] N.Mano, A.Kuhn, *Biosens. Bioelectron.* **2001,** *16*, 653.

[23] N.Mano, A.Thienpont, A. Kuhn, *Electrochem. Comm*. **2001**, *3*, 585.

6 Concluding remarks

An improved procedure for preparing NEEs is presented: the NEEs so obtained yielded voltammetric responses that agreed with the predictions of established electrochemical theory, allowing us to evaluate, by a standardization protocol, set up by us, NEE performances as far as signal/background ratio, reproducibility and life time are concerned.

Furthermore, we have presented a new method for assembling NEE, by using a screen printed support, so obtaining the new devices NEE/SPS which can take advantages of both electrodic system. This method is simple, low-cost and highly reproducible.

We have demonstrated, moreover, that the use of gold NEEs allows the direct determination of micromolar and even submicromolar concentrations of iodide by simple cyclic voltammetry, without requiring any preceding preconcentration of the analyte. This direct method of analysis has been applied successfully to the determination of iodide in pharmaceutical products and iodised edible salt.

We have finally presented a different NEE fabrication procedure in which the nanodisk electrode elements are substituted by short nanofibre elements in order to obtain 3D-NEE. Concerning this point, two main results are obtained: first, it has been demonstrated that 3D-NEEs show a different electrochemical behaviour with respect to fast and slow redox species; second, it has been showed the possibility to use 3D-NEE as electrochemical detectors for mediated biosensors.

Future research efforts need to be devoted for evolving from the present NEEs to more sophisticated systems. In fact because of the small dimension, the very favourable signal/background current ratio, the possibility to link various molecules directly on their surface and, not as the latest, the low cost, nanoelectrodes ensemble, either 2D-NEEs and 3D-NEEs, are expected to play a key role in the future development of advanced electrochemical sensors.

7 Acknowledgements

I wish to thank the whole group of Electrochemical Sensors of the University of Venice as well as all the people of the LACReM laboratory of the University of Bordeaux1. In particular, my thanks go to Professor Ugo, Professor Kuhn and to Dr. Moretto for showing and transmitting me their enthusiasm for research and guiding me during all these years.

It is a pleasure to acknowledge Professor Roberto Pilloton and Dr. Walter. Vastarella (ENEA Casaccia-Rome) for screen printed substrate, Professor Massimo Tormen (TASC, Area Science Park of Trieste) for FE-SEM images, Professor Stefano Polizzi (University of Venice) and Dr. Paolo Scopece (CIVEN, Venice) for TEM images and AFM measurements respectively.

APPENDIX A

Publications in international journals

- F.C.Pereira, L.M.Moretto, **M.De Leo,** M.V.Boldrin Zanoni, P.Ugo, Gold nanoelectrode ensembles for direct trace electroanalysis of iodide, *Analytica Chimica Acta 575 (2006) 16-24.*

- W.Wastarella. L.Della Seta, A.Masci, J.Mali, **M.De Leo**, L.M.Moretto, R.Pilloton, Biosensor based on gold nanoelectrode ensembles and screen printed electrodes, submitted to *International Journal of Environmental Analytical Chemistry.*

- **M.De Leo**, A.Kuhn, P.Ugo, 3D-ensembles of gold nanowires: preparation, characterization and electroanalytical peculiarities *Electroanalysis 79, 533, 2007.*

Presentations to international congress

- Communication to the 11th Young Investigators' Seminar on Analytical Chemistry, *YISAC*, held in Graz (Austria) from 30 June to 3 July 2004 entitled *"Electroanalysis with Nanoelectrode Ensembles (NEEs)"* M.De Leo, P.Ugo.

- Communication to the 12th Young Investigators' Seminar on Analytical Chemistry, *YISAC*, held in Sarajevo (Bosnia and Herzegovina) from 5 to 10 July 2005 entitled "*Advanced in the Electroanalytical Use of Nanoelectrode Ensembles"* M.De Leo, A.Kuhn, L.M.Moretto, P.Ugo.

- Communication to the 11th International Conference on Electroanalytical Chemistry, *ESEAC,* held in Bordeaux (France) from 11 to 15 June 2006 entitled "*Nanoelectrode Ensembles for Electrochemical Sensing Purposes"* M.De Leo, A.Kuhn, P.Ugo.